TEMPLATE SYNTHESIS OF MACROBICYCLIC CRYPTANDS AND THEIR SELECTIVE COMPLEXATION STUDIES

A Thesis Submitted
in Partial Fulfilment of the Requirements
for the Degree of
DOCTOR OF PHILOSOPHY

By

K. RAGUNATHAN

to the

DEPARTMENT OF CHEMISTRY
INDIAN INSTITUTE OF TECHNOLOGY KANPUR

FEBRUARY, 1993

TO MY PARENTS

S T A T E M E N T

I hereby declare that the matter embodied in this thesis is the result of investigations carried out by me in the Department of Chemistry, Indian Institute of Technology, Kanpur, India, under the supervision of Dr. P.K. Bharadwaj. In keeping with the general practice of reporting scientific observations, due acknowledgements have been made wherever the work described is based on the findings of other investigators.

K. RAGUNATHAN

IIT Kanpur
February 1st, 1993

DEPARTMENT OF CHEMISTRY
INDIAN INSTITUTE OF TECHNOLOGY, KANPUR INDIA

CERTIFICATE -I

This is to certify that Mr. K. RAGUNATHAN has satisfactorily completed all the courses required for the Ph.D. Degree programme. These courses include:

Chm 605 Principles of Organic Chemistry

Chm 624 Modern Physical Methods in Chemistry

Chm 625 Principles of Physical Chemistry

Chm 645 Principles of Inorganic Chemistry

Chm 681 Basic Biological Chemistry

Chm 646 Bioinorganic Chemistry

Chm 800 General Seminar

Chm 801 Graduate Seminar

Chm 900 Post-Graduate Research

Mr. K. Ragunathan successfully completed his Ph.D. qualifying examination on March 2nd., 1990

(Dr. P.K. Ghosh)
Professor and Head
Department of Chemistry
I.I.T. Kanpur

(Dr. Y.D. Vankar)
Professor and Convenor
Departmental Post Graduate Committee
Department of Chemistry
I.I.T. Kanpur

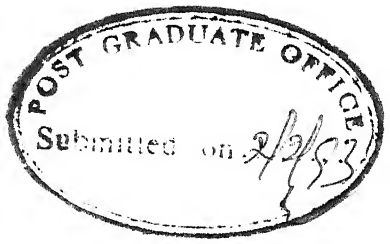

C E R T I F I C A T E - II

It is certified that the work contained in the thesis, **"TEMPLATE SYNTHESIS OF MACROBICYCLIC CRYPTANDS AND THEIR SELECTIVE COMPLEXATION STUDIES"** by K. Ragunathan, has been carried out under my supervision and the same has not been submitted elsewhere for a degree.

P. K. Bharadwaj

(Dr. P.K. Bharadwaj)
Department of Chemistry
Indian Institute of Technology, Kanpur

1st. February, 1993

ACKNOWLEDGEMENT

It is a great pleasure to express my heartfelt thanks to Dr. P.K. Bharadwaj for his unstinted guidance and stimulating discussion throughout the course of this work. It has been his encouraging words and timely assistance which preserved my enthusiasm during difficult periods. His constructive criticism and valuable suggestions helped me to develop scientific skill which instilled confidence in me to further my research interest. I am highly grateful to him for providing me a wonderful period in the laboratory.

I wish to express my profound thanks to

* Dr. S. Manogaran, Dr. Javed Iqbal, Dr. R.N. Mukherjee and Prof. S. Sarkar for the helpful discussions and extending their laboratory facilities.

* Prof. K. Natarajan, Prof. S. Shanmugam and Dr.K. J. Rajendra Prasad for their guidance during my M. Phil study which laid the foundation for my research career.

* Prof. C.W. Mak for the X-ray crystal structure.

* my colleagues Mr. S. Mandal, Dr. R. Shukla, Mr. P. Tarakeshwar, Mr. D. Chakraborti, Dr. B. R. Srinivasan, Dr. K. V. Surendranath, Mr. A. K. Verma, Miss J. Annapurna, Miss V.R.Latha, Miss R. Sridevi, Miss Jayati Sengupta, Mr. P. Ghosh and Miss Swati Misra for their ever helping hands, discussions and pleasant associations.

* Dr. K. Ramesh, Dr. P.K. Chowdhury, Messrs R. Maiti, S. K. Das, Jayaraman, B.K. Patel, U. Illangovan, M. Ray, S. Mahapatra, Balakrishnan and Sanjay Kumar for all their help and pleasant association.

* Kalyan, Tamil, Kundu, Shaji, Naren, Kasi, Immie, Govind, Ravikanth, Reddy, Johri, Saiffuddin, Ramsharan, Sampath,

Murali, Pandian, Pondimani, Nandi, Padmanabhan, Punnya Moorthy and all Hall IV and Hall V friends for enjoyable friendship and providing me a lovely campus life.

* Mrs. Dulali Bharadwaj and Mrs. Ramesh for providing a homely atmosphere.

* Messrs Kannaujia, Bhavsar, Ahmad and Rajgopalan for recording the spectra.

* RSIC, Lucknow for 400 MHz ^{1}H NMR, 100 MHz ^{13}C NMR, FAB-Mass and elemental analysis services.

* Messrs Misra and Ganguly for their skilful work to prepare this thesis.

I am highly indebted to my family members for their love, advice and patience.

K. Ragunathan

SYNOPSIS

The thesis entitled "Template Synthesis of Macrobicyclic Cryptands and Their Selective Complexation Studies" is divided into five chapters.

Chapter 1 gives a general account of the special features of cryptands as ligands for transition metal ions as well as uncharged molecules. The use of macrobicyclic cryptands as ligands for transition metal ions is of considerable current interest. As ligands they possess several desirable features like different donor atoms' topology, binding site rigidity, layer effects etc. that determine stability, selectivity and properties of their complexes with transition metal ions. Besides, the donor atoms in a cryptand are capable of imposing unusual coordination geometries onto metal ions owing to their neoplastic nature. This is of enormous importance in modelling the intrinsic active sites of metalloproteins. In case of cryptands having more than one receptor sites, polymetallic cryptates can be formed which might afford to study interactions between metal centres. Besides, secondary recognition of small molecules can be effected forming the so-called cascade complexes which is of importance in different areas of chemistry like selective transport, catalysis

and small molecular activation.

Chapter 2 discusses the scopes of the present work. Emphasis is given on the template synthesis of cryptands with different donor atoms' topologies as well as donor atom types. Synthesis of cryptands usually involves the use of high-dilution technique which is cumbersome and often leads to low yields of the desired products. On the other hand, synthesis using metal ions as templates can be achieved much more easily. In the present thesis alkali metal ions have been used as templates. Advantages of their use is discussed. The use of these cryptands as ligands for transition metal ions to mimic the intrinsic active sites of metalloproteins are discussed. This chapter also discusses the scopes of synthesizing cascade complexes as well as molecular complexes with cryptands.

Chapter 3 concerns with the synthesis of an octaazamacrobicyclic cryptand (Fig. 1) by [2+3] Schiff base condensation in presence of Cs^+ or Rb^+ ion as the template. The alkali metal ion is held in the cavity which can be transmetallated by Cu(II), Ni(II), Zn(II) and Mn(II) ions. The complexes isolated were probed by different spectroscopic, electrochemical and magnetic studies besides elemental analysis.

The cryptand has two potential receptor sites. It forms binuclear complexes with Cu(II) and Zn(II) when these metal ions are allowed to react with the cryptand in 2:1 molar ratio. The dicopper complex exhibits a peculiar seven-line EPR spectrum in solution attributed to two weakly interacting Cu(II) centres. The electronic spectrum is consistent with the trigonal bipyramidal geometry around each Cu(II) ion. The free ligand as well the zinc complex show a three-fold symmetry as revealed by the high field ^{1}H NMR studies. Cu(II), Ni(II) and Mn(II) ions form mononuclear hexacoordinate complexes with the chromophore, MN_6 when allowed to react in 1:1 molar ratio.

Chapter 4 presents a novel cryptand having three disulfide linkages (Fig. 2). This is also synthesized by [2+3] Schiff base condensation reaction in presence of Cs^{+} ion. In this case, however, the alkali metal ion is not bound inside the cavity. The cryptand readily forms hexacoordinated dicopper and dinickel complexes. The two metal ions inside the cavity donot interact as inferred from the spectroscopic, magnetic and electrochemical studies even though they are bridged by three disulfide groups.

Chapter 5 is divided into three sections. Section **A** describes the synthesis of a hetero-ditopic cryptand with three

bridging benzene groups (Fig. 3) by tripod-tripod Schiff base condensation in presence of Cs^+ ion. It has a recognition site for a Cu(II) or a Ni(II) ion at one end of the ellipsoidal cavity which provide four nitrogen donor atoms. These donor atoms impose a pseudotetrahedral coordination geometry onto the metal ions. The EPR spectrum of the Cu(II)-cryptate exhibits the smallest parallel hyperfine coupling ($A_{||}^{Cu} = 60 \times 10^{-4}$ cm^{-1}) observed todate for a Cu(II)-complex. Also, the Ni(II)-cryptate provides a rarely documented example of pseudotetrahedral NiN_4 coordination. Both the cryptates show secondary recognition and binds an azide group. The Cu(II)-cryptate forms an air-stable H_2S complex where the Cu(II)-S (of H_2S) bonding is revealed by changes in its spectroscopic properties compared to the original cryptate. This cryptate provides the first example of an air-stable Cu(II)-H_2S complex.

Section **B** presents the synthesis of a cryptand having a similar donor set with three bridging naphthalene groups instead of benzene (Fig. 4). This cryptand also enforces pseudotetrahedral geometry onto Cu(II) and Ni(II) which show similar spectroscopic properties as shown by corresponding Cu(II)- and Ni(II)-cryptates with the cryptand shown in Fig. 3. The Cu(II)-cryptate binds one H_2S molecule inside the cavity.

Section C discusses recognition of planar molecules like H_2O by these two hetero-ditopic cryptands. Crystal structural studies on the H_2O inclusion complexes are described here.

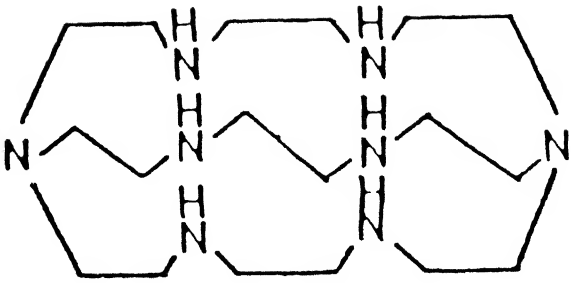

Fig. 1

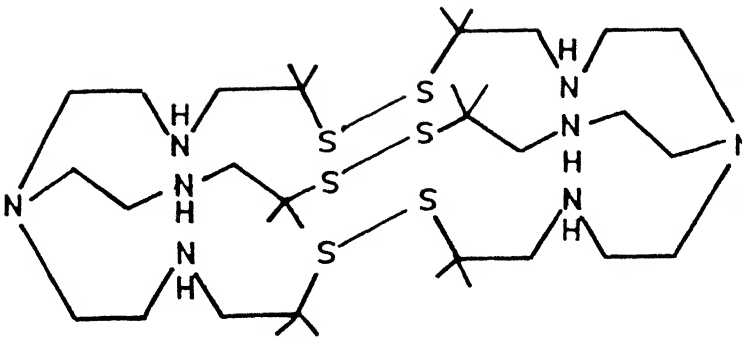

Fig. 2

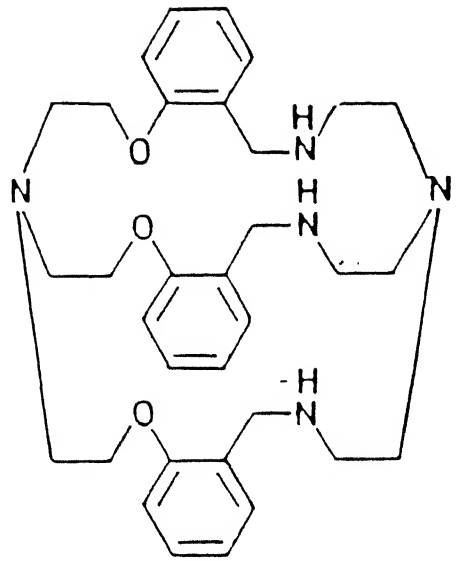

Fig. 3

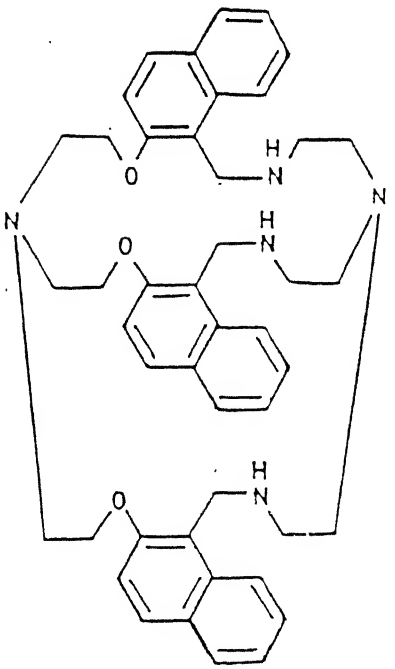

Fig. 4

CONTENTS

CHAPTER 1

INTRODUCTION

The name "cryptand" is derived from the Greek word "cryptos" meaning "cave" in order to express their special topological shapes [1,2]. These molecules have been proven to be of enormous importance in many areas of chemistry as well as biochemistry [3-5]. These macropolycyclic structures are able to provide suitable frameworks for arrangement in space of one or more receptor sites. These sites delineate molecular cavities into which the substrates penetrate, forming inclusion complexes whose geometry may be regulated via ligand design. As complexing agents, the cryptands permeate the area of molecular recognition [6-8] since their structural features determine the stability, selectivity and properties of their complexes with ions and neutral molecules. Cryptands can be designed to behave as single site (monotopic) or multisite (polytopic) molecular as well as metal ion receptors [9]. While monotopic receptors are capable of displaying functions [9] like recognition, catalysis selective transport etc., polytopic molecular receptors provide an entry into higher forms of molecular behaviour like co-

operativity, allostery and regulation. Polytopic receptors may have identical or different binding sites which may give rise to homo-and hetero-polynuclear complexes respectively.

The cryptands might have one or more cycles in their architecture and are denoted [10] by (n)-cryptands where "n" is the number of cycles. Thus, crown ethers (Fig. 1a) are (1)-cryptands. Macrobicycles (Fig. 1b) are (2)-cryptands and so on. Cryptands, as ligands, are superior to simple acyclic ligands due to certain desirable features in their structures which are discussed next.

1.1 Salient Features of Cryptands

1.1.1 Donor atoms' topology

The nature and number of subunits used for the construction of the cavity determines the shape of the donor atoms' array [2,9]. Thus, coaxial arrangement of two tripodal subunits linked by three bridges give the macrobicycle (Fig.1b) where the donor atoms describe an ellipsoidal cavity. Face to face linkage of two macrocycles results in a cylindrical macrotricycle (Fig.1c). Likewise, the cryptand shown in Fig. 1d has a spherical topology of the donor atoms. Of course, quite a number of other shapes for the cavity are possible to design which is limited only by

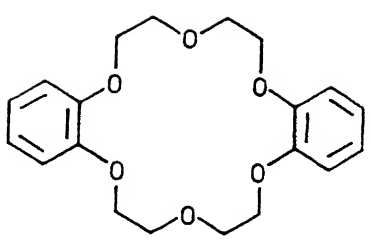

a

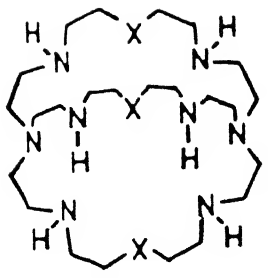

b

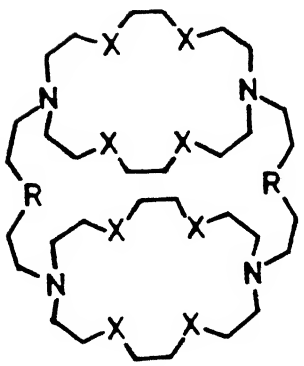

c

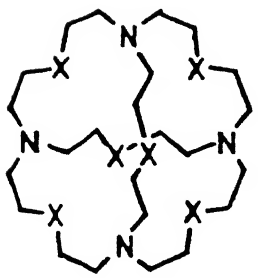

d

X = O,S

Fig. 1.1 Cryptands with different topologies of the donor atoms

one's imagination.

1.1.2 **Nature of the donor atoms**

By judicious choice of the subunits, different kinds of donor atoms like N, S, O, S_2, P etc. can be introduced into the ligand architecture [1,10-12] . It is appropriate to comment here that nature of donor atoms are very important in discriminating the binding of charged as well as uncharged guests. While macropolycycles with ethereal oxygens as the donor atoms preferably form [13] inclusion complexes with alkali as well as alkaline earth metal ions, those with thioether sulphur, amino nitrogens, etc. donors readily form [9,11] transition metal cryptates.

1.1.3 **Rigidity of the binding site**

Macropolycyclic architecture imposes [10,12,14] conformational and steric barrier which in turn determines the stability and selectivity of the complexation. An ideal situation will arise if the ligand donor set is preorganised [12] to impart a preferable coordination geometry for a particular metal ion and it is having least strain in that conformation. Because in that case, the metal complexation will be extremely facile and the stability should be high. Flexible structural

[10] units constructed of sp^3 hybridised atoms accommodate a large range of shapes and sizes than do those made from sp^2 or sp hybridised ones. Flexible chains can be multiply-linked into polyhedric shapes and severely limit the rotational freedom. Flat groups like aromatic rings can be used to rigidify the cavity. Groups like disulfides, amides etc. can also be used to construct a rigid cavity. The more rigid the cavity, the greater will be its discriminatory power against ions/molecules that are either larger or smaller than the cavity, since these will require severe ligand deformation for contact binding.

1.1.4 Cryptate effect

The inclusion complexes formed by cryptands are called cryptates [1]. The stability constants of these cryptates are found to be higher [13,15] by several orders of magnitudes compared to the complexes with open-chain polydentate ligands. This is called the cryptate effect. Studies on this phenomenon showed that this effect originates from both thermodynamic and kinetic quantities [14].

1.1.5 Layer effect

The cryptands provide a sort of organic skin [16] to the

bound species. As a result, the effect of the counterion and the medium will be at a minimum. The nature of the external surface of a cryptand, whether hydrophilic or lipophilic, determines its solubility pattern. The thickness of this organic skin will also determine the stability of the bound species since it affects the interaction between the bound species and the external medium. Adding alkyl/aryl groups to the cryptand as side chains can effectively isolate the ion/molecule trapped inside. Besides, the anion being isolated from the bound cations, can be used as catalysts, e.g. in anionic polymerisation [16].

1.2 Synthesis of Cryptands

The synthetic strategies for the preparation of cryptands can be classified broadly into two main classes: (1) high-dilution method and (2) the method of using a metal ion as a template.

1.2.1 High dilution method

This method [17] plays a dominant role in different types of ring closure reactions. Cyclizations taking advantage of the high dilution principle, usually start with open chain compounds having two or more functional groups. These functional groups

react leading to the formation of monomeric as well as oligomeric cyclization products. In order to suppress the formation of oligo-condensation products, a very low concentration of the educts is maintained in the reaction flask. The optimum concentrations of the educts is found out empirically. Nevertheless, there have been some developments in theoretical directions as well [18]. A large number of macrocycles, macrobicycles as well as macrotricycles have been synthesised by high dilution method. In fact, this is the major synthetic approach used for the synthesis of cage molecules [19]. The most common strategy for synthesizing cryptands involves the formation of macrocycles. Once a macrocycle is synthesized, the next step will be to add another chain to it to have the desired macrobicycle [19]. It is obvious that, a macrocyclic/macrobicyclic synthesis using the high-dilution technique is a time-consuming, cumbersome process. Besides, more often than not, the desired products are obtained in low yields alongwith a number of side products. Isolation of the pure product can sometimes be really an involved process.

1.2.2 **Template Synthesis**

A cyclisation step is sometimes made facile by using a metal

ion as a template [20]. One of the first examples of a metal ion facilitating the formation [21] of a macrocycle was the self-condensation of o-phthalonitrile to yield metal phthalocyanine complexes as illustrated in the Fig. 1.2.

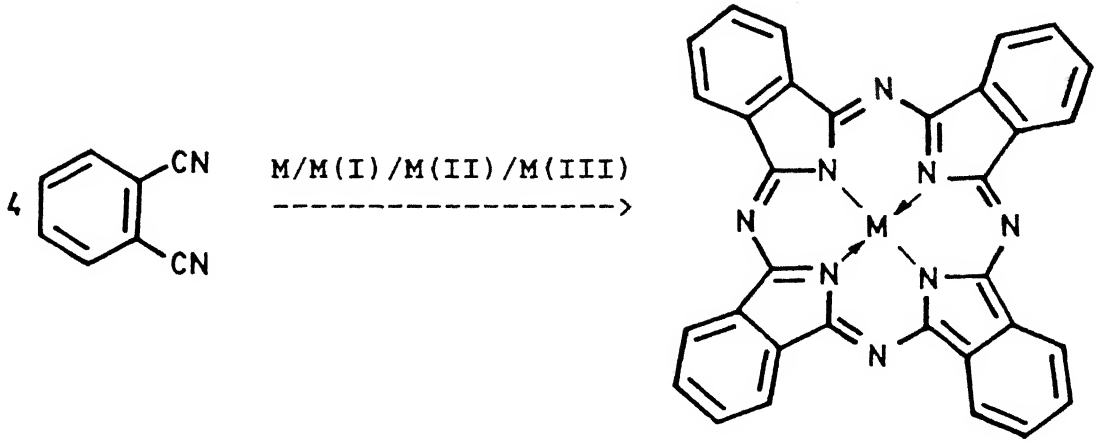

M = Na, Mg, Cu, Ni and Sb

M(I) = Na(I), K(I) and Cu(I)

M(II) = Ca(II), Mg(II), Ni(II) and Cu(II)

M(III) = Fe(III)

Fig. 1.2

The template effect can be of kinetic or of thermodynamic origin or can be a combination of both [20].

According to the kinetic template hypothesis [20], the geometric arrangement of ligands within the coordination sphere of a metal ion provides constraints that can be used to control the structure of a product formed by reactions of coordinated

ligands. Specifically, the coordination sphere of the metal ion may serve as a template to hold reactive groups in proper positions for sterically highly selective, multistep reactions. A large number of macrocycles have been synthesised on metal templates [20].

The contrasting thermodynamic coordination template effect [20] acts, not on the mechanism of the ligand forming process. It rather acts on stabilizing a ligand structure that might otherwise be disfavoured in the pure organic chemical system at equilibrium. The most important case of an equilibrium template process is the formation of the tetraazamacrocycles discovered [22] by Neil Curtis. Solutions of ethylenediamine in acetone react to form a variety of species whose relative abundances vary with conditions. Under certain experimental conditions, macrocycles I and II (Fig. 1.3) can be isolated in the absence of

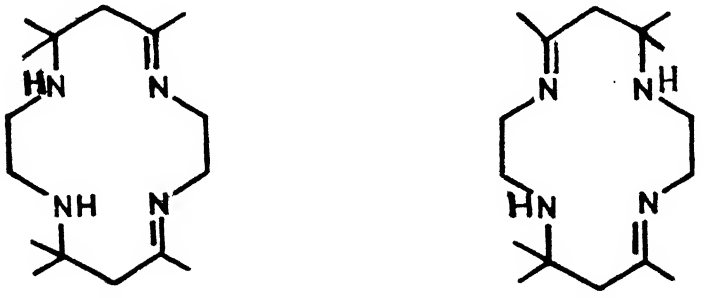

I II

Fig. 1.3

metal ions. However, it has been shown clearly that the presence of metal ions like Ni(II) and Cu(II) leads to the sequestering of the macrocycles by the metal ions because of the superior behaviour of the macrocycles as ligands. These are outside the scope of the present thesis and are not discussed.

Besides these two methods, other methods which found sporadic usage in the syntheses of cryptands include gauche effect [23], caesium effect [24], the rigid group principle [25], etc.

1.3 Ligating abilities of cryptands

The present section limits the discussion on the (2)-cryptands and their complex forming abilities to ions and neutral molecules. This is to provide the proper perspectives for the chapters to follow. For brevity, (1)- or (3)-cryptands are not included in the discussion although they are equally important.

1.3.1 Cryptands with oxygen donors

In 1967, Pedersen's pioneering discovery [26] of the crown ethers and their strong binding abilities [27] towards alkali metal ions, demonstrated that effective and selective complexation can be achieved with neutral synthetic organic

ligands. Selective binding of cations in solution is a distinctive feature of the solution chemistry of macrocyclic polyethers. The design and synthesis of new macrocyclic ligands with different cavity sizes, donor atom types, ring substituents, etc. have resulted in a large number and variety of compounds [1,28]. An extension of the macrocyclic chemistry is found in the case of (2)- and higher cryptands. Unlike a macrocycle, these macrobicyclic ligands encapsulate a metal ion due to their cage-like structures. Generally, the metal ion whose ionic radius best matches the radius of the cavity formed by the cryptand on complexation, will form the most stable complex. Macrobicyclic cryptands can assume any of the three conformations [29] according to the configuration of the two nitrogen bridge heads viz., in-in, in-out or out-out as illustrated in Fig. 1.4.

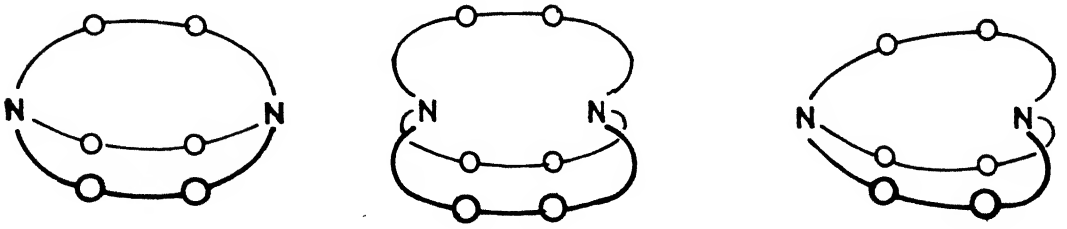

out-out in-in out-in

Fig. 1.4

For the complex formation reaction, the magnitude of steric strain of the ligand is an important factor to be considered. Lower the steric strain in the complex, more favourable will be the complex formation. An ideal situation will arise if the ligand donor set is preorganized to impart a preferable coordination geometry for a particular metal ion and it is having least strain in that conformation. Because in that case, the metal complexation will be extremely facile and the stability of the complex should be high. A few oxygen donor cryptands are given in Table 1.1.

The free [2.2.2] cryptand exists in the in-in conformation in the solid state as revealed [1] by its X-ray structure

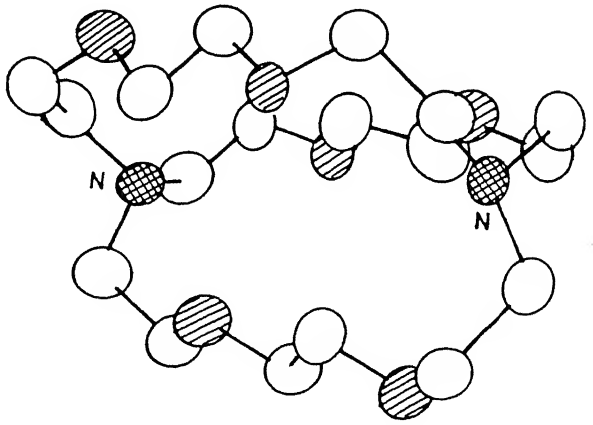

Fig. 1.5

(Fig. 1.5). This molecule shows some rigidity compared to acyclic/macrocyclic ligands and display [10] "peak selectivity".

However, cryptands having sizes greater than that of [2.2.2], show signs of flexibility in ion encapsulation. Lehn and Sauvage concluded [10] that these flexible cryptands show "plateau selectivity". Of course, rigid ligands which are too small to accommodate a metal ion may form 2:1 complexes [30]. Cryptands incorporating several ethereal donors, form an important part of supramolecular chemistry due mainly to their importance in a wide range of areas, particularly in biological systems and medical applications [3-6]. It has also breathed life into the chemistry of the otherwise uninteresting alkali and alkaline earth metal ions [31]. These cryptands have also been studied as selective complexing agents for toxic heavy metals [13]. However, the cryptands with the ethreal oxygen donors which act as hard donors have not been found to be useful complexing agents for transition metal ions.

1.3.2 **Cryptands with nitrogen and/or sulfur donors**

Introduction of nitrogen and/or sulfur in the place of oxygens in the macropolycyclic structures opened up a way for the exciting transition metal cryptate chemistry [9,13,32,33]. The design of ligands for the different transition metal ions requires the choice of classes of receptor molecules endowed with

the structural features that will confer strength and selectivity to the binding process. Of special interest, is the possibility to induce [34,35] a variety of special electronic, magnetic, electrochemical and photochemical properties. This is possible through designed modification of the structural features like the donor atoms' topology, rigidity of the binding sites and its size etc. Precisely, these are the properties which are very important in mimicking the intrinsic active sites [36] of metalloproteins.

In an intrinsic active site, the amino acid side chains of the protein backbone provide the donor atoms for the metal ion(s). The unusual properties of metal ions at these sites [36,37] compared with those of the simple complexes, arise due to unusual coordination environments which in turn result from conformationally imposed constraints upon amino acid side chains that comprise the ligands for the metal ion(s). This imposition of an irregular geometry in an intrinsic active site, is designed by nature to achieve a condition energetically favourable to carry out its assigned biological role(s). In a suitably designed cryptand, the donor atoms being somewhat neoplastic in nature, can enforce an irregular coordination geometry on to a

metal ion [13,32,38]. Thus, cryptands are perhaps the best suited as abiological ligands to mimic the electronic structure and bonding of an intrinsic active site. However, no systematic studies are available in the literature in this direction. Of course, any such exercise has the ultimate aim to understand the structure and functional relationship of metalloproteins at the molecular level.

Cryptands can include one or more metal ions depending on the cavity size and the disposition of donor atoms. Thus, both mono- and bi-nuclear cryptates have been studied with transition metals some of which are listed in the Tables 1.2-1.3. These tables do not intend to provide an exhaustive list of transition metal cryptates. Only a few representative complexes are shown. It is relevant to point out here that there is a growing interest [39,40,41] in polynuclear metal assemblies because an increasing number of active centres in metalloproteins are found to contain more than one metal atoms [42-45]. In what follows, some of the mononuclear and polynuclear transition metal cryptates have been discussed. This discussion is biased towards the studies of electronic structure and bonding properties of the transition metal cryptates.

1.3.3 Mononuclear cryptates

The cages [32] of sepulchrate (Fig. 1.6A) and sarcaphagine (Fig. 1.6B) belong to the cryptand family and they form highly stable complexes with a number of first-row transition metal ions. Sargeson and coworkers, synthesized these cage molecules (Fig. 1.6) on Co(III), Pt(IV), Ir(III) and Rh(III) [46] ion as the template. The redox properties of the metal complexes were of

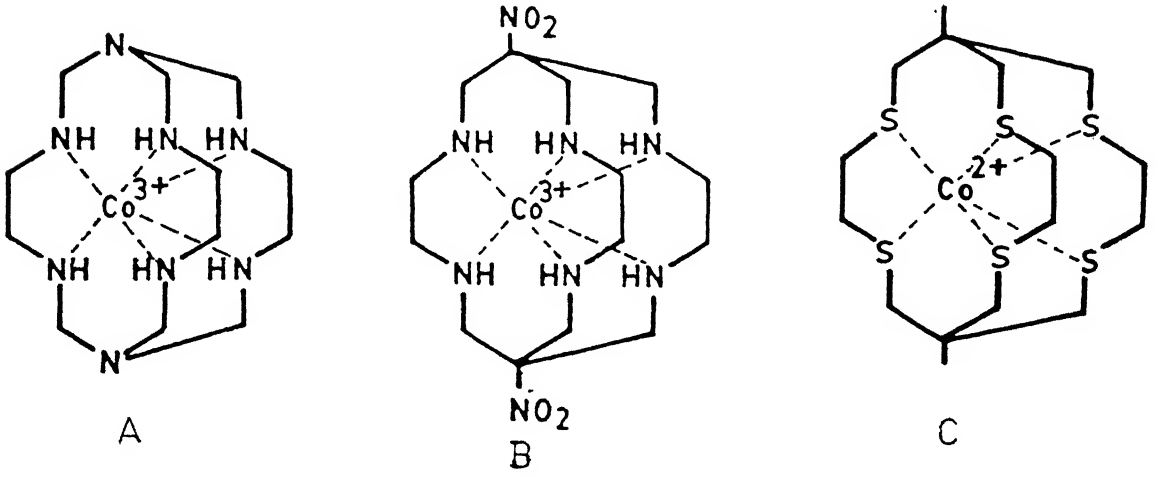

Fig. 1.6

the early captivating features of the cage chemistry [46]. For Co(III)/(II) sepulchrate ions, despite the insulating organic coat, the electron self exchange rate was 10^5 fold greater [46a] than that for the parent $[Co(en)_3]^{3+/2+}$ ions. The cage hole appears to be a little large for Co(III) and a little too small for Co(II). Thus, the strain generated in the ligand by the

encapsulation of the ion explains the increased electron self-exchange rate. If the ligand frame work is such that the stereochemistry about the metal is ion strained in a way that helps the system towards transition state then a more rapid electron self-exchange rate can be expected relative to the unstrained system. This expectation is incorporated in the entatic state hypothesis [36] of metalloenzyme redox processes. Cu(II)/Cu(I) systems, for example, could be constrained to largely the same stereochemistry in the two oxidation states by the rigidity of the enzyme donor system. Such arrangement could lead to rapid reversible electron transfer reactions. The sulphur analogue of the sarcaphagine (Fig. 1.6C) has been synthesised [46e] recently. A few other mononuclear transition metal cryptates have been reported which are collected in the Table 1.2. The small cavity cryptand, 1 illustrated in Fig. 1.9 imposes a trigonal bipyramidal geometry [47] around the metal ion Cu(II) and the cryptate [1 Cu(II)]Br_2 shows a great inertness towards strong acid solutions, no change being observed over a period of months in both HCl and $HClO_4$ (3 mol dm^{-3} aqueous solutions). Thus, the stability of this cryptate is unprecedented.

1.3.4 Binuclear Cryptates

Macrobicyclic ligands having two receptor sites may form dinuclear cryptates (Table 1.3). The ligand O-bistren (1) forms dinuclear cryptates with Zn(II), Cu(II), Ni(II), Mn(II) and Co(III). The ellipsoidal cavity takes up two metal cations one at each end. The powder EPR spectrum of blue [2 Cu(II) 1] complex show a weak signal at g = 4 indicating some coupling between the two Cu^{2+} ions. The electronic spectrum shows similarity to that of the metalloenzyme, hemocyanin [42]. A binucleating cryptand having two NS_3 donor sets bridged by three-carbon aliphatic chains have been synthesized [49] by high dilution method. This compound can incorporate two Cu(II) ions inside the cavity. These ions do not interact magnetically as its magnetic susceptibility and EPR spectral results indicate.

1.3.5 Tri- and poly-nuclear cryptates

Arranging more than one metal cations inside the cavity of the ligand might lead [34,35] to molecular wires and molecular magnets which is mainly directed towards the development of materials with novel properties. Metal ions assembled together in a multimetal system can exhibit drastically different magnetic properties from those of individual ions due to electron exchange

phenomena [41]. Also, long range spin-exchange interactions may shed light on mechanisms of long range electron tunnelling [50]. Recently Mandoza et. al. [51] reported the first trinuclear Ag(I)- and Cu(I)-Ag(I)-Cu(I) hetero-trinuclear cryptates (Table 1.3). The three metal ions are arranged (Fig. 1.7) in a row, held at well-defined distances and bound in two different

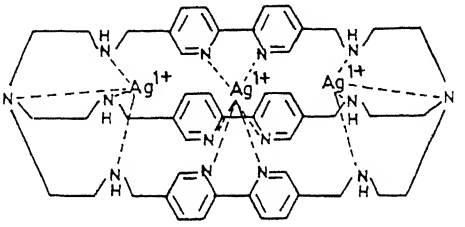

Fig. 1.7

environments. This clearly indicates the potential of macropolycylic ligands in arranging the metal ions in space in a specific sequence. The ligand design plays a major role in the multimetal assembling process. Arranging specific donor sets in a specific disposition might lead to specificity in arranging the metal ions. Beer et.al. synthesised [52] the cryptand, **10**, (fig 1.10) with three externally oriented 2,2'-bipyridyl transition metal recognition sites. The hetero-polymetallic cryptate of Cu(I) and Ru(II), Zn(II) and Ru(II) have been studied. The

Ru(II) photo- and electro-chemical properties are perturbed by the internally bound Zn(II) ions. A polyaza tris-ferrocene macrobicyclic cryptand, **13** (fig1.10) forms hetero-polymetallic cryptates with Zn(II) and Cu(I).

1.3.6 **Cascade Complexes**

Both mono- as well as poly- nuclear cryptates can further add on to substrates forming cascade complexes [9]. These complexes (Table 1.4) form via a sequential, double selection process: selection of the cation(s) by the cryptand, selection of the substrate controlled by the nature and arrangement of the complexed cation(s). Cascade complexes may display several exciting properties: (i) selective fixation and transport of substrates, (ii) catalysis of multicenter-multielectronic processes, (iii) activation of the fixed substrates, (iv) condensation or cross-reaction (thermal or photochemical) of different substrates brought together and held in proximity.

Investigations pertaining to the formation of cascade complexes with dinuclear cryptates have been made sporadically [48,49,53-56]. In contrast, such studies with mononuclear cryptates are not well known [57,58]. Oxidation [53a] of the

dinuclear Co(II) complex of o-bistren gives the -peroxo, -hydroxo species (Fig. 1.11-1). Addition [48] of H_2O, CN^-, N_3^- to the dicopper cryptate with O-bistren (1 in Table 1.3) lead to changes in the electronic spectra indicating [48] the formation of cascade complexes. The cascade complex shown in Fig. 1.11-3 crystallizes [56] from the corresponding dinuclear cryptate where CO_2 is bound as CO_3 ion. Illustrations of few other cascade complexes are shown in Fig. 1.11.

1.3.7 **Molecular Cryptates**

The binding of molecular substrates represents also a major area of supramolecular chemistry. It makes use of various molecular interactions [59,4] like electrostatic, hydrogen bonding, donor-acceptor, van der Waals as well as hydrophobic effects. Specific groups may serve as anchoring sites through which substrate molecules attach to complementary sites in the receptor molecules. Extensive use has been made of H-bonding interactions and well-defined coordination patterns have been identified and characterised by crystal structure determination when H-bonding is involved [60]. Interactions such as donor-acceptor and van der Waals forces are less directive and may present a softer dependence [61] on distances and angles. This is

also the case for hydrophobic (solvophobic) effects which can nevertheless make a high contribution to the complex stability especially for lipophilic receptors [62] like cyclophanes (or) cyclodextrins in aqueous solution which is, however, out of scope for discussion here.

Strong binding in molecular complexes require multiple interactions due to weaker interactions involved compared to transition metal cryptates. This is very important for neutral molecules binding through hydrogen bonds and dipole-dipole interactions. The stability of the complexes formed through hydrogen bonding of acidic OH, NH, CH to acceptor sites (O, N) are comparatively low [63]. Suitably designed receptor molecules are capable of forming selective and stable supramolecular species through neutral hydrogen bonding array in the appropriate coordination patterns.

Table 1.1 N,O-Donor Cryptands

Cryptand	Method of Preparation	Transition Metal Cryptates Studied	Reference
1	HD or Na(I) template	Cu(II)	15,64
2	HD	Co(II) and Ni(II)	66,65
3	HD	Cu(II), Ni(II) and Co(II)	67
4	HD	Fe(III)	68
5	Fe(III) template	Fe(III)	69

HD = high dilution

Illustrations of the cryptands are given in Fig. 1.8

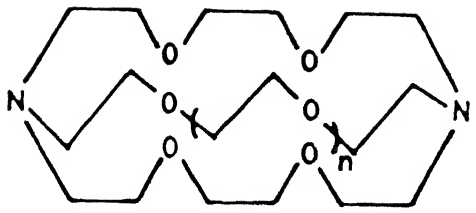

n = 1

1

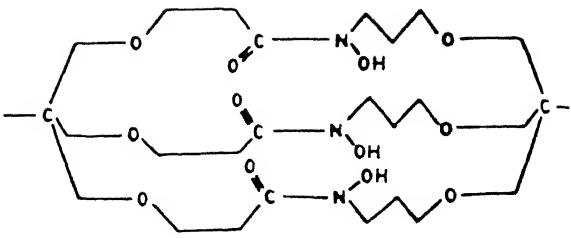

4

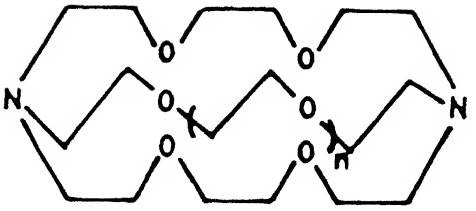

n = 0

2

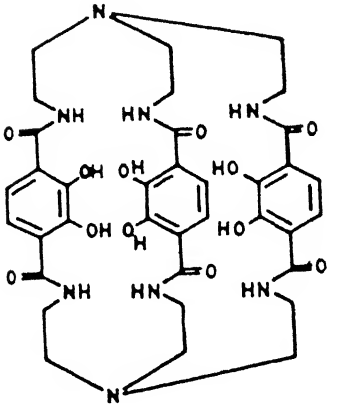

5

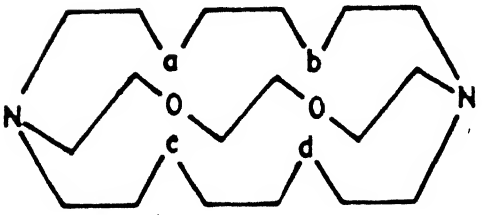

3

1 a = b = c = O and d = NCH_3

2 a = b = O and c = d = NCH_3

3 a = b = c = d = NCH_3

4 a = b = NH and c = d = O

Fig. 1.8 N,O-donor cryptands as collected in Table 1.1

Table 1.2 Mononucleating N- and/or S-Donor Cryptands

Cryptand	Method of Preparation	Transition Metal Cryptates Studied	Reference
1	HD	Cu(II)	47
2	Co(III),Pt(IV), Rh(III) & Ir(III) template	Cr(III),V(III),V(IV), Mn(II),Mn(III),Fe(II), Fe(III),Co(II),Co(III), Cu(II),Ni(II),Ni(III), Rh(III),Pt(IV) & Ir(III)	32,46a,c,d
3	Co(III),Rh(III) & Ir(III) template	Co(III),Rh(III) & Ir(III)	46b,c
4	Cs(I) template	Co(II)	46e
5	Co(III) template	Co(III)	46f
6	Ca(II) & Sr(II) template	Cu(II),Mn(II),Co(II) Fe(II) & Fe(III)	70

HD = high dilution

Illustrations of the cryptands are given in the Fig. 1.9

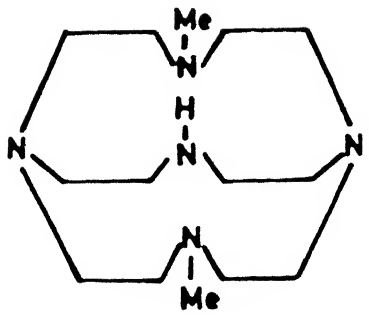

1

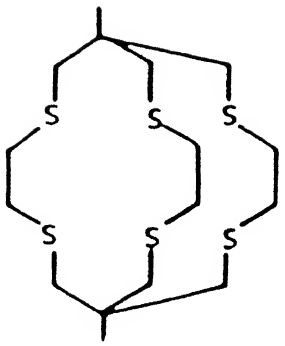

4

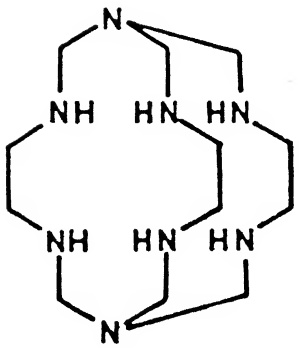

2

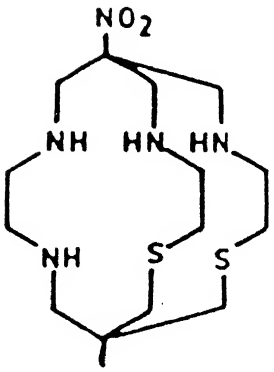

5

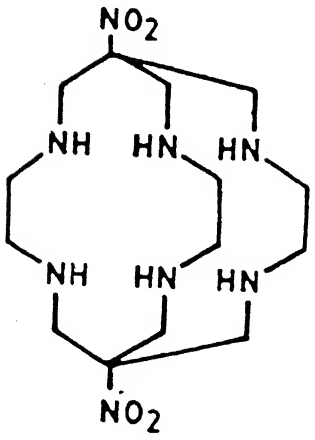

3

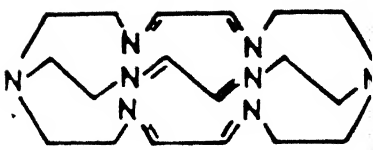

6

Fig. 1.9 Mononucleating N- and/or S-donor cryptands as in Table 1.2

Table 1.3 Di- and Poly-nucleating Cryptands

Cryptand	Method of Preparation	Transition Metal Cryptates Studied	Reference
1	HD (or) Cs(I) & K(I) template	Cu(II), Zn(II) & Co(II)	48,71
2	HD	Cu(II)	49
3	Ca(II) & Sr(II) template	Cu(II)	72
4	Ag(I) template template	Cu(I)	39
5	HD	Cu(II) & Co(II)	56
6	HD or Ag(I) template	Cu(II),Ni(II) & Co(II)	73
7	HD	Cu(I)	74
8	HD	Cu(II)	75
9	HD	Cu(I)-Ag(I)-Cu(I) Ag(I)-Ag(I)-Ag(I)	51
10	HD	Cu(I)-Ru(II)$_3$-Cu(I) Zn(II)-Ru(II)$_3$-Zn(II)	52
11		Zn(II)-Fe(II)$_3$-Zn(II)	52

HD = high dilution

Illustration of the cryptands are given in Fig. 1.10

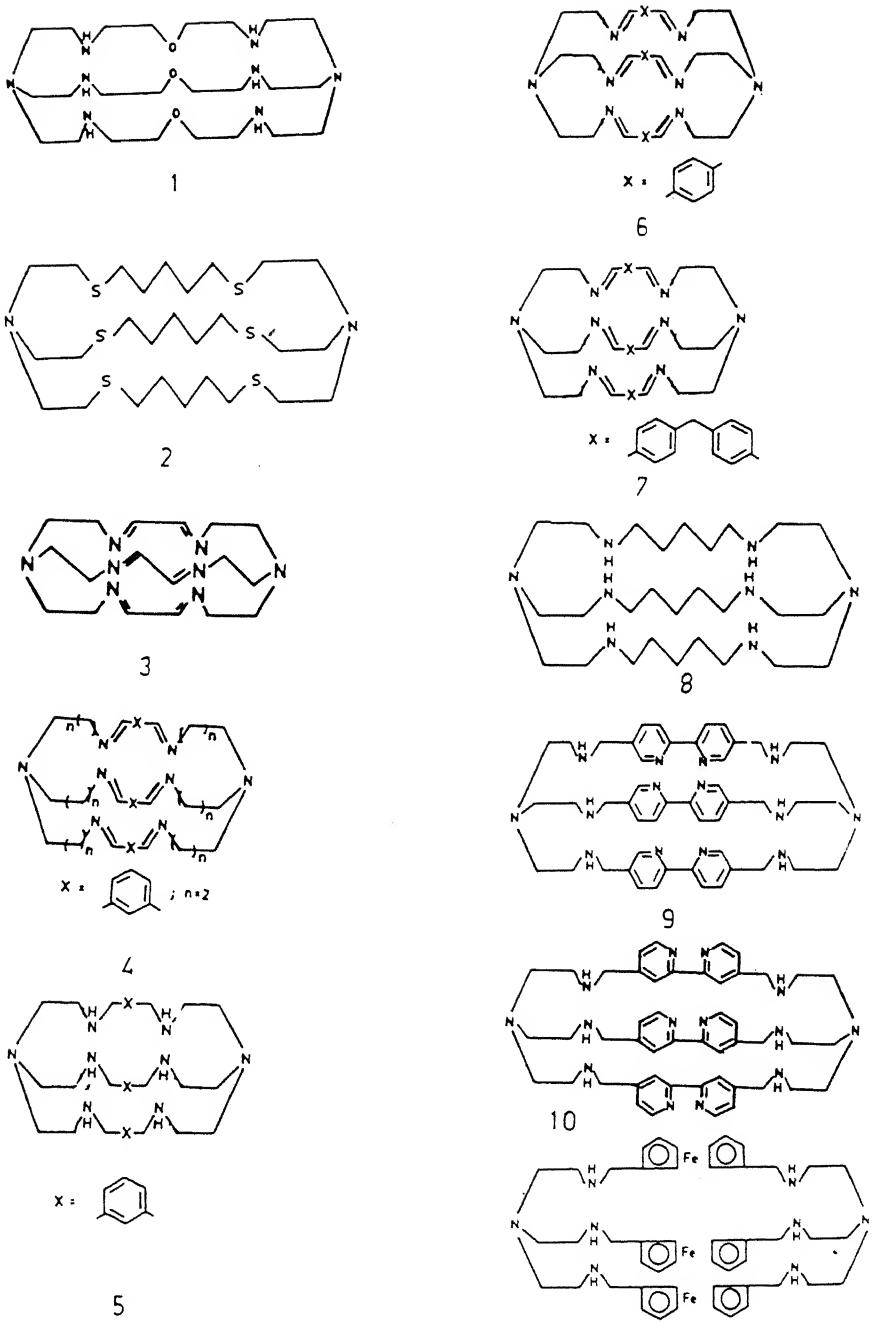

Fig. 1.10 Di- and Poly-nucleating cryptands as in Table 1.3

Table 1.4 Cascade Complexes

Complex	Metal ion(s)	Substrate	Reference
1	Co(III)	OH^-, O_2^{2-}	53a
2	Cu(II)	H_2O, CN^-, N_3^-	48
3	Cu(II)	CO_3^{2-}	56
4	Cu(II)	OH^-	53b
5	Cu(II)	F^-	58
6	Co(II)	N_3^-	55

Illustrations of the cascade complexes are given in Fig. 1.11

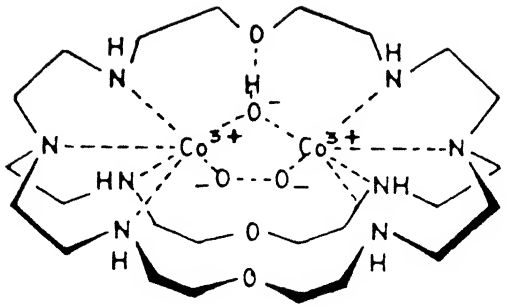

1

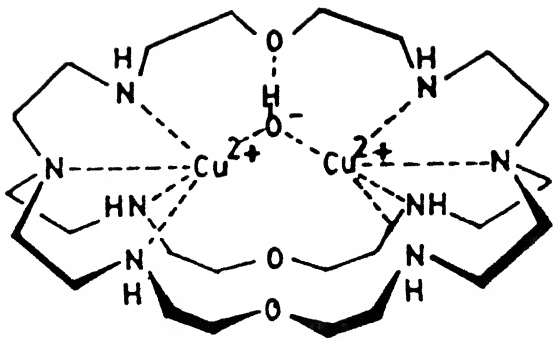

4

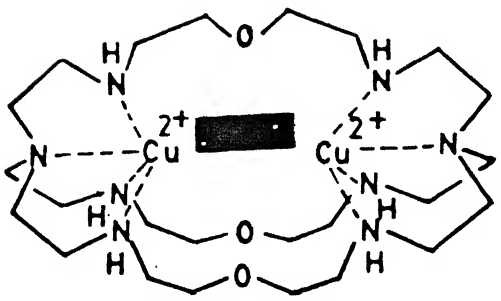

2

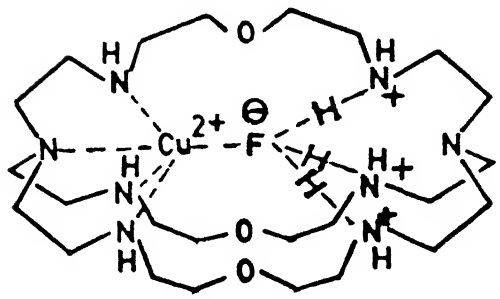

5

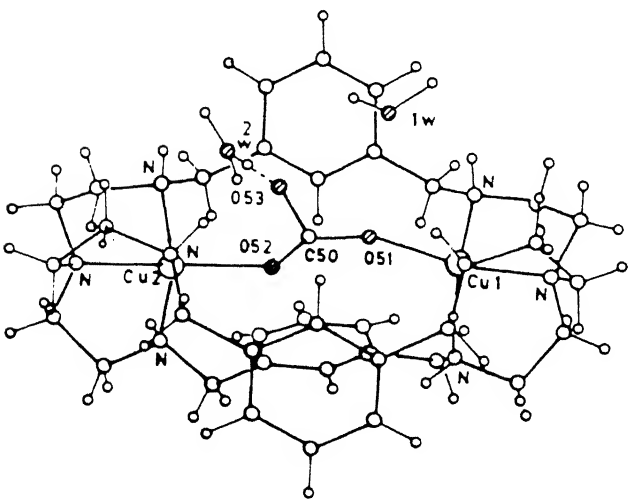

3

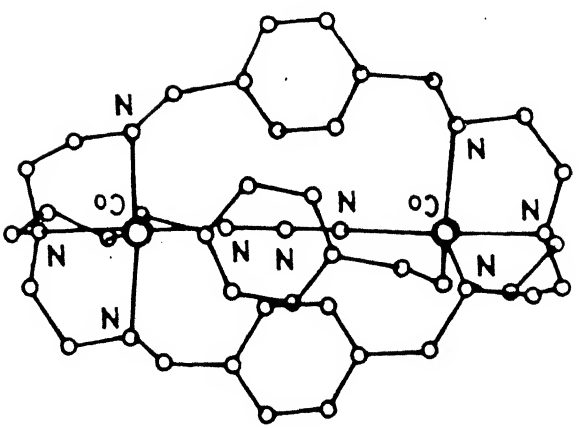

6

Fig. 1.11 Cascade complexes as collected in Table 1.4

Chapter 2

Scope of the Work

Synthesis of cryptands for ligating transition metal ions is of considerable current interest. Cryptands bearing nitrogen and/or sulfur donors readily form inclusion complexes with transition metal ions. Depending upon the size of the cavity, nature of the donor atoms and their topology, one or more metal ions can enter the cavity forming cryptate complexes. As ligands, these molecules possess several desirable features like predesigned three-dimensional donor atoms' topolgy, binding sites' rigidity, layer effects etc. which make them superior to simple acyclic or macrocyclic ligands. However, widespread use of these compounds as ligands for transition metal ions are yet to take place owing mostly to the difficulties involved in their synthesis. The usual method of synthesis involves utilising the high dilution techniques [17] which are cumbersome and afford only low yields of the desired products. Also, isolation of the pure product mixed with a number of bye-products can often be extremely difficult. Synthesis using templates provide an alternative method [20] which gives much higher yields of the

desired products. Besides, the numbers as well as amounts of the bye-products can be kept at the minimum.

Alkali metal ions have been used in the synthesis of macrocycles ever since the pioneering work of Pedersen was done for the synthesis of crown ethers [26]. However, these metal ions have not been used systematically for the synthesis of cryptands. Alkali metal ions form kinetically labile complexes [76]. Therefore, if an alkali metal ion, being used as the template, gets trapped inside the cryptand during its synthesis, it can be easily trans-metallated with a transition metal ion. So, a systematic investigation on the use of alkali metal ions as templates in the synthesis of cryptands is highly desirable. The template effect can be used in the following two ways:

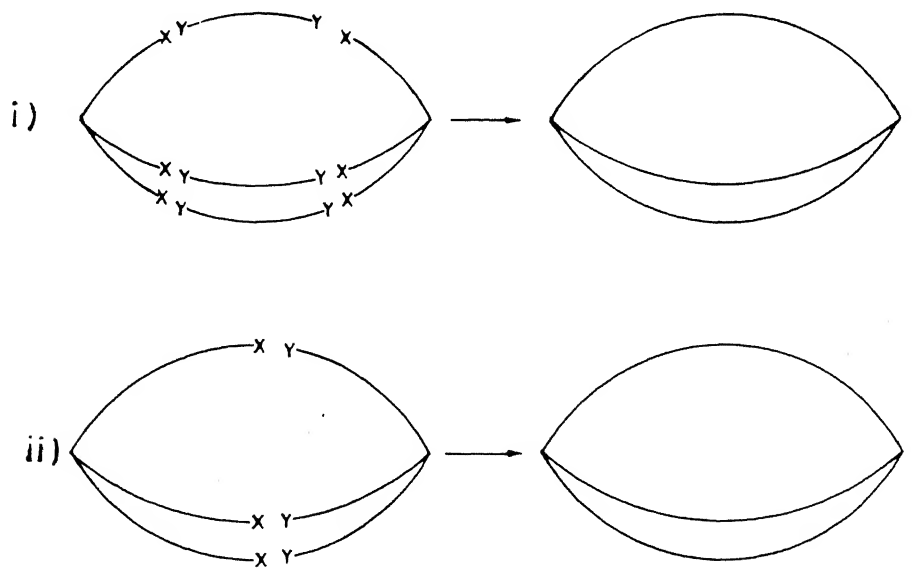

Fig. 2.1 Formation of macrobicyclic cryptands from acyclic components

In case of (ii) the two tripodal units can come together and join to form the cryptand **A**. In case of (i) a spacer unit can join the two tripods leading to the cryptand **B**. Thus, under both situations, the cryptand can be synthesized in one step. Schiff base condensation reaction can be used effectively as it requires only mild conditions and hence is a popular method [39,51,52,56]

A number of first-row transition metal ions have been used in synthesizing inclusion complexes with cryptands having nitrogen and/or sulfur donor atoms. Emphasis in such studies were placed on evaluating thermodynamic properties of such complexes. Sporadic studies have also been made on the electronic structure and bonding of the metal cryptates. However, no reports are available where imposition of a desired coordination geometry onto the transition metal ions have been studied. Due to neoplasticity of the donor atoms in a cryptand, it is possible to achieve metal complexes in unusual coordination symmetries. The active sites in a large number of metalloproteins are intrinsic [37] in nature. An intrinsic active site generates an unusual coordination environment at the metal binding site due to conformationally imposed constraints upon amino acid side chains

that comprise the ligands for the metal ion. The imposition of an irregular geometry onto a metal ion at the active site is designed by nature to achieve a condition energetically favourable [36] to carry out its assigned biological role(s). However, this leads to two important problems: (i) spectroscopic studies of the native proteins may yield data that are difficult to interpret and (ii) it is quite unrealistic to expect to synthesize a complex which is a detailed model for an intrinsic active site. In a suitably designed cryptand, however, a desired coordination geometry can be enforced upon a metal ion like the protein matrix does in an intrinsic active site. The rigidity of the donor sites can be enhanced by introducing groups like disulfides, aromatic rings, etc. With disulfides in the macrobicyclic rings, it is also possible to study metal-disulfide interactions which have important bioinorganic relevance [77]. Metalloproteins' active sites usually reside in hydrophobic pockets. Adding aliphatic/aromatic groups as the side groups in the macrobicyclic rings will increase the hydrophobicity to a significant extent around the donor groups. This will more closely match the active site environments.

For cryptands having two distinctly different receptor sites, it is possible to form metal cryptates where the metal ion

occupies only one site leaving the other site vacant. This is specially true if one site has oxygen donors while the other site has nitrogen donors. Small neutral molecules or anionic fragments can occupy this site and get bonded to the metal ion trapped inside. This type of secondary recognition [9] is important in selective fixation and transport of a given substrate as well as in the development of new catalytic systems.

Apart from metal ion recognition, neutral molecular recognition [7] is an important area of research today. Formation of inclusion complexes of the neutral molecules by the host cryptands is a topic of fundamental importance in many areas of chemistry as well as biochemistry [3,4]. The present thesis aims at investigating some the aforesaid aspects of the chemistry of cryptands.

Chapter 3

SYNTHESIS OF AN OCTAAZAMACROBICYCLIC CRYPTAND AND ITS LIGATING ABILITIES TOWARDS Mn(II), Ni(II), Cu(II) AND Zn(II) IONS

The incorporation of the tripodal unit, tris(2-aminoethyl) amine, $N(CH_2CH_2NH_2)_3$ in the macrobicycles was achieved first by Lehn and coworkers [74]. Since then, a variety of cryptands incorporating this unit have been synthesised and used as ligands for transition metal ions (Table 1.3; chapter 1). Most of the first-row transition metal ions have high affinity for nitrogen donor ligands and these metal ions readily form inclusion complexes with the cryptands incorporating these donor atoms. Cryptands, where the two coaxial tren {tren = tris(2-aminoethyl)amine} units are separated by spacers of considerable length, may form bimetallic cryptates. The distance between the metal centres can be varied via ligand design. For a large separation, the metal ions may behave as independent centres [39,56,73]. Decreasing the spacers' length might lead to bimetallic cryptates with metal-metal interactions [48,72] and/or cooperative binding of small molecules or anions like CO, CN^-,

imidazolate etc. Besides, dinuclear transition metal cryptates may provide models for the dinuclear active sites present in some metalloproteins [42-45]. Antiferromagnetic coupling has been observed [78,79] in different biomolecules like the dicopper sites in hemocyanin tyrosinase and laccase. Also, multi-metal interactions might lead to molecular magnets [35] with unusual conductivity as well as magnetic properties.

This chapter describes the one-pot synthesis of an octaazamacrobicyclic cryptand by [2+3] Schiff base condensation of tren and glyoxal followed by reduction with $NaBH_4$. The condensation step undergoes smoothly in presence of Rb(I) or Cs(I) ion acting as the template. The resulting Rb(I)- or Cs(I)-cryptate that forms in high yields, can be transmetallated readily with metal ions like Mn(II), Ni(II), Cu(II) and Zn(II). The cryptand behaves both as monotopic and ditopic receptor depending upon the nature of the metal ion and/or the reaction conditions. This all-nitrogen cryptand, synthesised previously [80] by Lehn and coworkers using the high-dilution technique, acts as an anion receptor upon protonation. Also, Hunter et.al.[70] have synthesised the Schiff base analogue using Sr(II) ion as the template and have probed its ligating abilities towards transition-metal ions.

3.1 EXPERIMENTAL SECTION

3.1.1 **Materials.**- Reagent grade chemicals tris(2-aminoethyl)amine, glyoxal, copper(II)perchlorate hexahydrate, nickel(II)perchlorate hexahydrate, manganese(II)acetate tetrahydrate and zinc(II) nitrate tetrahydrate acquired from Aldrich, were used as received. $NaBH_4$, rubidium chloride, cesium chloride and the solvents were acquired from SD Fine Chemicals, India. The solvents were purified prior to use following standard procedures [81].

3.1.2 **Analysis and Measurements**

The elements carbon, hydrogen and nitrogen were analysed by standard microanalytical techniques at the Indian Institute of Technology, Kanpur or at the Central Drug Research Institute, Lucknow, India.

Infrared spectra were recorded either on a Perkin-Elmer model 580 grating spectrophotometer or on a model 1600 Perkin-Elmer FT-IR spectrophotometer using KBr pellets. A polystyrene film was used as the reference.

^{1}H-NMR data were recorded either on a Bruker WP-80FT (80 MHz) instrument or on a Bruker WM 400FT (400 MHz) instrument. For

brevity, not all the NMR spectra taken are shown although all the NMR data are presented.

Magnetic susceptibility measurements were made with a Cahn Faraday Balance using $[CoHg(SCN)_4]$ as the standard. Diamagnetic corrections were applied in all the cases.

Electron paramagnetic resonance (EPR) spectra were recorded on a varian E-109 spectrometer operating at the X-band using DPPH as the external standard. EPR spectra were taken at room temperature (298 K) and at liquid nitrogen temperature (77 K).

Conductivity data were collected on an Elico Model CM-82T conductivity bridge for dilute solutions (ca. 10^{-3}M). The instrument was calibrated using standard KCl solutions.

Melting points were obtained using an electrical melting point apparatus (PERFIT) and were uncorrected.

The electronic spectra of solutions were recorded on a Perkin Elmer Lambda-2 UV-VIS spectrophotometer at 298 K using freshly purified solvents.

Cyclic voltammetric measurements were performed using a PAR model 370-4 electrochemistry system : 174A, polarographic analyzer; 175, universal programmer; and RE 0074, X-Y recorder. Potentials are reported at 298 K relative to a saturated calomel

reference electrode (SCE) and are uncorrected for liquid junction potentials. A sealed all-glass cell was used. The auxiliary electrode, which consisted of a platinum flag sealed in soft glass, and the reference electrode were separated from the working solution by means of a fritted bridge filled with the same solvent and supporting electrolyte. Uncompensated solution resistance in the cell configuration was minimized by placing the tip of the reference electrode as close to the working electrode as possible and using an approximately constant ratio of $[NBut_4]ClO_4$ as supporting electrolyte and solute concentration of (100:1). A PAR G0021 glassy carbon electrode was used as the working electrode. The system was calibrated [82] against ferrocene, and tris(2,2'-bipyridyl)iron(II) perchlorate. All measurements were made under an atmosphere of nitrogen. The potentials are reported as E_f { $E_f=0.5(E_{pa}+E_{pc})$ }.

FAB-mass (positive ion) data were recorded on JEOL SX 102/DA-6000 Mass Spectrometer/Data Systems using Argon (6KV, 10 mA) as the FAB gas. The accelerating voltage was 10 kV and the spectra were recorded at 298 K. m-Nitrobenzyl alcohol (NBA) or glycerol was used as the matrix. Some of the matrix peaks that appeared when NBA was used were at m/z values of 136, 137, 154, 289, 307 and in the case of glycerol the matrix peaks were at m/z

values of 93 and 185. For the metal complexes, the peaks always showed isotropic distribution.

3.1.3 Synthesis of the cryptand, L^1

The synthesis of the cryptand was achieved in two steps as illustrated in the Fig. 3.1. The Schiff base precursor (hereafter $L^{1'}$) was synthesised by [2+3] condensation of tren with glyoxal in presence of Rb(I) or Cs(I) ion. The alkali metal ion brings together the reactive groups which then undergo facile condensation reaction leading to the desired product in appreciable yields. However, the alkali metal ion gets trapped inside the cryptand during its synthesis. Using a transition metal ion as the template do not give the desired Schiff-base. Only a mixture of indefinite composition is obtained.

3.1.3a Synthesis of $[L^{1'} \subset Rb]Cl$, 1

Tren (0.73 g; 5 mmol) and CsCl (0.42g; 2.5 mmol) were dissolved in methanol (500 ml). To this stirred solution at 50°C, was dropwise added a solution of glyoxal (0.44g; 7.5 mmol) in methanol (200 ml) over a period of 8 hr. After the addition was complete, the resulting solution was stirred at 65°C for a further 8 hr period. The resulting light yellow solution was

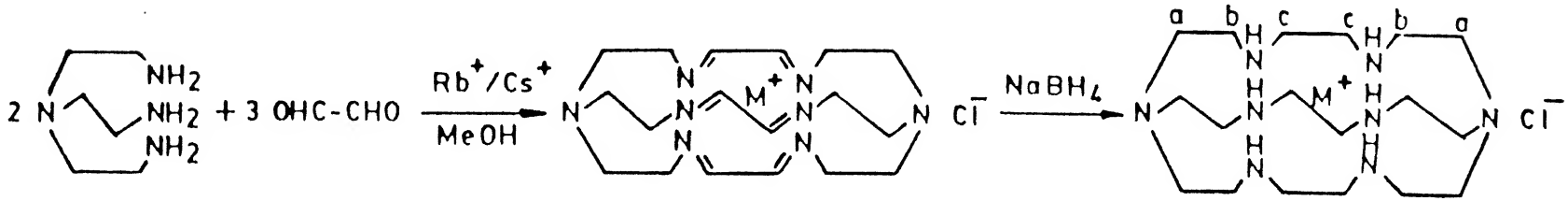

Fig. 3.1 Synthetic scheme for the ligand, **L1**

cooled to room temperature, decolourised with activated charcoal and the volume reduced to 10 ml in a rotary evaporator. The solution was kept in a dessicator, over concentrated H_2SO_4, when **1** was obtained as a colorless microcrystalline solid. Yield 60%. IR(KBr): A strong peak at 1650 cm^{-1} is obtained corresponding to the imine linkages [83]. The Schiff base turns yellow in air in two days due to decomposition.

3.1.3b **Synthesis of** $[L^1_C Rb]PF_6$, **2**

The compound **1** (0.48 g; 1 mmol) was dissolved in methanol (100 ml) and to this solution, excess $NaBH_4$ (0.50 g) was added and refluxed for 4 hr. After the reflux was over, methanol was completely removed. To the resulting solid distilled water (20 ml) was added and warmed. Then water was completely removed and the resulting residue was extracted with dry CH_3CN (3 x 25 ml). On evaporation of the CH_3CN a gummy mass was obtained. This was dissolved in water (10 ml) and to this, NH_4PF_6 (0.1 g; 1 mmol) was added, stirred for 10 minutes and the solution was filtered. On slow evaporation, colorless needles were obtained in 85% yield. m.pt. 125-127^oC.

IR (KBr): Two strong peaks at 850 and 565 cm^{-1} due [84] to anionic (PF_6) was observed. The imine peak was absent (Fig.

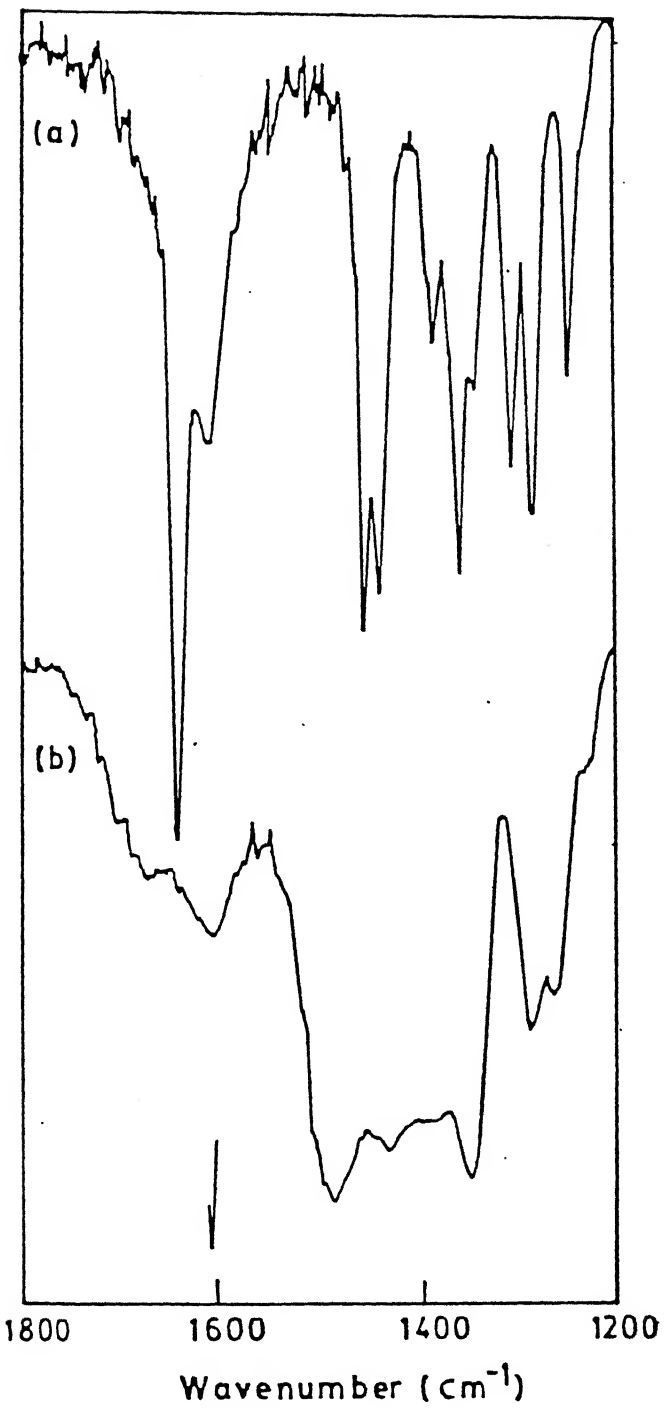

Fig. 3.2 Infrared spectra of the ligands in the region, 1200-1800 cm^{-1}; (a) $L^{1'}$ (b) L^{1}

3.2).

^{1}H-NMR (400 MHz, D_2O, ppm): 4.8 (s, HOD); 3.21 (s, 12H, H^c); 3.02 (s br, 12H, H^b) and 2.7 (s br, 12H, H^a). Designation of the protons are shown in the Fig. 3.1.Spectrum is shown in Fig. 3.3.

3.1.3c Synthesis of $[L^1 \subset Cs]Cl$, 3

This was prepared by following the above procedure using CsCl instead of RbCl. Yield 55% (overall).

^{1}H-NMR (400 MHz, D_2O, ppm): 4.8 (s, HOD); 3.19 (s, 12H, H^c); 3.09 (s br, 12H, H^b) and 2.7 (s br, 12H, H^a).

3.1.4 Transmetallation Studies

Transmetallation studies were done with the complex, 3 or its rubidium analogue.

3.1.4a Synthesis of $[L^1 \subset Zn(II)_2](NO_3)_4$, 4

To a solution of 3 (0.24 g; 0.5 mmol) in methanol (15 ml) was added $[Zn(H_2O)_4](NO_3)_2$ (0.26 g; 1 mmol) in methanol (10 ml) and refluxed for 30 minutes. Then the solution was filtered and the filtrate allowed to evaporate at room temperature. The colorless solid thus obtained was collected by filtration and recrystallized from acetonitrile. Yield 35%.

^{1}H-NMR (400 MHz, D_2O, ppm); 4.8 (s br, HOD); 3.59 (s, 12H, H^c); 3.30 (s br, 12H, H^b) and 2.85 (s br, 12H, H^a).(Fig. 3.4).

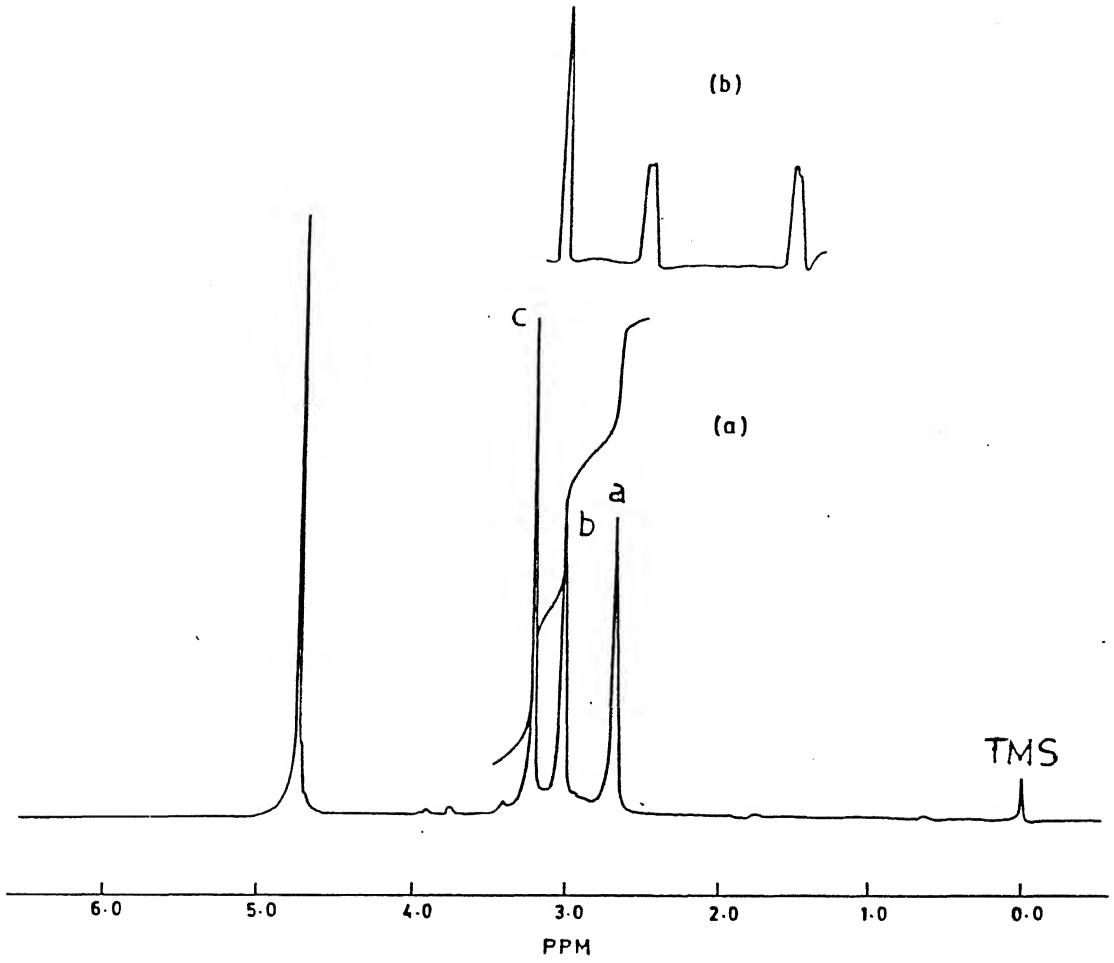

Fig. 3.3 400 MHz ^{1}H-NMR spectrum of **2**; (a) the entire spectrum (b) resonance enhanced spectrum in the region 2.6-3.3 ppm

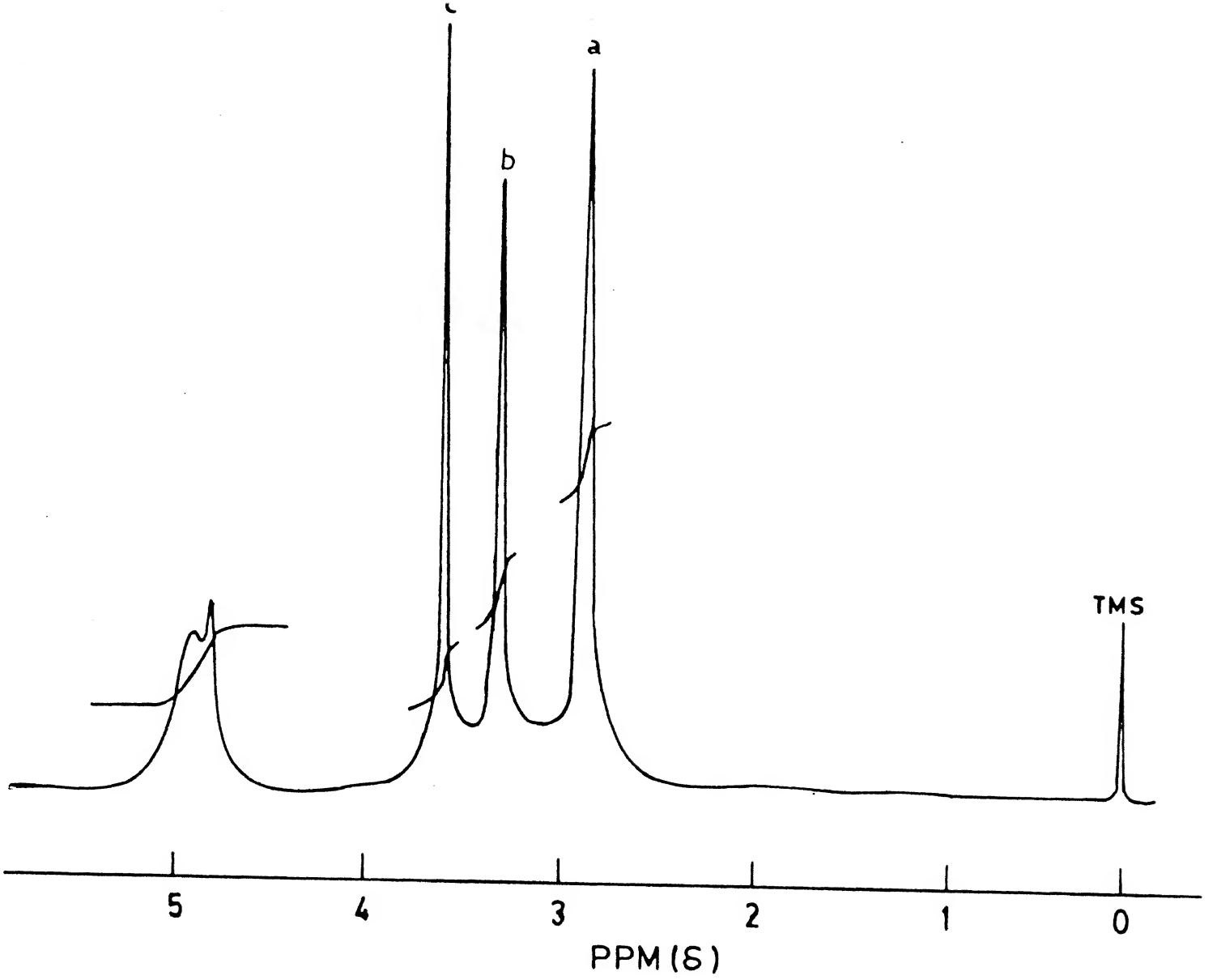

Fig. 3.4 400 MHz ^{1}H-NMR spectrum of **4**

3.1.4b Synthesis of $[L^1_{\subset} Cu(II)_2(ClO_4)](ClO_4)_3$, 5

$[Cu(H_2O)_6](ClO_4)_2$ (1.1 g; 3 mmol) dissolved in methanol (50 ml) was added dropwise to a warm solution (40°C) of 3 (0.51 g; 1 mmol) in methanol (250 ml). After the addition was over, the resulting blue solution was allowed to reflux for 30 min and then cooled to room temperature. The blue microcrystalline solid that separated was collected by filtration and washed with dry methanol (30 ml). Yield 72%.

3.1.4c Synthesis of $[L^1_{\subset} Cu](ClO_4)_2$, 6

$[Cu(H_2O)_6](ClO_4)_2$ (0.37 g; 1 mmol) dissolved in methanol (10 ml) was added dropwise to a solution of 3 (0.51 g; 1 mmol) in methanol (50 ml) and after stirring for 30 minutes filtered. The filtrate on slow evaporation afforded a greenish blue solid which was collected and washed with cold methanol (10 ml) and air-dried. Yield 72%.

The FAB-mass spectrum of **6** showed three prominent peaks around m/z 632, 532 and 431, which were due to the molecular ion, liberation of one and two perchlorate ions respectively. The FAB-mass spectrum is shown in Fig. 3.5.

3.1.4d Synthesis of $[L^1_{\subset} Ni(II)](ClO_4)_2$, 7

To a solution of 3 (0.26 g; 0.5 mmol) in methanol (25 ml)

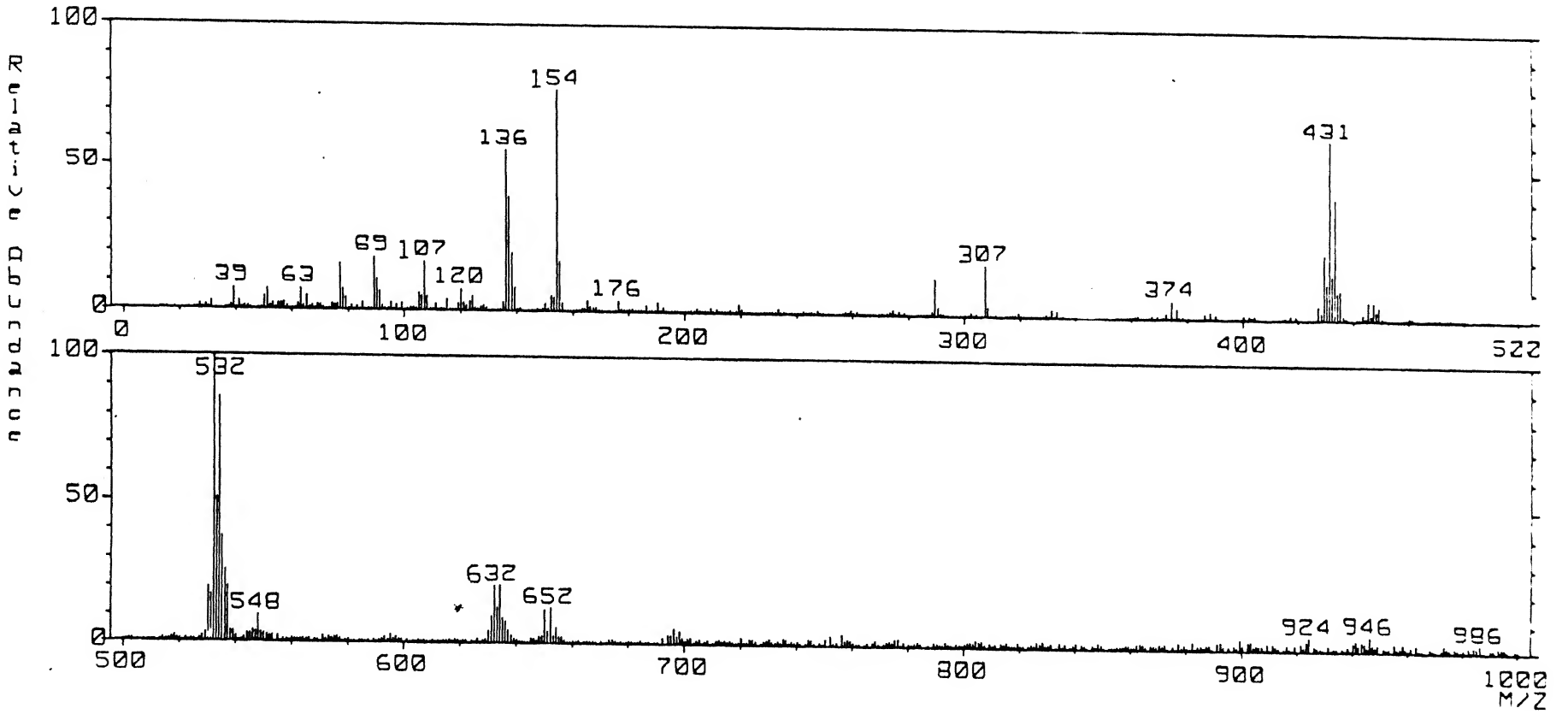

Fig. 3.5 FAB-mass spectrum of the cryptate, 6

was added a solution of $[Ni(H_2O)_6](ClO_4)_2$ (0.18 g; 0.5 mmol) in methanol (10 ml) and refluxed for an hour. After cooling to RT, the solution was filtered and allowed for slow evaporation which afforded the desired complex as a purple solid. The complex was recrystallized from CH_3CN. Yield 68%.

The FAB-mass spectrum of 7 showed three prominent peaks around m/z 625, 527 and 426, which were due to the molecular ion, liberation of one and two perchlorate ions respectively. The FAB-mass spectrum is shown in Fig. 3.6.

3.1.4e Synthesis of $[L^1_C Mn(II)](ClO_4)_2$, 8

Manganese (II) acetate tetrahydrate (0.25 g; 1 mmol) dissolved in methanol (10 ml) was added to 3 (0.51 g; 1 mmol) in methanol (20 ml) and refluxed for 90 min and the solution was then allowed to cool to room temperature. To this solution, sodium perchlorate monohydrate (0.24 g; 2 mmol) was added and stirred for 10 minutes. The almost colorless solid that crashed out was collected by filtration and recrystallized from dimethyl sulphoxide. Yield 80%.

The FAB-mass spectrum showed two prominent peaks around m/z 524 and 424 produced by the liberation of one and two perchlorate ions respectively. The spectrum is shown in Fig. 3.7.

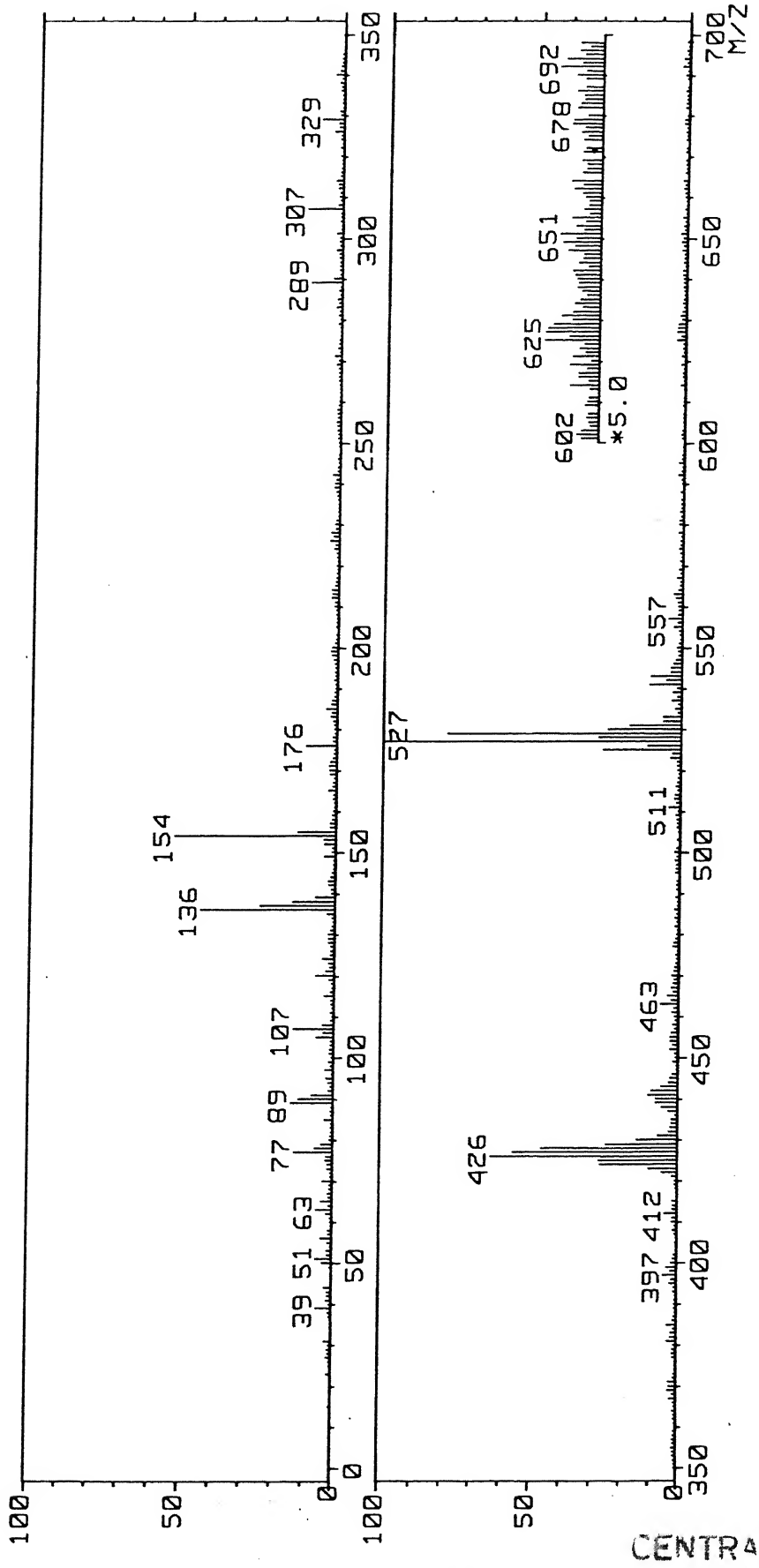

Fig. 3.6 FAB-mass spectrum of the cryptate, 7

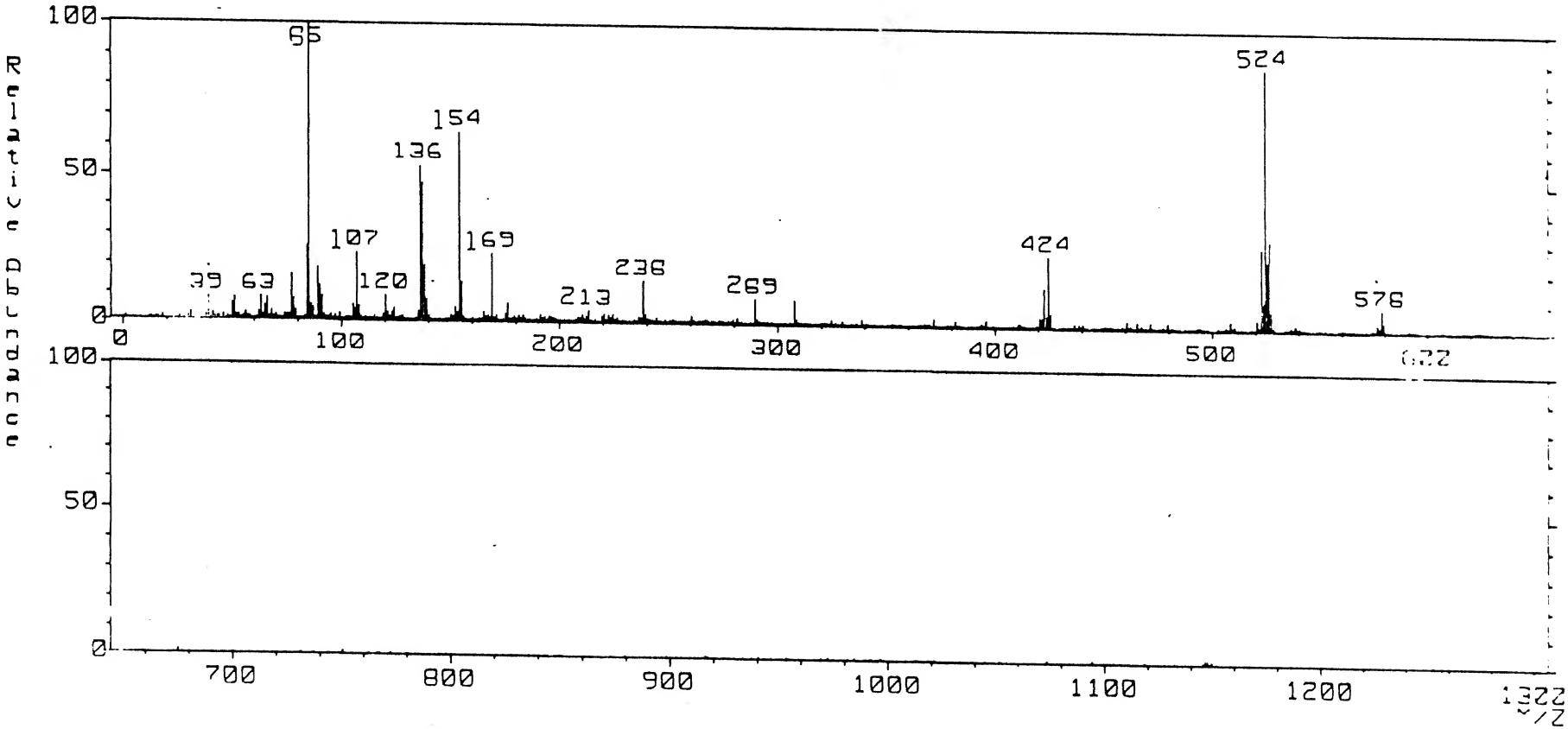

Fig. 3.7 FAB-mass spectrum of the cryptate, **8**

Analytical data for all the complexes are collected in Table 3.1.

3.2 Results and Discussion

3.2.1 Template action of Rb(I) or Cs(I) ion

Cs(I)/Rb(I) ion acts as the template in the preparation of the cryptand, L^1. In the process, the metal ion is trapped inside the cavity of the resulting cryptand. Like the structurally similar [2.2.2] cryptand [85] bearing the N_2O_6 donor set, the metal ion's radius and the cavity size match for the binding process.

The ^{1}H-NMR spectrum of Cs(I)/Rb(I) cryptate showed three equal intensity peaks (Fig. 3.3) for the three kinds of protons H^a, H^b and H^c (for designation of the protons refer to the Fig. 3.1) present in the molecule. This indicates that C_3 symmetry is present in the alkali metal cryptates. The peaks due to the protons H^a and H^b are broad and the resonance enhanced spectrum (Fig. 3.3) shows ill resolved triplets for these protons.

3.2.2 Transmetallation reactions

The alkali metal ion trapped inside the cavity can be readily displaced by the ions studied. In this way, both

mononuclear as well as dinuclear cryptates have been synthesised. Dinuclear cryptates have been obtained with Zn(II) and Cu(II) when the corresponding metal perchlorate salt and the alkali metal cryptate are refluxed in methanol in 1:2 molar ratio. Cu(II) also forms a mononuclear cryptate when allowed to react in 1:1 molar ratio at RT. Unlike the Cu(II) and Zn(II) ions, Ni(II) and Mn(II) ions always form mononuclear cryptates irrespective of the molar ratio of the reactants. In what follows, characterization of the individual metal cryptates by different physicochemical techniques are described..

3.2.3 $[L^1 \subset Zn(II)_2](ClO_4)_4$, 4

The molar conductivity of this complex was found to be 490 $ohm^{-1}cm^2mol^{-1}$ in CH_3CN at 295 K. While only a few conductivity data are available [86] for complexes other than 1:1 electrolytes in acetonitrile, a value of above 450 $ohm^{-1}cm^2mol^{-1}$ has been attributed [86] as the average value for 1:4 electrolytes. As complexes of zinc(II) do not have diagnostic electronic spectral bands, it is not possible in the absence of a single-crystal X-ray diffraction study to establish firmly whether the metal ions are inside or outside the cavity of the cryptand. We have not been able to grow suitable single crystals of this compound but

in the X-ray crystal structure of a related mixed dinuclear copper(II)-zinc(II) complex [87], the Zn(II) ion is bound to four nitrogens of a tren ligand. Also, solution studies [88] of Zn(II)-tren systems indicate that Zn(II) may be coordinated to the four nitrogens of the tren ligand. If the two Zn(II) ions are inside the cavity and each is bound to four nitrogens, then the proton NMR spectrum of the complex should be quite similar to that of the rubidium cryptate. This is found to be so with a slight downfield shifting of the three peaks observed (Fig. 3.4).

3.2.4 $[L^1 \subset Cu(II)_2(ClO_4)](ClO_4)_3$, 5

The dicopper complex , 5 is stable in air and soluble in common organic solvents as well as water. The molar conductivity of the dicopper complex in acetonitrile is found to be 370 $ohm^{-1}cm^2mol^{-1}$ at 298 K. A value of 380 ohm^{-1} cm^2 mol^{-1} has been attributed [86] as the average value for 1:3 electrolytes. In this case, therefore, the dicopper complex can be formulated as $[L^1 \subset Cu(II)_2(ClO_4)](ClO_4)_3$ with one perchlorate co-ordinated to copper(II) ion(s) in acetonitrile solution.

In the infrared spectrum of the complex, strong signals appear at 1143, 1116 and 1090 cm^{-1} besides moderately strong peaks at 1011, 996 and 818 cm^{-1}. The alkali-metal complex of the

ligand with chloride as counter ion does not absorb appreciably at these positions. It can be suggested, based on literature data [89,90] that both coordinated and uncoordinated perchlorates are present.

Two ligand-field and one ligand-to-metal charge-transfer (LMCT) transitions are observed in the electronic absorption spectrum of the complex in acetonitrile at 298 K (Table 3.2). The spectrum is shown in Fig. 3.8. The shape and position of the ligand-field bands remain almost unchanged in DMF at room temperature. The strong band at 280 nm is attributed [91] to a σ(N)---> Cu(II) LMCT transition. Of the two ligand-field bands, the stronger one appears at 750 nm while the weaker one appears at a higher energy (630 nm). A regular trigonal-bipyramidal CuN_5 chromophore usually gives two ligand-field transitions [92] in this region with greater absorption intensity for the lower energy transition although exceptions to this general observation are known [93]. The shapes of the ligand-field bands agree well with the complexes $[Cu(tren)X]^{n+}$ ($X = NCS^-$ or NH_3; $n = 1$ or 2) where the coordination geometry around copper is trigonal bipyramidal [94]. The present macrobicyclic ligand may be considered as consisting of two tren units separated by two carbon spacers (Fig. 3.1). Two copper ions can be easily fitted

into the macrobicycle and the fifth co-ordination site is possibly provided by a bridged perchlorate. For trigonal bipyramidal geometry the ground state orbital [92,94] is d_z2. The absorption at 750 nm is then due to the transition, d_{xy},$d_{x^2-y^2}$ ----> d_z2 which is allowed in C_3 or D_{3h} local symmetry and the less intense one at 630 nm is due to the d_{xz}, d_{yz} ---->d_z2 transition which is allowed in C_3 local symmetry only [94]. The relative intensities of the two bands are not very different which suggests [94a] that the effective local symmetry is lower than D_{3h}. The ligand-field bands are well separated from the charge-transfer band and so the high intesities of these transitions cannot be due to an intensity stealing mechanism [95]. However, if both the coppers are in a +2 oxidation state, the intensities are within the range found for trigonal-bipyramidal copper(II) complexes [94]. When this perchlorate complex is treated with six equivalents of sodium azide, the colour of the solution slowly changes to green at 296 K. After 4 hr, the two ligand-field bands are replaced by a very broad signal (Fig. 3.9; Table 3.2) similar to that for $[Ag(Cu(NH_3)_2(SCN)_3)]$ in which the co-ordination geometry around Cu(II) is trigonal bipyramidal [96a]. Also a new band appears at

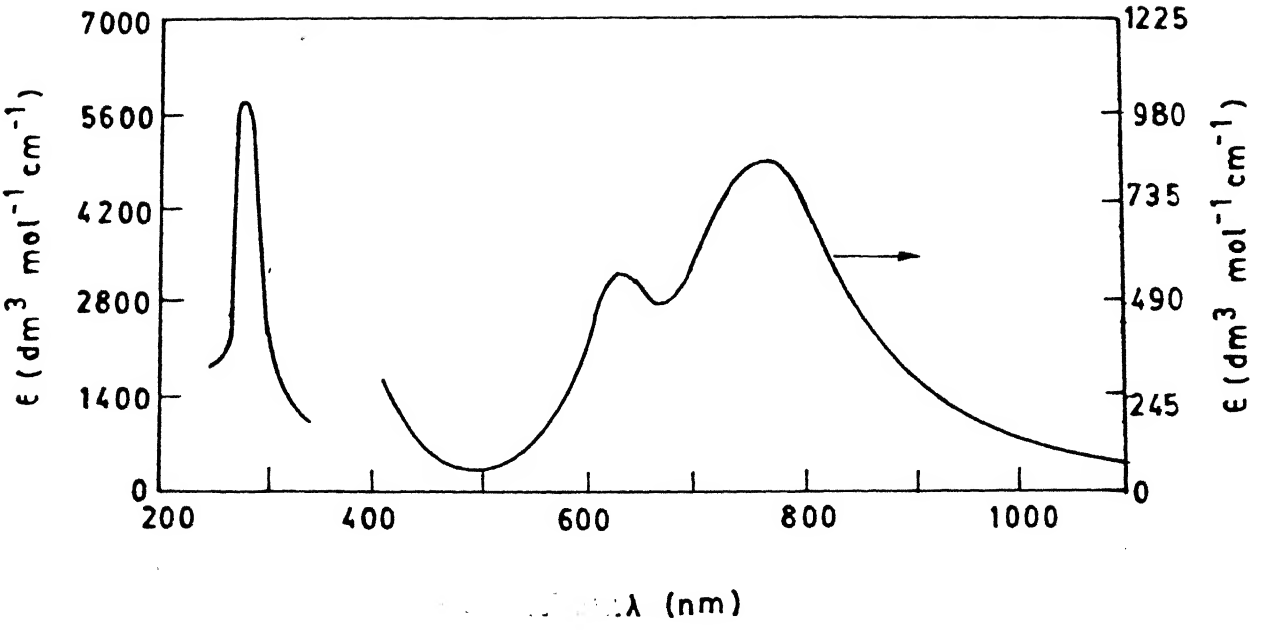

Fig. 3.8 Electronic absorption spectrum of the cryptate, **5** in acetonitrile

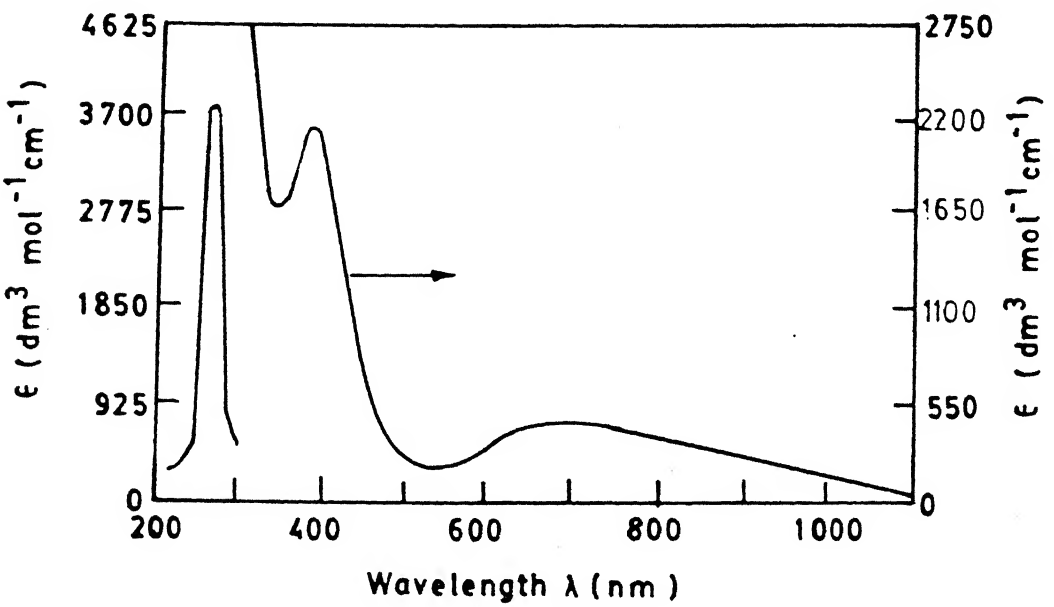

Fig. 3.9 Electronic absorption spectrum of the cryptate, **5** in acetonitrile taken 4 hr after the azide treatment

380 nm suggestive of azide co-ordination [48,96b,c].

The effective magnetic moment value for the dicopper complex after applying diamagnetic corrections, is found to be 1.61 (μ_{eff}/μ_B) at 303 K per copper which is slightly lower than for discrete monomeric copper(II) complexes [96] and can be attributed to the existence of a weak antiferromagnetic interaction between the two copper(II) ions in the complex.

The EPR spectral data of the complex are given in Table 3.3. The EPR spectrum in the solid state displays a broad signal (Fig. 3.10) centred near g_{av}= 2 at room temperature with a very weak signal at g = 4 observed only at high power. The signal near g_{av}= 2 becomes more asymmetric upon cooling to liquid-nitrogen temperature (77 K) as shown in Fig 3.10. The signal near g = 4 could not be observed due to poor signal:noise ratio at high power. The solid-state spectrum is typical of magnetically concentrated copper(II) dimeric complexes [92a] and is not indicative of the solid-state stereochemistry. In the solution phase, the shape of the spectrum depends upon the solvent. At room temperature in acetonitrile, a seven-line spectrum centred at g_{av}= 2 is observed which coalesces to a symmetric absorption at 77 K (Fig. 3.11). The A_{av} value is found to be about 74 x 10^{-4} cm^{-1}. A seven-line spectrum at room temperature near g = 2 with

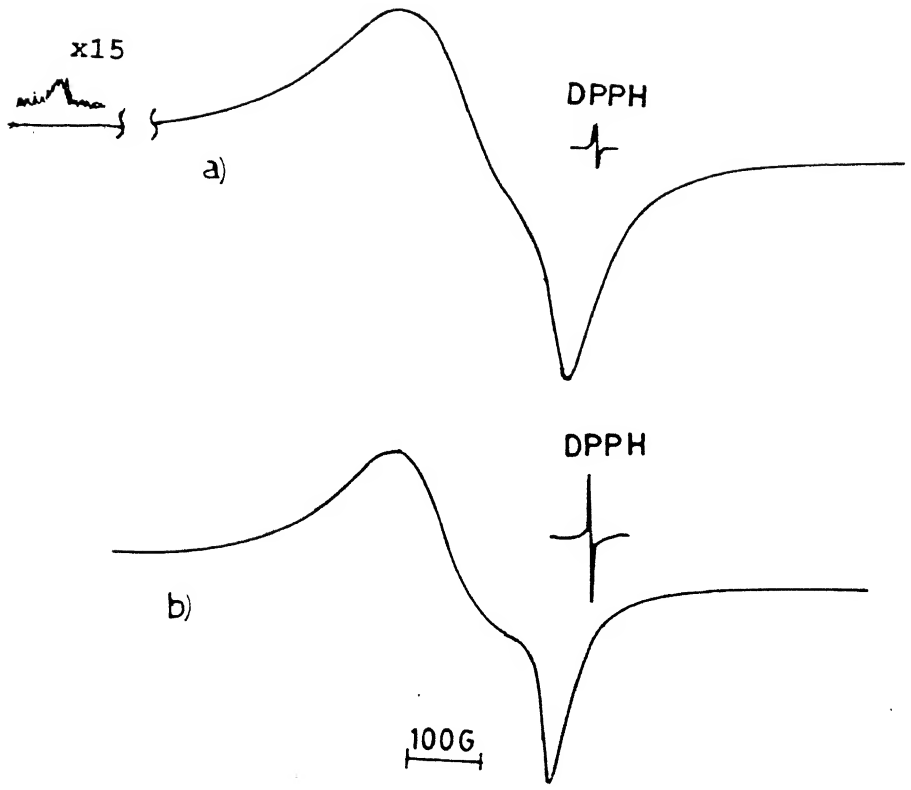

Fig. 3.10 Solid state EPR spectra of 5 at (a) 298 K and (b) 77 K

-1 is also observed in DMF medium which at 77 K,
ven-line spectrum (Fig. 3.11) with an increased
103 x 10^{-4} cm^{-1}). The weak signal at g=4 is not
ion. The EPR data can be explained as follows:
s are in a +2 oxidation state and owing to poor
ly a very weak interaction (2J ---> 0) exists
ons. In this situation, the dominant mechanism
e EPR spectrum is the dipolar interaction [97]
between the two Cu(II) ions. This splits the $\Delta M_s = \pm 1$ transition at $g_{av} = 2$ and the $\Delta M_s = \pm 2$ transition at g = 4 appears as a weak signal. In acetonitrile solution, the seven-line spectrum is replaced by a broad signal at $g_{av} = 2$ at low temperature apparently due to structural changes upon cooling. Hunter et. al. [70] reported a seven-line spectrum for the dicopper Schiff-base complex in DMF as due to the presence of a single electron delocalised over the two copper centres. This would suggest a mixed-valence Cu(I)Cu(II) species despite the formulation of the complex as $[Cu_2L^1(ClO_4)_4]$. These authors do not report any signal near g = 4, nor do they report the spectra in acetonitrile solution. Reports are available describing multi-line EPR spectra and a six-line spectrum was obtained [93] for the complex

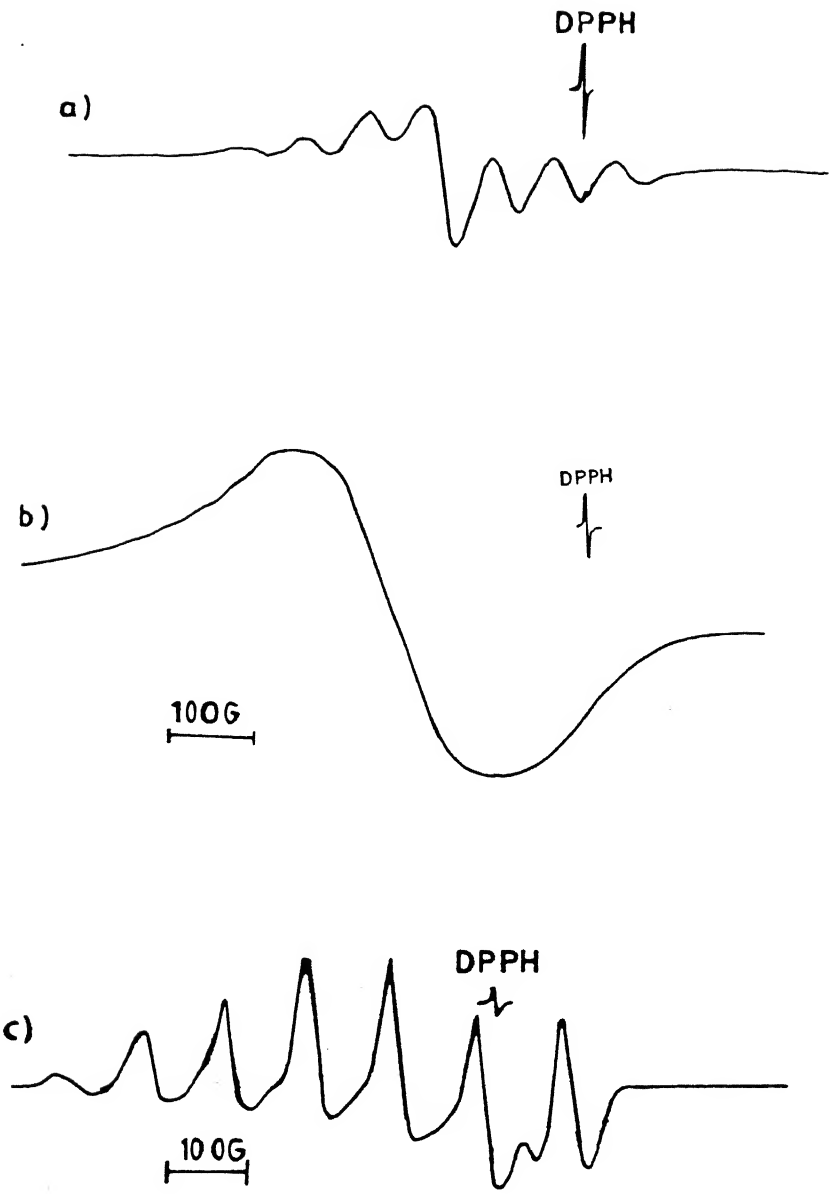

Fig. 3.11 Solution EPR spectra of **5**; (a) in MeCN at 298 K (b) in MeCN at 77 K (c) in DMF at 77 K

$[Cu(ntb)I]BF_4.2MeOH.4H_2O$ [ntb = tris(2-benzimidazolylmethyl)amine] at 77 K. A similar observation was made [98] in case of polycrystalline $[Cu(N\text{-}CH_2CH_2NMe_2)_3]I]I$ doped into the isomorphous zinc salt where the shape of the spectrum persists up to 133 K. The spectra were rationalised by presuming some overlap of two sets of resonances from two Cu(II) centres with slightly different stereochemistries. It is obvious, however, that only an X-ray structural analysis of the dicopper complex can provide a clearer picture of the structure and bonding. On addition of azide to the dicopper cryptate, the EPR signal vanishes.

Cyclic voltammetry of this complex at 298 K in acetonitrile (**ca.** 1×10^{-3} mol dm^{-3}) show two anodic responses at +1.2 and +1.3V but no cathodic peak is found on scan reversal. When the voltage scan on the negative side is probed, two cathodic peaks, at -0.6 and -1.6 V are observed. However, on scan reversal, only a sharp peak appears at about -0.2 V attributable to the oxidation of copper deposited on the electrode. Similar observations have been made [99] on other Cu(II)-systems. An analysis of the cyclic voltammetric study is complicated due to the irreversibility of the electrode processes.

3.2.5 $[L^1 \subset Cu(II)](ClO_4)_2$, 6

The FAB-mass spectrum (Fig. 3.5) gives a clear evidence for the formation of the mononuclear Cu(II)-cryptate. The base peak at m/z = 632 with isotropic distribution corresponds to the ion, $[L^1 Cu(II)](ClO_4)]^+$. The conductivity value of 242 $ohm^{-1}cm^2mol^{-1}$ in acetonitrile corresponds [86] to the 1:2 electrolytic nature of this complex. The infrared spectrum showed a strong and broad band centered at 1100 cm^{-1} attributable [100] to the presence of the ionic perchlorates.

The electronic spectrum (Fig. 3.12) of this cryptate is consistent with a distorted octahedral CuN_6 chromophore [101]. It shows two broad d-d bands at 802 and 669 nm and one LMCT band at 278 nm (Table 3.2). The charge transfer band at 278 nm is attributable [91] to the σ(N)---> Cu(II) transition. The Cu(II) ion is present here at the middle of the cavity bonded to six nitrogens in a distorted octahedral geometry. This gives rise [101] to two d-d bands: the lower energy band is due to the transition, d_z2 --->$d_{x^2-y^2}$ while the higher energy band is due to the transitions, d_{xy} ----> $d_{x^2-y^2}$ and d_{xz},d_{yz} ----> $d_{x^2-y^2}$. The ligand field bands in this complex and in 5, show appreciable differences (Table 3.2). On this basis, the coordination geometry around Cu(II) for the two cases are likely to be different. The

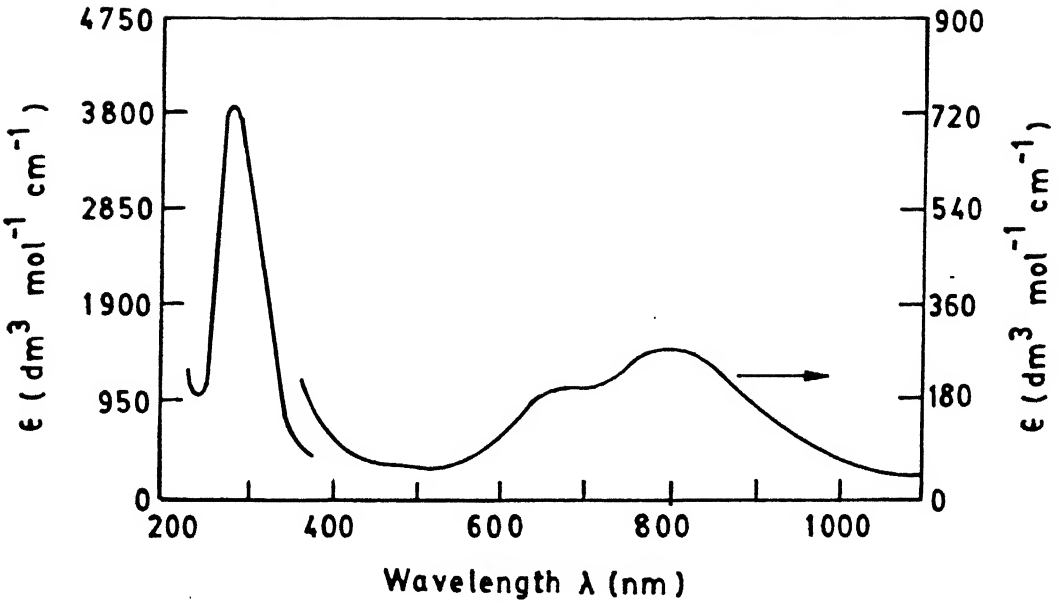

Fig. 3.12 Electronic absorption spectrum of **6** in acetonitrile

mononuclear Cu(II) cryptate of the corresponding Schiff base analogue of the cryptand, L^1, gives only one broad ligand field band [70].

The EPR spectral data of this complex are provided in Table 3.3. The EPR spectra of the cryptate in solid state do not give any information about the geometrical feature of the Cu(II) ion. A broad band at g_{av} = 2.09 (at 298 K and 77 K) is obtained (Fig.3.13). The 298 K solution spectrum of the cryptate in CH_3CN shows a rhombic signal with g values of 2.19, 2.14 and 2.06, due to the distorted environment around the Cu(II) ion. The g_z region showed ill-resolved hyperfine coupling (A_z = 70 x $10^{-4}cm^{-1}$). At 77 K the spectrum changes to an axial type (Fig. 3.13) with $g_{\parallel}$ = 2.26 and $g_{\perp}$ = 2.13 with $A_{\parallel}$ = 65 x 10^{-4} cm^{-1}, indicating a tetragonal geometry for the Cu(II) ion. However, the $A_{\parallel}$ value is quite small compared to typical tetragonal complexes [102]. A distortion of the coordination geometry away from tetragonal symmetry leads [103] to smaller value of $A_{\parallel}$. The room-temperature effective magnetic moment of 1.92 (μ_{eff}/μ_B) is in agreement with a discrete mononuclear Cu(II) complex [104].

Cyclic voltammetric experiments on this cryptate are

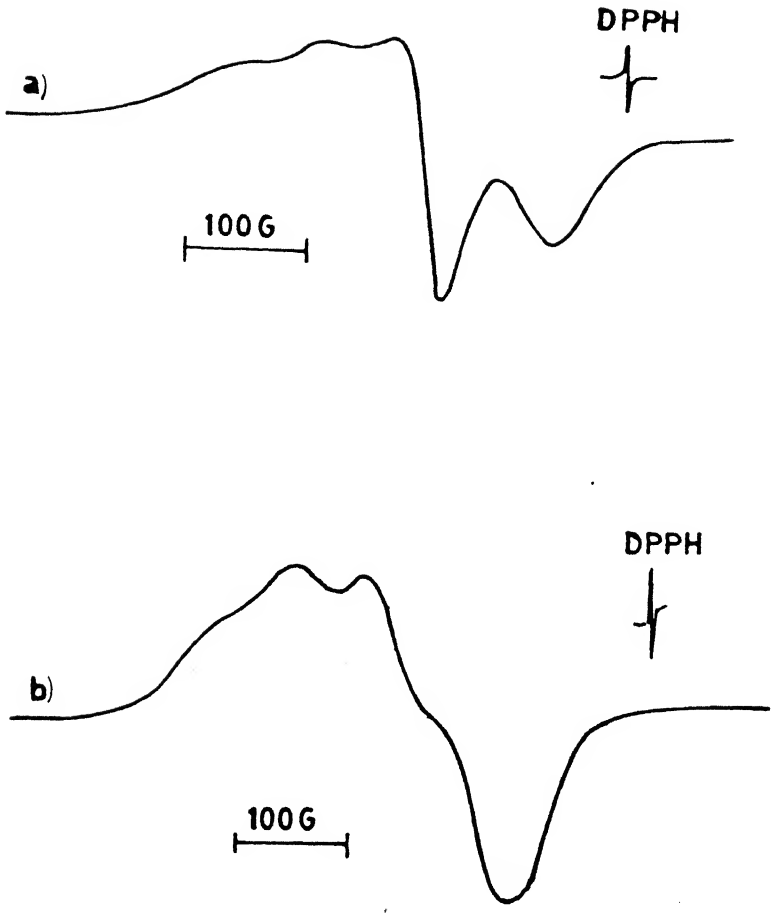

Fig. 3.13 EPR spectrum in acetonitrile of the cryptate, **6**;
(a) at 298 K (b) at 77 K

side, no well-defined peak can be observed upto +1.64 V. However, on scanning in the negative side, two cathodic peaks occur at -0.7 and 1.4 V, although the corresponding anodic peaks are absent. Instead, a sharp and strong anodic peak at -0.2 V appears which is attributable [99] to the oxidation of metallic copper deposited on the electrode surface. Thus, electrochemically generated reduced products decompose instantaneously.

3.2.6 $[L^1 \subset Ni(II)](ClO_4)_2$, 7

FAB-mass spectrum shows the base peak due to the ion, $\{[L^1 Ni](ClO_4)\}^+$. Conductivity data in acetonitrile (242 $ohm^{-1}cm^2mol^{-1}$) is consistent [86] with the formulation, $[L^1 \subset Ni](ClO_4)_2$. The cryptate formed with the Ni(II) ion is found to be always mononuclear, irrespective of the concentration of the metal ion used unlike in the case of Cu(II).

The infrared spectrum of 7 shows a strong and broad peak centering around 1100 cm^{-1} attributable to the ionic perchlorates [100].

The room temperature (299 K) effective magnetic moment of 2.82 (μ_{eff}/μ_B) indicates the metal ion is present in near octahedral geometry [104] ruling out the possibility of square planar or tetrahedral geometry.

The electronic spectrum of this cryptate is shown in Fig. 3.14 while the data are given in Table 3.2. The spectrum in DMF showed three low intensity (ϵ_{max} < 40 $dm^3 mol^{-1} cm^{-1}$) bands at 983, 573 and 346 nm and an medium intensity band (ϵ_{max} = 480 $dm^3 mol^{-1} cm^{-1}$) at 273 nm. The 273 nm band, being too high in energy to be a ligand field band, is assigned to σN--->Ni(II) LMCT transition comparing with the mononuclear Cu(II)-cryptate. A regular octahedral Ni(II) complex shows [105] three spin allowed transitions with intensities less than 30 $dm^3 mol^{-1} cm^{-1}$. Distortion from regular octahedral geometry is reflected by the intensities and sometimes by the splitting of these bands. Here, the Ni(II) ion is present in a very slightly different stereochemistry from octahedral as reflected by the intensities of the three ligand field bands. The bands can be assigned to the transition originating from the $^3A_{2g}$ ground state to the three excited states $^3T_{2g}$, $^3T_{1g}$ and $^3T_{1g}(P)$.

3.2.7 $[L^1_C Mn(II)](ClO_4)_2$, 8

This cryptate is air-stable and soluble only in DMSO. The FAB-mass spectrum of the complex shows (Fig. 3.7) a strong peak at m/z 524 with isotropic distribution corresponding to the -mono cation, $\{[L^1_C Mn(II)](ClO_4)\}^+$. The molar electrical conductivity

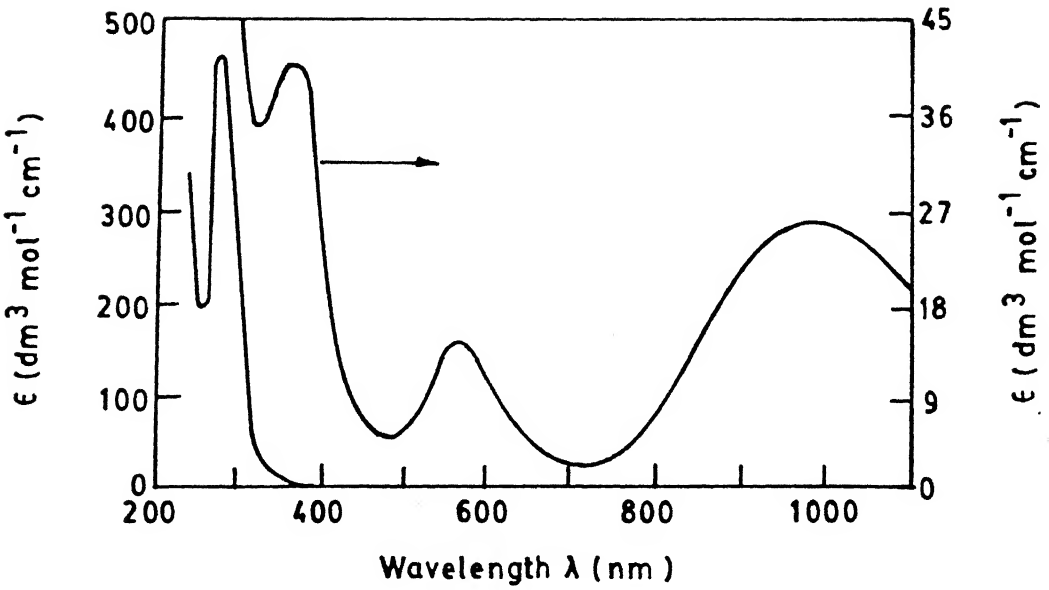

Fig. 3.14 Electronic absorption spectrum of the cryptate, **7** in DMF

of the cryptate in DMSO is found to be 140 $ohm^{-1}mol^{-1}cm^{2}$ corresponding to a 1:2 electrolyte [86].

The infrared spectrum of 8 shows a strong and broad peak near 1100 cm^{-1} attributable to the presence of the ionic perchlorates [100].

The electronic spectrum of the cryptate in DMSO gives an extremely low intensity (ϵ_{max} = 3 $dm^{3}mol^{-1}cm^{-1}$) band centering at about 850 nm. The ligand field transitions in a high spin d^{5} system (S=5/2) are both parity and spin forbidden [106]. This explains the extremely weak ligand field band for this Mn(II)-cryptate. In the solid state, the cryptate is pale pink in color in bulk quantities. The charge transfer transitions could not be located due to interference from the solvent.

The room temperature (301 K) effective magnetic moment (μ_{eff}/μ_{B}) is 5.69 corresponding to a high spin (S=5/2) Mn(II) complex [104].

The EPR spectrum of the cryptate is shown in Fig 3.15 while the data are given in Table 3.3. The spectrum in the solid state, at 298 K, gave an anisotropic signal with the g values : g_1 = 2.4 , g_2 = 1.9 and g_3 = 1.6 . The anisotropic g valus suggest [107] that the symmetry around Mn(II) is lower than cubic. The 298 K solution spectrum shows a charateristic [107]

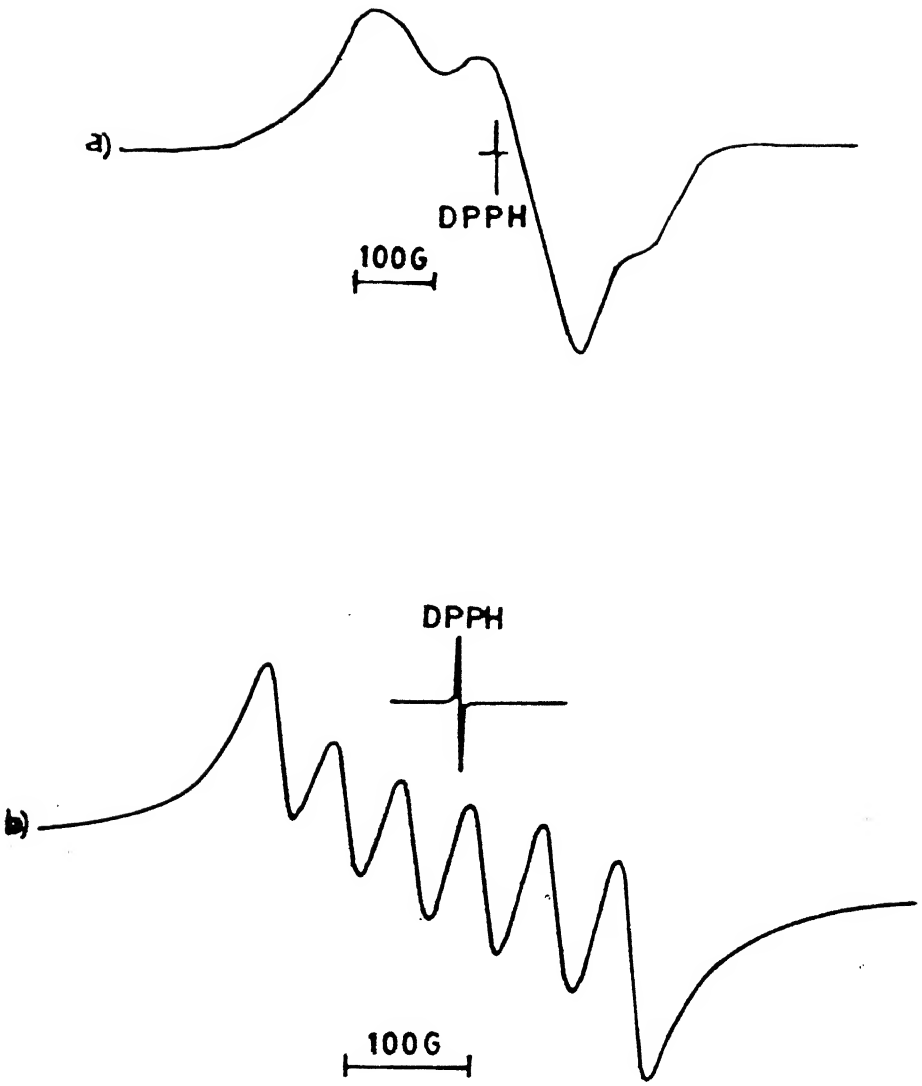

Fig. 3.15 EPR Spectra of the cryptate, **8** at 298 K;

(a) solid-state (b) in DMSO

six-line pattern centering at g = 2.01. The spectrum of the cryptate in DMSO glass (at 77 K) is very similar to the solid state spectrum at 298 K.

The cyclic voltammogram of the cryptate in DMSO shows an irreversible cathodic peak at -0.75 V in the negative voltage scan. When the voltage scan is done in the positive direction an irreversible anodic peak appears at +1.0 V. Thus, both reduced and oxidised states undergo rapid decomposition.

3.3 Conclusion

The results discussed above indicate clearly that the octaazamacrobicycle can be synthesized in high yields using Rb(I) or Cs(I) ion as the template. The cryptand shows different recognition sites for different metal ions. For Cu(II) and Zn(II) ions, which readily form four-coordinate complexes, the recognition sites are at the two ends of the cavity that provide N_4 donor sets. In contrast, Ni(II) as well as Mn(II) recognize the middle of the cavity forming hexadentate cryptates with the MN_6 chromophore. However, Cu(II) can form hexadentate CuN_6 cryptate as well.

Table 3.1 Elemental Analyses of the Complexes

Cryptate	Analysis (%)					
	Found			Calcd		
	C	H	N	C	H	N
2	35.25	7.2	19.5	35.95	7.05	18.65
3	39.96	7.63	20.35	40.10	7.85	20.78
4	28.60	5.70	21.95	28.85	5.65	22.4
5	23.95	4.65	12.60	24.15	4.75	12.50
6	34.45	6.71	17.32	34.13	6.68	17.69
7	34.82	6.13	17.52	34.39	6.73	17.83
8	34.10	6.52	18.34	34.60	6.78	17.93

Table 3.2 Electronic Absorption Spectral Data of the Complexes

Cryptate	λ_{max}/nm	ϵ_{max}/dm^3 mol^{-1} cm^{-1}	Assignment
5	750	880	d_{xy}, $d_{x^2-y^2}$ ----> d_{z^2}
	630	590	d_{xz}, d_{yz} ----> d_{z^2}
	280	5570	σ(N) ---> Cu(II) LMCT
5'*	680(br)	500	$d_{x^2-y^2}$, d_{xy} ----> d_{z^2} d_{xz}, d_{yz} ----> d_{z^2}
	380	2150	N_3^- -----> Cu(II) LMCT
	280	3820	σ(N) -----> Cu(II) LMCT
6	802	280	d_{z^2} -----> $d_{x^2-y^2}$
	669	210	d_{xy}, d_{xz}, d_{yz} ----> $d_{x^2-y^2}$
	278	3800	σ(N)-----> Cu(II) LMCT
7	983	26	$^3A_{2g}$ -----> $^3T_{2g}$
	573	18	$^3A_{2g}$ -----> $^3T_{1g}$
	346	40	$^3A_{2g}$ -----> $^3T_{1g}$(P)
	273	480	σ(N)-----> Ni(II) LMCT

* 5' is the dicopper cryptate after treatment with sodium azide. The spectrum recorded after 4 hr. No further change in the spectrum was observed after 4 hr.

Table 3.3 EPR Spectral Data of the Cryptates 5, 6 and 8

Cryptate	g_{av}	A^{Cu}_{av}	g_1	g_2	g_3	$A^{Cu}_{\parallel}$	
5	2.08						(298 K solid sample)
	4.09*						
	2.08						(77 K solid sample)
	2.10	74					(298 K in MeCN)
	7 lines						
	2.09						(77 K in MeCN)
6	2.09						(298 K solid sample)
	2.09						(77 K solid sample)
			2.19	2.14	2.06	70	(298 K in MeCN)
				$g_{\perp}$=2.13; $g_{\parallel}$=2.26		65	(77 K in MeCN)
8			2.4	1.9	1.6		(298 K solid sample)
	2.01	96					(298 K in MeCN)
	6 lines						

* observable only at high gain

Unit for A^{Cu} is $cm^{-1} \times 10^{-4}$

CHAPTER 4

SYNTHESIS OF A MACROBICYCLIC CRYPTAND HAVING DISULFIDE LINKAGES AND ITS COMPLEXING ABILITIES TOWARDS Cu(II) AND Ni(II) IONS

Cryptands with more than one receptor sites provide systems to study polynuclear metal complexes [51,52,56,74]. Variation of ligand design can afford to give systems where the distances between metal ions can be varied easily [9]. In case of short distances between the metal ions, interactions between them can be probed. On the other hand, when the distance between the metal ions is significant, small substrates may be introduced between the two leading to its activation [53,55]. Multimetal centres are increasingly given attention [35] for their interesting magnetic properties and their role as catalysts in redox processes. Cryptands, besides providing multimetal pockets for the binding of metal ions, can also impose a coordination geometry onto metal ions owing to their inherent rigidity. Groups like a disulfide can lead to increased rigidity of the donor atoms of a cryptand. The ligand described in this chapter has a slipped ellipsoidal cavity as illustrated in Fig. 4.1. Two metal ions may enter the cavity to form dinuclear cryptates. The present cryptand is the

first known such molecule having three disulfide linkages incorporated in the rings. Metal-disulfide interactions have important bioinorganic relevance [77]. In the electron transfer reactions of metalloproteins, the metal disulphide interactions are believed to be involved [108]. The removal of excess copper, associated with Wilson's disease, by administering D-penicillamine is predicted [109] to involve copper-disulfide bond formation. Model studies on metal-disulfide interactions would be helpful to understand these phenomena. Reports are available [110] on the studies of Cu(I)-disulfide bonding. In contrast, Cu(II) [108,109,111] and Ni(II)-disulphide [112-114] interactions are only sporadically investigated. Also, detailed spectroscopic studies are absent on these systems. In recent years, other transition metal disulphide interactions have been reported [115-118]. All these involve multidentate ligands to enforce the disulfide interactions onto the metal ions. The present cryptand is synthesized using Cs(I) ion as the template by [2+3] Schiff base condensation of tren and diisobutyraldehyde disulfide followed by reduction with sodium borohydride. This cryptand has been treated with Cu(II) and Ni(II) salts in excess to isolate homo-dinuclear complexes.

4.1 Experimental Section

4.1.1 Materials

Reagent grade isobutyraldehyde, sulfurmonochloride, tris(2-aminoethyl) amine, CsCl, $[Cu(H_2O)_6]$ $(ClO_4)_2$, $[Ni(H_2O)_6]$ $(ClO_4)_2$ sodium borohydride and picric acid were from Aldrich. These were used as received. All the solvents were from SD Fine Chemicals and were purified prior to use following standard methods [81].

4.1.2 Measurements

Elemental analyses for C, H, N, and S were done at the Central Drug Research Institute, Lucknow, India. ^{13}C-NMR spectrum for the ligand was recorded in $CDCl_3$ first at 20.1 MHz using a Bruker WP 80 machine and further confirmed by recording at 100 MHz using a Bruker WM 400 spectrometer. All other physical measuremets were made as described in the section 3.1.2 in chapter 3.

4.1.3 Synthesis of the cryptand

The cryptand synthesis was achieved via several steps as illustrated in the Schematically in Fig. 4.1.

4.1.3a Preparation of diisobutyraldehyde disulfide

The diisobutyraldehyde disulphide was prepared by the

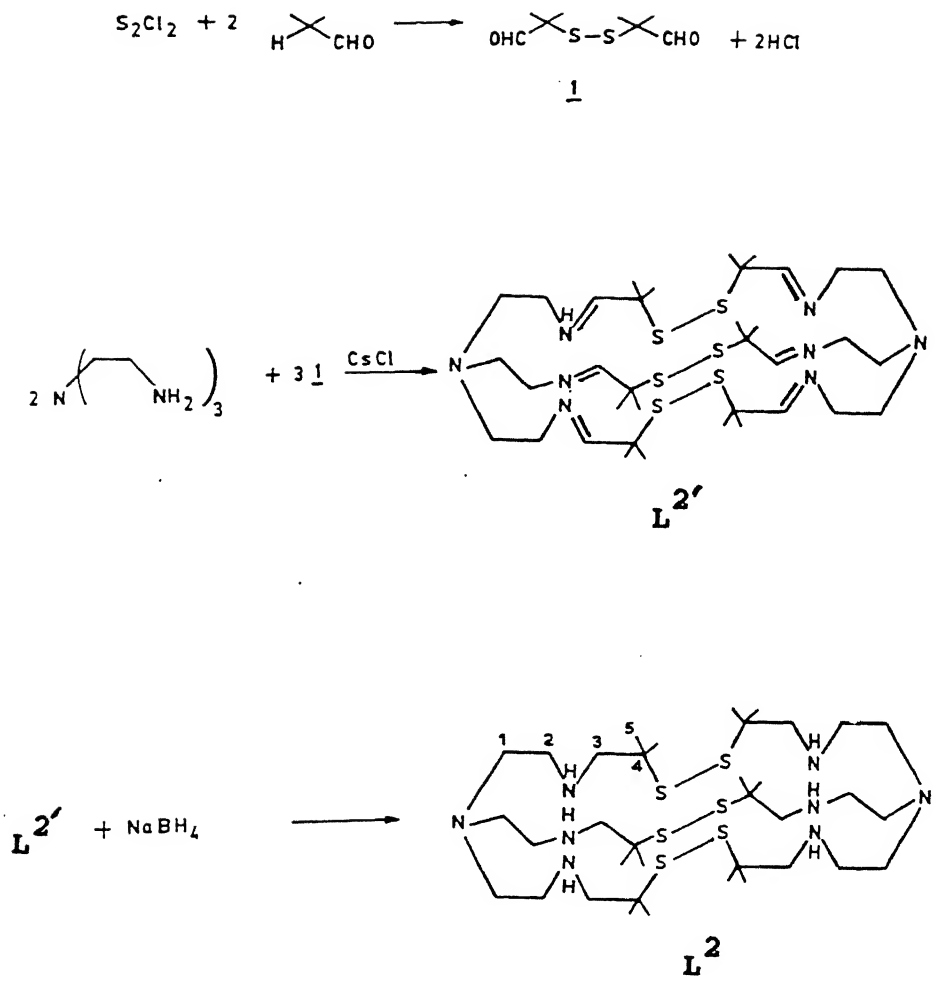

Fig. 4.1 Synthetic scheme for the cryptand, L^2

:hermally induced radical reaction between sulfur monochloride ınd isobutyraldehyde. The radical generated by the homolytic :leavage of the bond between sulfur and chlorine reacts with ısobutyraldehyde to give the diisobutyraldehyde disulfide. The reaction was performed following a modified literature procedure [119]. Freshly distilled isobutyraldehyde (5.8 g; 0.08 mol) was mixed with CCl_4 (15 ml) and warmed upto 40°C. To this warm solution, sulphur monochloride (5.4 g; 0.04 mol) in CCl_4 (15 ml) was added dropwise while stirring continuously. As soon as S_2Cl_2 comes into contact with isobutyraldehyde, copius evolution of HCl gas takes place which was driven out of the reaction vessel by occasional passage of nitrogen gas. Total addition time was 2 hr and the temperature of the reaction mixture was maintained at 40°C for another 48 hr, for completion of the reaction. After this period, CCl_4 was removed by distillation at low pressure and the resulting pale yellow thick liquid was washed several times with distilled water to remove dissolved HCl. Finally the desired product was obtained as a colorless liquid upon fractional distillation (15 mm; 90-100°C). Yield 80%.

^{1}H-NMR (80 MHz, $CDCl_3$,ppm) 1.4 (s, 12H, CH_3); 9.1 (s, 2H, CHO). The spectrum matches with the one reported [119].

4.1.3b Preparation of the Schiff base, L^2

Tris(2-aminoethyl)amine (0.73 g; 5 mmol) and CsCl (0.42 g; 2.5 mmol) were dissolved in 3% aqueous tetrahydrofuran (400 ml) by stirring and warming upto 40°C under an Argon atmosphere. To this stirred solution, was added a solution of diisobutyraldehyde disulphide (1.5 g;7.5 mmol) in tetrahydrofuran (150 ml) over a period of 6 hr and the resulting pale yellow solution was stirred at 40°C for a further 6hr. Then all THF was removed at low pressure to obtain a colorless solid which was found to be unstable and decomposed to yellow flakes in contact with air. However, it could be used to synthesize the dicopper(II) cryptate which was found to be stable in air although highly hygroscopic.

4.1.3c Reduction of the Schiff base to the cryptand, L^2

The Schiff base once formed was reduced <u>in situ</u> by refluxing with excess of $NaBH_4$. To the Schiff base formed in the above reaction, solid $NaBH_4$ (0.6 g) was added in portions over a period of 15 min at about 25°C. After the addition was complete, the solution was allowed to reflux for 8 hr. Then, tetrahydrofuran was completely removed at low pressure and excess $NaBH_4$ was decomposed by shaking the residue with 10 ml of water. The desired cryptand being insoluble in water formed oily droplets

which could be extracted with chloroform (2 x 50 ml). The crude ligand, L^2, obtained was finally purified by neutral alumina column. The major impurities were removed by eluting with $CHCl_3$. The pure product was eluted with the mixed solvent, $CHCl_3$ & MeOH (2:1 ratio by volume). Removal of the solvent gave a pale yellow oil in 52% yield. As reported [120,121] in the literature $NaBH_4$ did not cleave the disulfide bond as evidenced by the FAB-mass spectrum (Fig. 4.2) which shows the molecular ion peak at m/z 816 corresponding to the cryptand L^2.

^{1}H-NMR (400 MHz, $CDCl_3$, ppm), 1.35 (s, 36H, CH_3); 2.6 (t, 12H,1); 2.75 (overlapped t and s, 24H, 2 and 3). The spectrum is shown in Fig. 4.3.

^{13}C-NMR (100 MHz, $CDCl_3$, ppm) 27.5 (C 5), 47.5 (C 1); 49.6 (C 4); 53.0 (C 2); 59.1 (C 3). The spectrum is shown in Fig. 4.4. The atom numbers for both the ^{1}H-NMR and ^{13}C-NMR spectra are as shown in the Fig. 4.1.

FAB-mass: Found m/z = 816 $[L^2]^+$. Calculated for $C_{36}H_{78}N_8S_6$ is 815.46.

4.1.3d Hexa-picrate derivative of L^2

The picrate derivative was prepared to further characterize the cryptand. To a solution of L^2 (0.20 g; 0.25 mmol) in

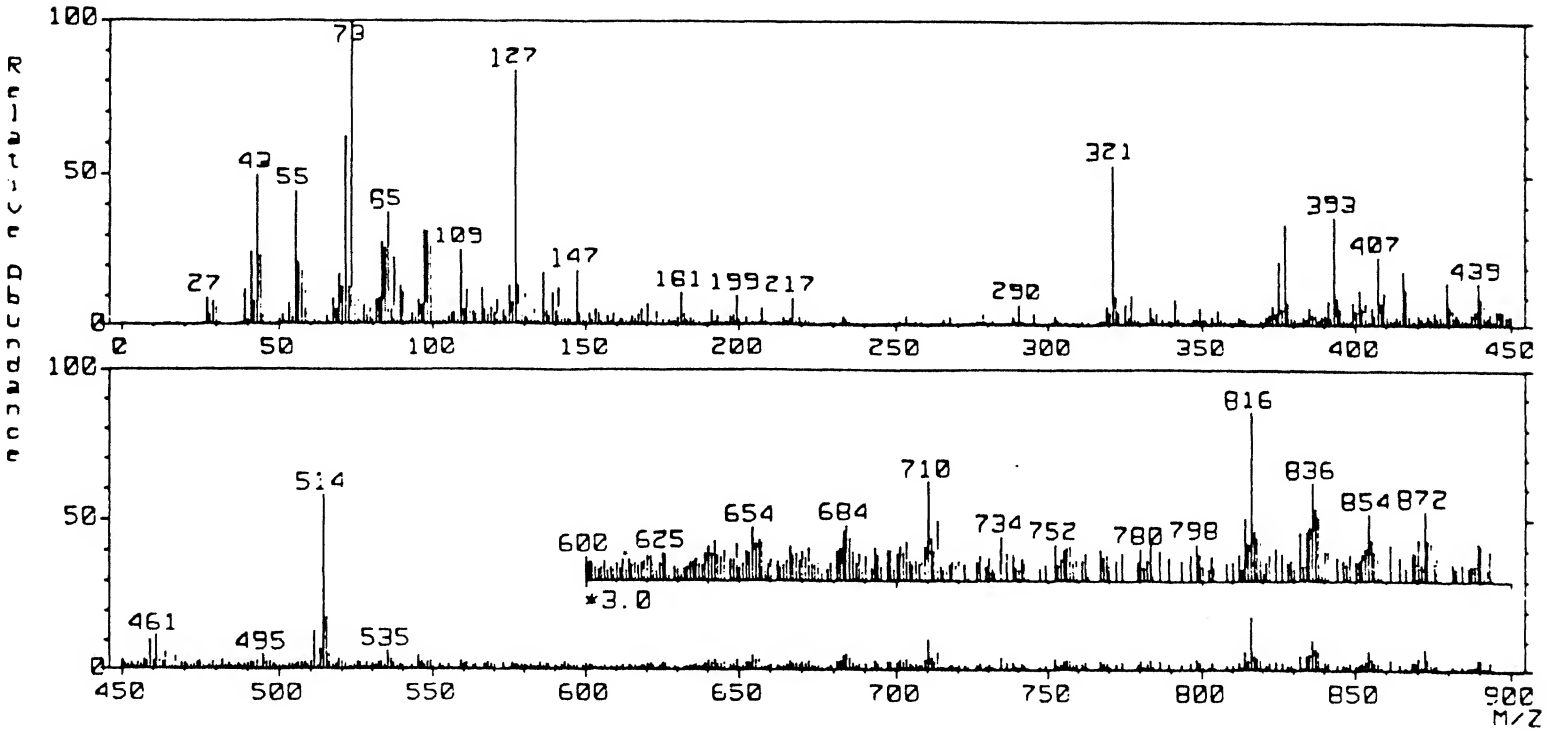

Fig. 4.2 FAB-mass spectrum of the cryptand, L^2

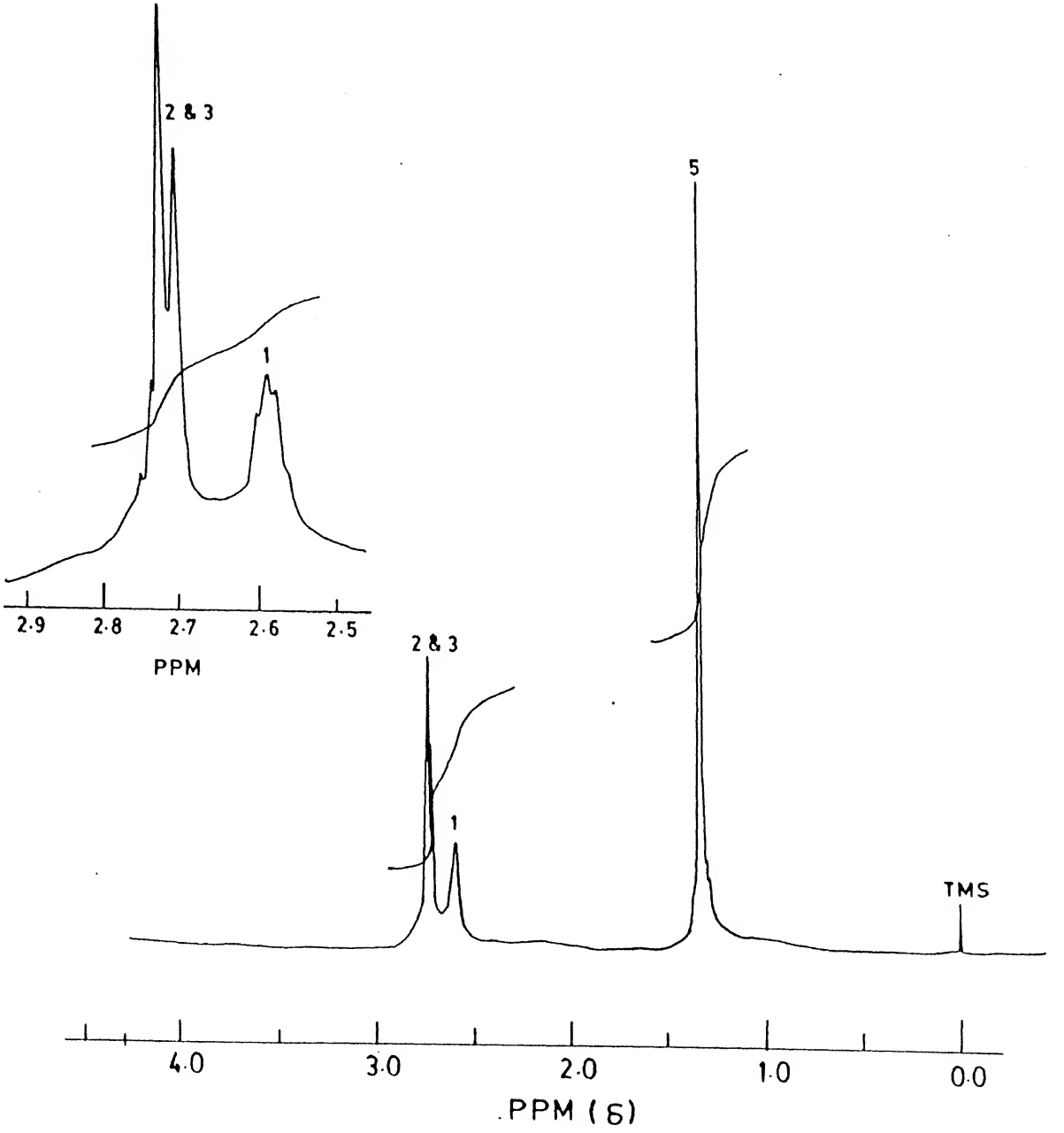

Fig. 4.3 400 MHz ^{1}H-NMR spectrum of L^{2}

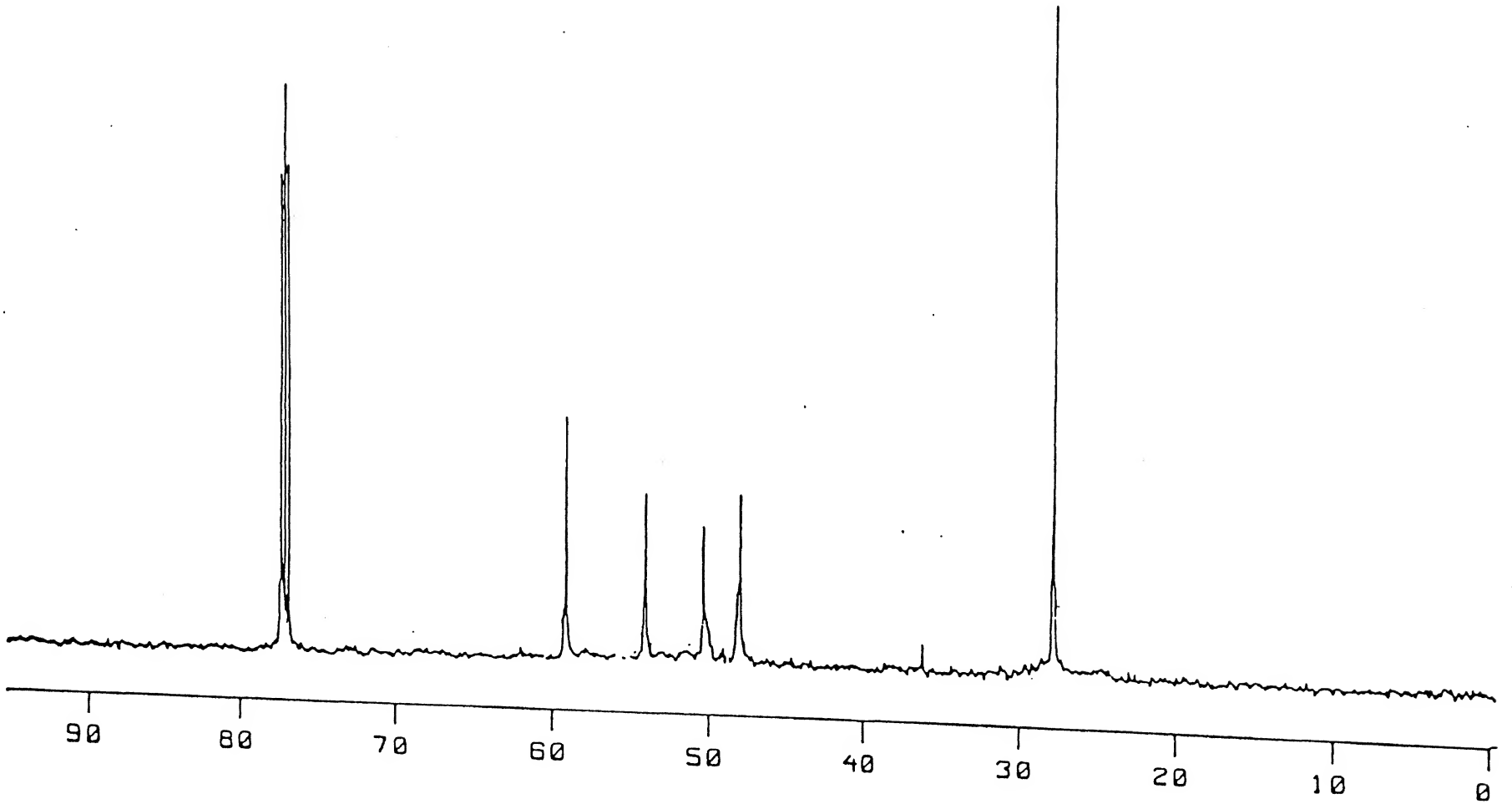

Fig. 4.4 100 MHz ^{13}C-NMR spectrum of L^2

chloroform (10 ml), was added a solution of picric acid (0.34 g; 1.5 mmol) in benzene (10 ml) with stirring at 40°C. A bright yellow precipitate appeared immediately which was collected by filtration and dried in vacuo. Yield 85%.

Analysis: Found C, 39.76; H, 4.19; N, 16.45 and S, 8.89 %. $C_{72}H_{96}N_{26}O_{42}S_6$ requires C, 39.49; H, 4.42; N, 16.63 and S, 8.78 %. The elemental analysis indicates that it is a hexa-picrate. It has been found [122] by other workers that an acid does not protonate the two bridgehead nitrogens easily. It can protonate only the secondary amino nitrogens present in the macrobicyclic rings. Therefore, the present result is consistent with the previous studies.

^{1}H-NMR (400 MHz, (d_6-DMSO + $CDCl_3$), ppm): 1.3 (s, 36H, 5); 2.9 (d, 12H, 1); 3.9 (overlapped t & s, 24H, 2 & 3) and 8.7 (s, 12H, aromatic). The spectrum is shown in Fig. 4.5.

4.1.4 Complexation studies

The cryptand L^2 or its precursor $L^{2'}$ synthesised does not include the Cs(I) ion as in the case of octaazamacrobicyclic ligand described in chapter 3 apparently due to the large size and the slipped nature of the cavity (vide infra). Complexation of transition metal ions by this ligand can be easily achieved as

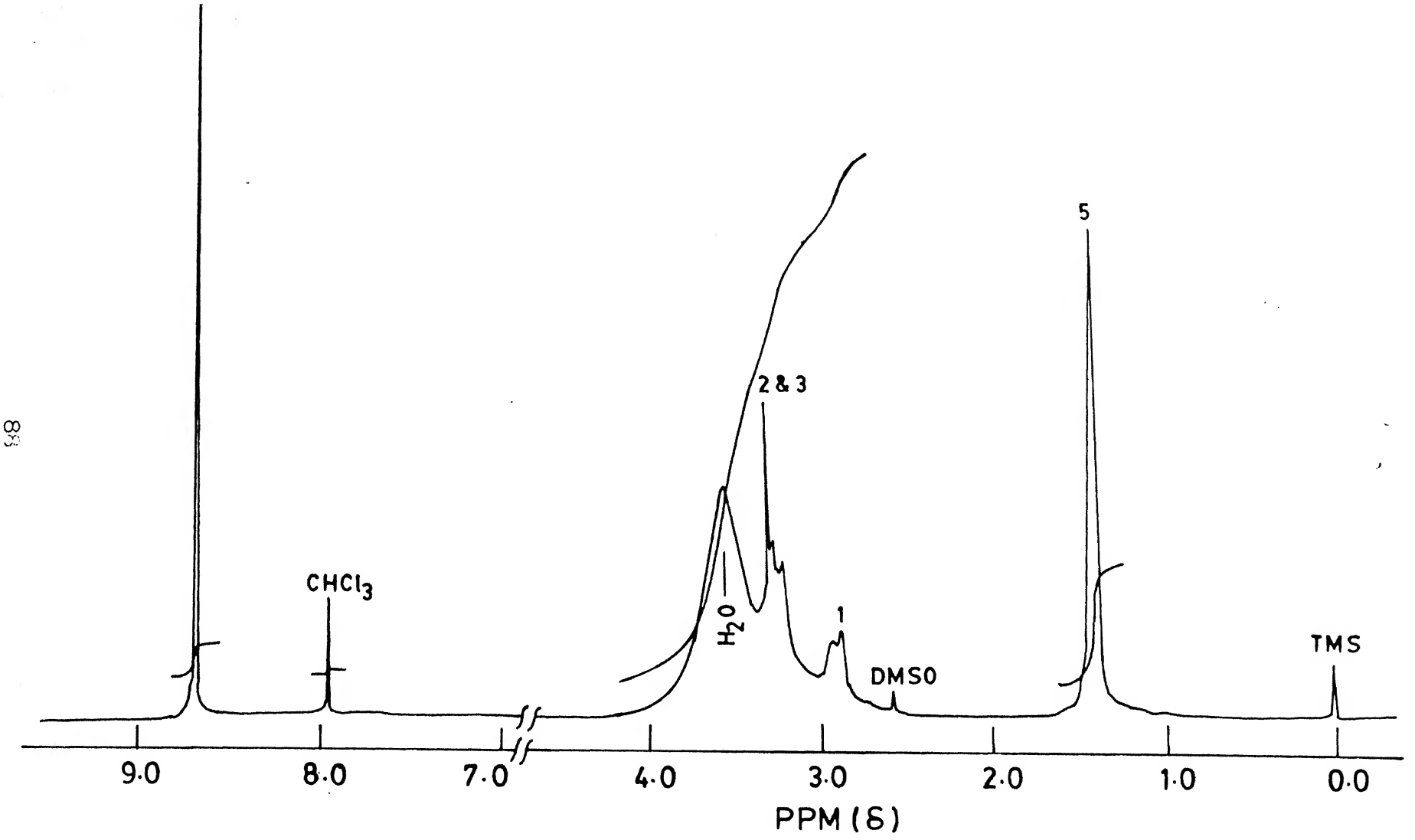

Fig. 4.5 400 MHz ^{1}H-NMR spectrum of the hexa-picrate derivative of L^{2}

described below.

4.1.4a Synthesis of $[L^{2'}\subset Cu(II)_2](ClO_4)_4$, 1

A solution of copper perchlorate hexahydrate (0.37 g; 1 mmol) in MeOH (20 ml) was added to a solution of the ligand $L^{2'}$ (0.4 g; 0.5 mmol) in methanol (20 ml) and stirred for 10 minutes. Then chloroform (50 ml) was added to the green solution obtained and kept at $5^{o}C$ overnight. The green solid deposited was collected by quick filtration and dried in vacuo. Yield 40%. This complex was quite hygroscopic in nature.

4.1.4b Synthesis of $[L^{2}\subset Cu(II)_2](ClO_4)_4$, 2

The cryptand L^2 (0.4 g; 0.5 mmol) was dissolved in ethanol (10 ml) and to this solution copper(II)perchlorate hexahydrate (0.37 g; 1 mmol) dissolved in ethanol (5 ml), was added with stirring at RT. The green solid crashed out was collected by filtration, washed with ice cold ethanol (3 ml) and vacuum dried. The green powder is slightly hygroscopic. Yield 54%.

4.1.4c Synthesis of $[L^{2}\subset Ni(II)_2](ClO_4)_4$, 3

To a solution of the ligand L^2 (0.4 g; 0.5 mmol) in methanol (20 ml), a solution of nickel(II)perchlorate hexahydrate (0.37 g; 1 mmol) in methanol (10 ml) was added with stirring at RT. The

solution was stirred for a further 1/2 hr and methanol was removed in a rotary evaporator. The resulting purple powder was washed several times with water and vacuum dried. Yield 63%. Elemental analyses for the three complexes are given in Table 4.1.

4.2 Results and Discussion

4.2.1 The ligands L^2 and $L^{2'}$ are the first set of cryptands with disulphide groups incorporated in the ligand architecture. They were prepared by one-pot [2+3] Schiff base condensation reaction between tris(2-aminoethyl)amine and diisobutyraldehyde disulphide on Cs(I) ion template. However, when Rb(I) was used instead of Cs(I), no pure product could be isolated. The Cs(I) ion is not bound inside the cavity. This is due to the slipped nature of the cavity and the mismatch in size of the metal ion and the macrobicyclic cavity. The macrobicycle has a slipped ellipsoidal cavity, as evident from the CPK model owing to the three disulphide groups. The dihedral angle, described by the C-S-S-C framework, depends [123] upon the substituents on the α-carbon atoms. It is 90° in HSSH and in the case of diisobutyldisulphide dihedral angle is 69°. In the present case, the α-carbon atoms are also disubstituted like in diisobutyraldehyde. Therefore, the

dihedral angle of the C-S-S-C framework will be closer to 69°. As a result, the two bridgehead nitrogens will not be coaxial.

The 400 MHz ^{1}H-NMR spectrum (Fig. 4.3) of L^{2} is somewhat broadened owing to the slipped ellipsoidal structure of the cryptand. The spectrum in the expanded version shows a broad triplet at δ 2.6 and arises from the protons on C_1. Another triplet at δ 2.75 which has totally different shape and symmetry and is double the intensity of the other triplet. This is because of the overlap of a singlet arising from the protons on C_3 and a triplet arising from the protons on C_2. All the methyl groups appear as a singlet at δ 1.35.

The ^{13}C-NMR spectrum (Fig. 4.4) is simple and shows 5 peaks corresponding to 5 kinds of carbon present in the molecule.

The cryptand forms a hexapicrate derivative when six equivalents of picric acid is added to one equivalent of the cryptand. All the secondary nitrogens are protonated as shown by the downfield shift of the proton NMR signals for the protons on C_2 and C_3 compared to that of the free ligand L^{2}. The protons on C_1 are also downfield shifted but the magnitude δ 0.3 is much less compared to δ 1.25 for the protons on C_2 and C_3. The signal for the protons on C_1 appears as a broad unsymmetrical doublet

and those for the protons on C_2 and C_3 appear as a triplet which has no symmetry and explainable shape. The methyl groups appear as a singlet at δ 1.4. The aromatic protons' resonance appear as a singlet at δ8.7.

4.2.2 Synthesis of dinuclear cryptates

As expected the cryptand, L^2, forms dinuclear cryptates with the metal ions Cu(II) and Ni(II) when two equivalents of a Cu(II) or a Ni(II) salt is stirred with one equivalent of the cryptand. With the precursor, $L^{2'}$, a dinuclear Cu(II) cryptate has also been synthesised. The cryptates are characterised by different spectroscopic techniques which is discussed next.

4.2.2a Dicopper Cryptates 1 and 2

The molar electrical conductivity in acetonitrile for **1** and **2** were 495 and 510 $ohm^{-1}cm^2mol^{-1}$ respectively at 298 K. These values are consistent [86] with the 1:4 electrolytic nature of the cryptates and thus can be formulated as $[ACCu(II)_2](ClO_4)_4$ (A = L^2 or $L^{2'}$). Infrared spectrum of each exhibits a strong and broad absorption band centred around 1100 cm^{-1} attributable to the presence of anionic perchlorates.

The electronic spectral data of **1** at 298 K in acetonitrile are collected in Table 4.2 while the spectrum is shown in Fig.

4.6. The free ligand does not absorb significantly at wavelengths longer than 280 nm. The spectral band positions do not change to any noticeable extent upon changing the solvent from acetonitrile to methanol implying no coordination by the solvent molecules. The electronic spectrum of the Schiff base dicopper cryptate showed 5 bands at 275, 385, 465, 605 and 745 nm. The broad bands that occur at 605 and 745 nm are assignable to ligand field transitions of a hexadentate Cu(II) complex having approximately D_{3h} symmetry [124]. The strong band at 275 nm is assignable as the σ(N)---> Cu(II) charge transfer absorption involving an imine nitrogen and Cu(II). The rest two bands at 385 and 465 nm are too low in energy to be σ(N)-->Cu(II) LMCT transitions. A number of theoretical studies [123] suggest that the enregy difference between the two highest occupied MO's of a disulfide depend upon the substituents in the α-carbon atoms. Accordingly, with the α-carbon atoms bearing two methyl substituents, the energy difference between the HOMO and the SHOMO in the present cryptand should be about 0.65 ev. Taking this at its face value, the two bands at 385 and 465 nm are attributable to the LMCT transitions from the SHOMO and the HOMO respectively to the d-vacancy. The electronic spectrum of a CuN_4S

chromophore built from an N_4-macrocycle and a hydrosulfide ($\bar{S}SCH_2CO_2^-$) shows [125] two bands at 390 and 465 nm assigned as LMCT transitions originating from the two highest occupied orbitals of the hydrosulfide moiety. These two orbitals are well separated from the core-like orbitals. Also, a pentacoordinated Cu(II) complex with an acyclic ligand bearing one disulphide group in the middle and two terminal amino groups have been reported [111] where the fifth N is provided by N-methyl imidazole or CH_3CN. This complex shows three strong bands located at 275, 335 and 445 nm. Although no hexadentate Cu(II) complex with disulfide as one of the ligands has been studied spectroscopically, the bands at 385 and 465 nm are assigned as the LMCT transitions involving disulfides and Cu(II).

The cryptate, **2**, shows five bands at nearly the same positions (Table 4.2) as in the case of **1** except the d-d bands which are slightly red shifted here. These bands are similarly assigned. The spectrum is shown in Fig. 4.7.

The effective room temperature magnetic moment values (μ_{eff}/μ_B) are found to be 2.04 and 1.98 per copper for **1** and **2** respectively. These values indicate the absence of magnetic interaction between the two Cu(II) centres even though they are bridged by three disulphide groups. Due to the slipped

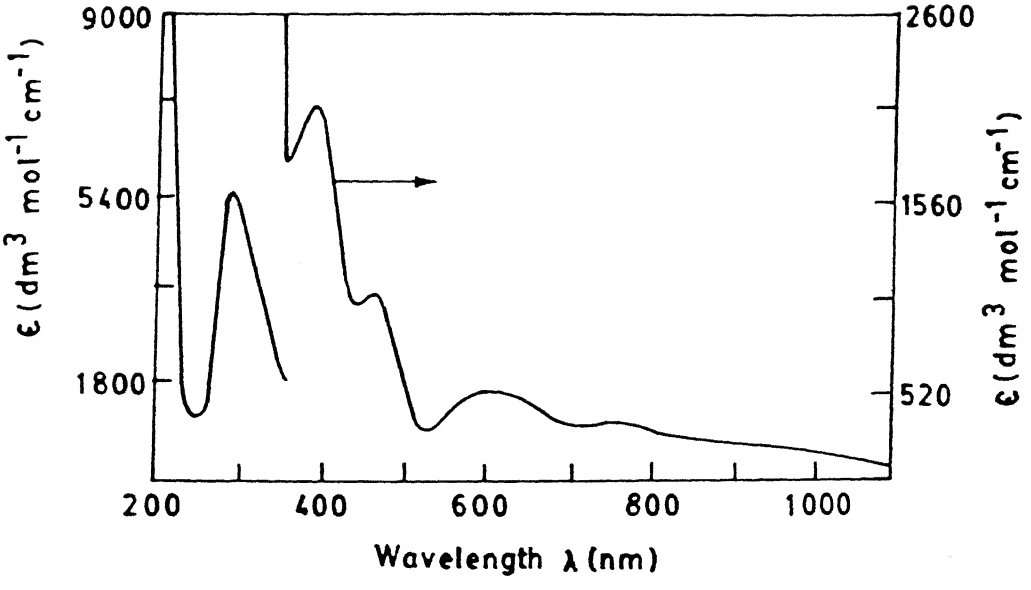

Fig. 4.6 Electronic absorption spectrum of 1 in acetonitrile

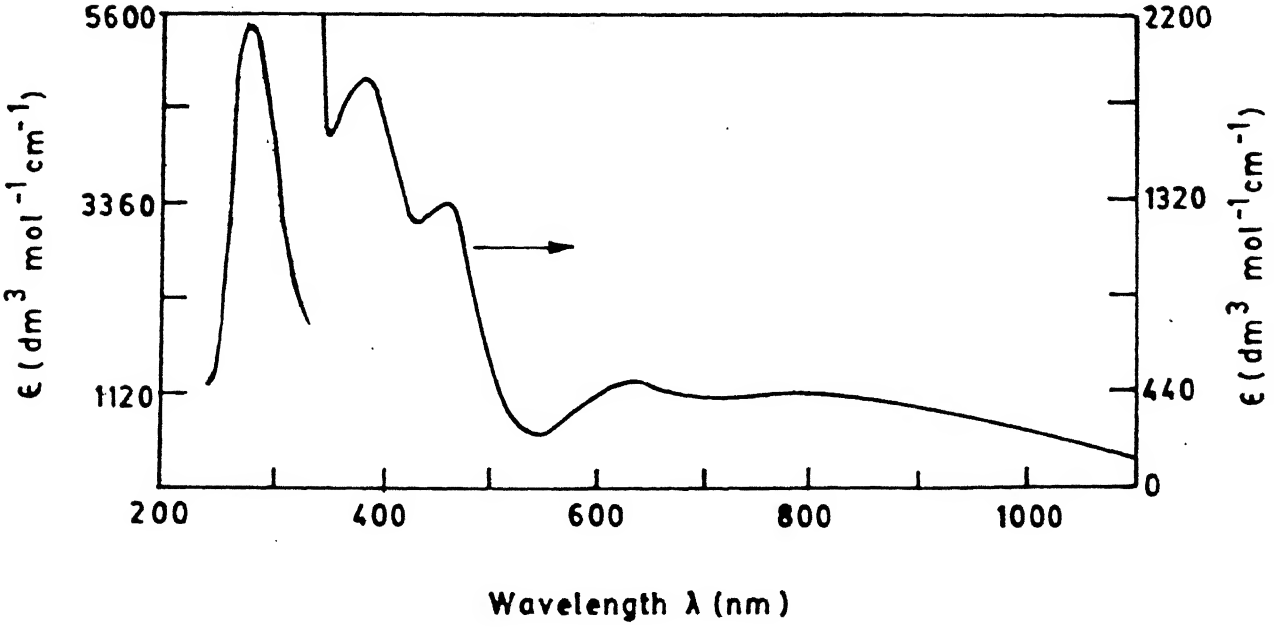

Fig. 4.7 Electronic absorption spectrum of 2 in acetonitrile

ellipsoidal nature of the cavity, the possibilities for magnetic interaction either by super exchange pathway or by direct overlap of orbitals of Cu(II) centres are absent.

The EPR spectral data are given in Table 4.3 while the spectra in solution are shown in Fig. 4.8. The electron paramagnetic spectra at 298 and 77 K of the complexes **1** and **2** in the solid state show only broad bands near g_{av}= 2 and are not indicative of the stereochemistry of these cryptates. At 298 K, the spectra in CH_3CN show characteristic four-line signals near g_{av}= 2 for both **1** and **2**. No signal near g = 4 is found either in the solid state or in solutions of **1** and **2** which indicates that there is no interaction between the metal centres. Even residual interactions, including magnetic dipolar interactions as small as a few wavenumbers can be enough to yield spectra very different from the spectra of individual spins [126]. At 77 K in acetonitrile glass, each spectrum changes to an axial one indicating the presence of a three-fold symmetry around the metal ions. The spectra are consistent with the $d_{x^2-y^2}$ ground state for the metal ion. In case of hexadentate CuN_6 complexes which show static Jahn-Teller distortion, the EPR spectra are significantly rhombic in nature [127]. Since the spectra are axial in these

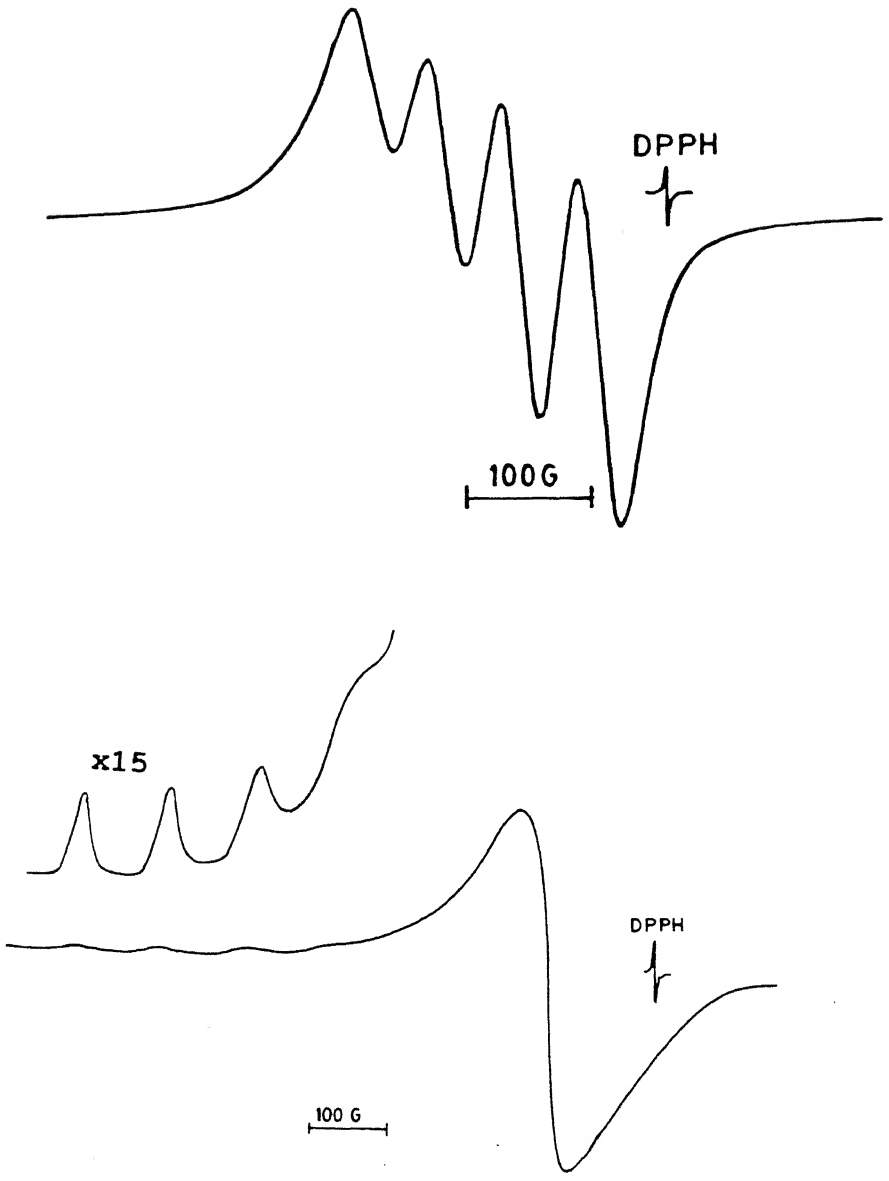

Fig. 4.8 Solution EPR spectrum of **1**; (a) at 298 K (b) at 77 K

cases, it is concluded that the donor atoms in the cryptand being neoplastic, are able to overcome the Jahn-Teller distortion forces. The $A_{\parallel}^{Cu}$ values are small as each Cu(II) is bonded to three sulfurs which are known [128] to reduce hyperfine coupling.

The electron transfer properties of the two dicopper cryptates were probed by cyclic voltammetry at 298 K in acetonitrile. The cyclic voltammogram (Fig. 4.9) of the cryptate **1** shows a quasi-reversible response at E_f = +0.14 V with ΔE_p = 95 mV. In case of **2**, the response (Fig. 4.9) occurs at E_f = -0.17 V with ΔE_p = 115 mV. The following characteristics were observed : ΔE_p value increases by 35 mV (for **1**) and 40 mV (for **2**) with the increase in the scan rate from 100 mVs^{-1} to 200 mVs^{-1}; i_{pa}/i_{pc} 1.1 at all the scan rates employed. The free ligands do not show any redox activity in the region, -0.5 to +0.5 V. Also, the corresponding dinickel cryptate does not show (vide infra) any cyclic response in the same region. Thus, the responses are attributed to be metal-centred. The difference in the E_f values of **1** and **2** is due to the difference in σ-donor ability [129] of the amine nitrogens compared to the imine nitrogens. Due to increased σ-donor ability of the amino nitrogen compared to that of imine nitrogen, the Cu(I) state is more destabilised and the reduction occurs at negative potential with increased ΔE_p. The

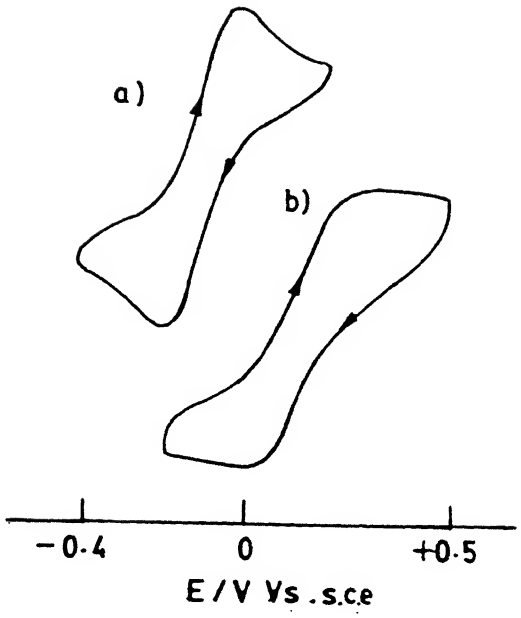

Fig. 4.9 Cyclic voltammogram of the dicopper cryptates at 100 mV s^{-1} (a) for **1** (b) for **2**

exhaustive controlled potential coulometric experiments done on **1** at -0.06 and on **2** at -0.35 V gives n = 1.96 and 1.99 e^- respectively. These results indicate that the cyclic responses are associated with the transfer of two electrons and the two Cu(II) centres are undergoing reduction at the same potential for both **1** and **2**. When quickly frozen in liquid nitrogen temperature, no EPR signal of the reduced product can be observed in either case. The cyclic responses are, therefore, assigned to the following redox reactions :

$$[L^{2'}_{C}Cu(II)_2]^{4+} + 2e^- = [L^{2'}_{C}Cu(I)_2]^{2+}$$

$$[L^{2}_{C}Cu(II)_2]^{4+} + 2e^- = [L^{2}_{C}Cu(I)_2]^{2+}$$

Redox data are available [130] for the dicopper complexes with cryptands incorporating one or two tren units. Cu(II) is tetracoordinated with four nitrogens from the tren unit in these systems where the counter ion is perchlorate. In such systems, no cyclic responses are seen either in the positive or in the negative scan implying instantaneous decomposition of the oxidised or the reduced species formed. Our results indicate that each copper ion is hexacoordinate through three nitrogens and three sulfurs in a grossly trigonal prismatic fashion and the

sulphur coordination results in quasi-reversible response in cyclic voltammogram since sulphur coordination known to destabilise Cu(II) oxidation state [131].

4.2.2b **Dinickel Cryptate, 3**

The ligand L^2 which provides two N_3S_3 donor site for Cu(II) can provide the same sites to Ni(II) also, since Ni(II) prefers hexacoordination over distorted tetrahedral which will be the case if the metal ion recognizes the N_4 donor site at the two ends of the cavity. As expected, when two equivalents of nickel perchlorate hexahydrate was allowed to react with one equivalent of the cryptand L^2, a dinickel cryptate readily formed as a light purple solid. The solid is slightly hygroscopic. Its molar conductivity in acetonitrile is 520 ohm^{-1} cm^2 mol^{-1} that corresponds [86] to a 1:4 electrolyte. In the infrared spectrum, a strong and broad absorption band appears centering at about 1100 cm^{-1} indicating [100] the presence of anionic perchlorates.

The electronic spectral data of 3 is collected in Table 4.2 and shown in Fig. 4.10. Three ligand field transitions are observed for the dinickel complex. The model studies indicated that the geometry around each Ni(II) ion would be closer to trigonal prismatic. For trigonal prismatic arrangement of donor

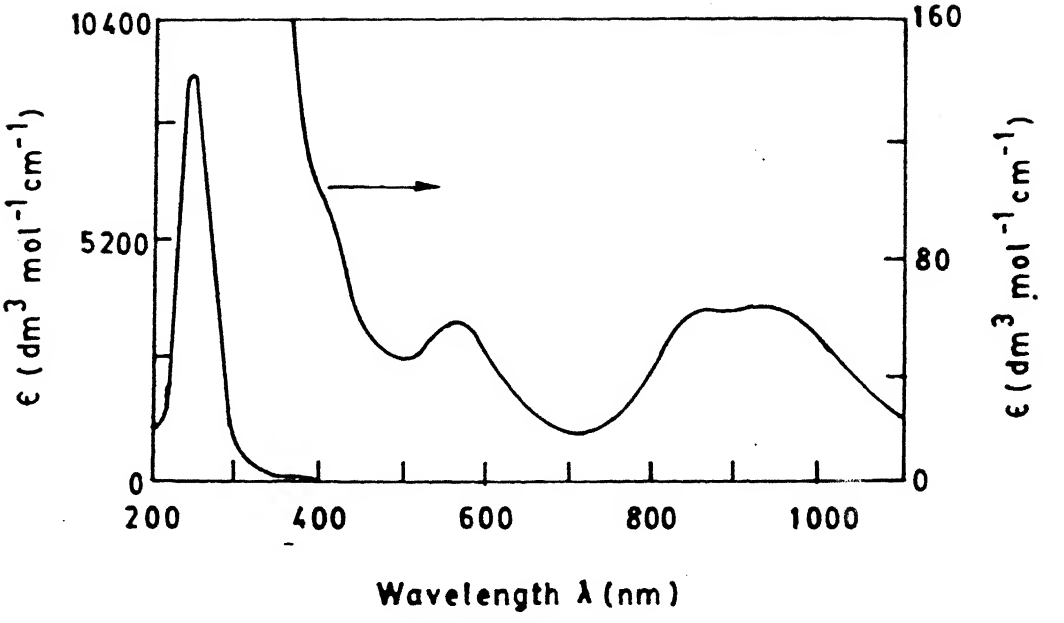

Fig. 4.10 Electronic absorption spectrum of 3 in acetonitrile

atoms around Ni(II), three spin allowed transitions [132] are expected : $^3A_{2g} \rightarrow {}^3T_{2g}$, $^3A_{2g} \rightarrow {}^3T_{1g}$ and $^3A_{2g} \rightarrow {}^3T_{1g}(P)$. Intensities of these transitions usually lie below 100 $dm^3 mol^{-1} cm^{-1}$ which is also observed here. The absorptions due to LMCT transitions involving disulfide and Ni(II) have not been reported. These bands are expected to occur at higher energies compared to the transitions observed in case of **1** and **2** because of lower optical electronegativity of Ni(II) with respect to Cu(II) in the same coordination symmetry [133]. A shoulder appears at 405 nm which should be a LMCT transition involving the disulfides and Ni(II). The corresponding band in the cryptates, **1** and **2**, appears around 485 nm. The other LMCT bands in **3** are mixed with the intra-ligand transitions.

The room temperature magnetic moment (μ_{eff}/μ_B) is 2.9 per nickel. This value lies within the normal range for trigonal prismatic Ni(II) complexes [132]. This value also suggests that there is almost no magnetic interaction between the two Ni(II) centres.

The cyclic voltammetric experiments were performed on **3** in acetonitrile at 298 K. On scanning in the negative side a cathodic peak appears at -0.55 V but the corresponding anodic peak is absent. When scanned in the positive side, two anodic

peaks at +0.95 and +1.45 V are observed although no corresponding cathodic peaks are seen. The cyclic voltammetric results indicate that the oxidised and the reduced species formed electrochemically undergo instantaneous decomposition.

4.3 Conclusion

This study provides the first example of a cryptand having three disulfide linkages incorporated in the rings. This cryptand is theoretically capable of acting as a multi-site receptor. However, both Cu(II) and Ni(II) recognize the site that provide N_3S_3 coordination. The two metal ions behave independently because of the slipped ellipsoidal structure of the cryptand.

Table 4.1 Magnetic Moment (301K) and Elemental Analysis of the Cryptates

Cryptate	μ_{eff}/μ_B	Analysis							
		Found				Calculated			
		C	H	N	S	C	H	N	S
1	2.04	32.71	5.27	8.19	14.32	32.55	5.01	8.44	14.48
2	1.98	32.62	5.71	8.49	14.26	32.26	5.87	8.36	14.35
3	2.9	32.81	5.86	8.67	14.58	32.5	5.91	8.42	14.46

1.2 Electronic Absorption Spectral Data of the Cryptates

Cryptate	λ_{max}/nm	ϵ_{max}/$dm^3 mol^{-1} cm^{-1}$	Assignment
1	745	376	dz^2--->dx^2-y^2
	605	516	t_{2g}--->dx^2-y^2
	465	1010	(S_2)-->Cu(II) LMCT
	385	2010	(S_2)-->Cu(II) LMCT
	275	5400	σ(N)-->Cu(II) LMCT + intra-ligand absorption
2	776	420	dz^2--->dx^2-y^2
	633	502	t_{2g}--->dx^2-y^2
	460	1339	(S_2)-->Cu(II) LMCT
	385	1922	(S_2)-->Cu(II) LMCT
	288	5370	σ(N)-->Cu(II) LMCT + intra-ligand absorption
3	925	63	$^3A_{2g}$-->$^3T_{2g}$
	856	63	$^3A_{2g}$-->$^3T_{1g}$
	552	60	$^3A_{2g}$-->$^3T_{1g}$(P)
	405	102	(S_2) -->Ni(II) LMCT
	262	8925	σ(N)-->Ni(II) LMCT + intra-ligand absorption

Table 4.3 EPR Spectral Data of the Dicopper Cryptates

Cryptate	g_{av}	A^{Cu}_{av}	$g_{\parallel}$	$g_{\perp}$	$A^{Cu}_{\parallel}$	
1	2.09	-	-	-	-	(298 K solid sample)
	2.08	-	-	-	-	(77 K solid sample)
	2.10	60	-	-	-	(298 K in MeCN)
	-	-	2.35	2.09	110	(77 K in MeCN)
2	2.08	-	-	-	-	(298 K solid sample)
	2.07	-	-	-	-	(77 K solid sample)
	2.11	63	-	-	-	(298 K in MeCN)
	-	-	2.36	2.09	114	(77 K in MeCN)

Unit of $A^{Cu}_{\parallel}$ is $cm^{-1} \times 10^{-4}$

Chapter 5

SYNTHESIS OF CRYPTANDS WITH HETERO-DITOPIC RECEPTOR SITES AND THEIR COMPLEXING ABILITIES TOWARDS Ni(II),Cu(II),Zn(II) IONS AND H_2O MOLECULE

Cryptands having two identical donor sites form homo-dinuclear cryptates in which the metal centres show similar redox, magnetic and structural properties when they are far apart or the individual properties change according to the influence of the one metal ion on the other. When the cryptand has two binding sites of different nature, hetero-dinuclear cryptates can be isolated. Also, if a metal ion recognizes only one site leaving the other site empty, then small molecules or charged fragments can occupy this vacant site. The metal ion already included inside the cavity can influence such binding processes or it might be the inherent property of the vacant site itself to bind such molecules or ions. In this way, unstable molecular fragments (or) gaseous molecules like CO, CO_2, H_2S etc. can be fixed in the cavity. This kind of cavitand chemistry might afford to investigate the electronic structure and bonding of the resulting complexes which might otherwise not be possible due to

their highly unstable nature. Moreover, they can find application in controlling environmental pollution by acting as scavangers. It is also possible for the metal binding site to impose an unusual coordination geometry onto the metal ion, which is possible by judicious choice of donor atoms' topology and provide rigidity to the ligand structure. In that case, the electronic properties of the metal ion can be tuned to activate the bound species. Macrobicycles with hetero-ditopic receptor sites, where one subunit provides N(S) donor atoms and the other subunit provides O donor atoms, may present a way to the kind of studies mentioned above. The site with N(S) donors can recognise a transition metal ion leaving the other site empty for small molecules or ions.

This chapter is divided into three sections. The section **A** describes the synthesis of a hetero-ditopic macrobicyclic cryptand with donor sets of N_4 and NO_3 at the two end (Fig 5.1) and flat benzyl groups between them. The tripodal N_4 subunit imposes a pseudotetrahedral geometry onto metal ions like Cu(II) and Ni(II). The vacant site can recognise N_3 and H_2S which have been studied spectroscopically.

Section **B** describes the synthesis of another hetero-ditopic

receptor with same sets of donor atoms as in Section **A** but the bridging units here are naphthyl instead of benzyl groups. The receptor properties towards the metal ion Zn(II), Cu(II) and Ni(II) have been probed. The electronic spectroscopy reveals the effect of naphthyl bridges instead of benzyl bridges on coordination geometry of these metal ions. An air-stable Cu(II) complex with H_2S included inside the cavity has also been characterised.

Section **C** discusses the molecular recognition properties of the two cryptands towards H_2O. Both the cryptands, L^3 and L^4, give single crystals where one water molecules is included inside the cavity. A novel water cryptate with the cryptand, L^3 has been studied by x-ray crystallography.

SECTION A

5.1 Experimental Section

5.1.1 **Materials.**- Reagent grade salicylaldehyde, tris(2-aminoethyl)amine and triethanolamine (Aldrich) were used as received. Thionyl chloride, $NaBH_4$ and all the solvents (SD Fine Chemicals, India) were purified prior to use following standard procedures [86].

5.1.2 **Methods.**- Elemental analysis for C, H, and N were done at the Central Drug Research Institute, Lucknow, India. Physicochemical data on the complexes were collected as described in chapters 3 and 4.

5.1.3 Synthesis of the Cryptand, L^3

Synthesis of the cryptand (L^3) was attempted following two different routes as shown schematically in Fig. 5.1 and 5.6. In either scheme, the synthesis involves a number of steps. The synthesis according to the Scheme outlined in Fig. 5.1 is described next.

5.1.3a Tris(2-chloroethyl)amine hydrochloride

This compound was prepared by following a literature procedure [134]. Triethanolamine (4.6 g; 3 mmol) was dissolved in chloroform (10 ml) and added dropwise with stirring to a solution of thionyl chloride (14.7 g; 0.12 mol) in chloroform (10 ml). After the addition was complete, the reaction mixture was stirred for another 1 hr and the volatile components of the reaction mixture were distilled off. The crystalline mass left behind was recrystallised from acetone. Yield 92%. m.pt. 128°C (lit. 127-130°C).

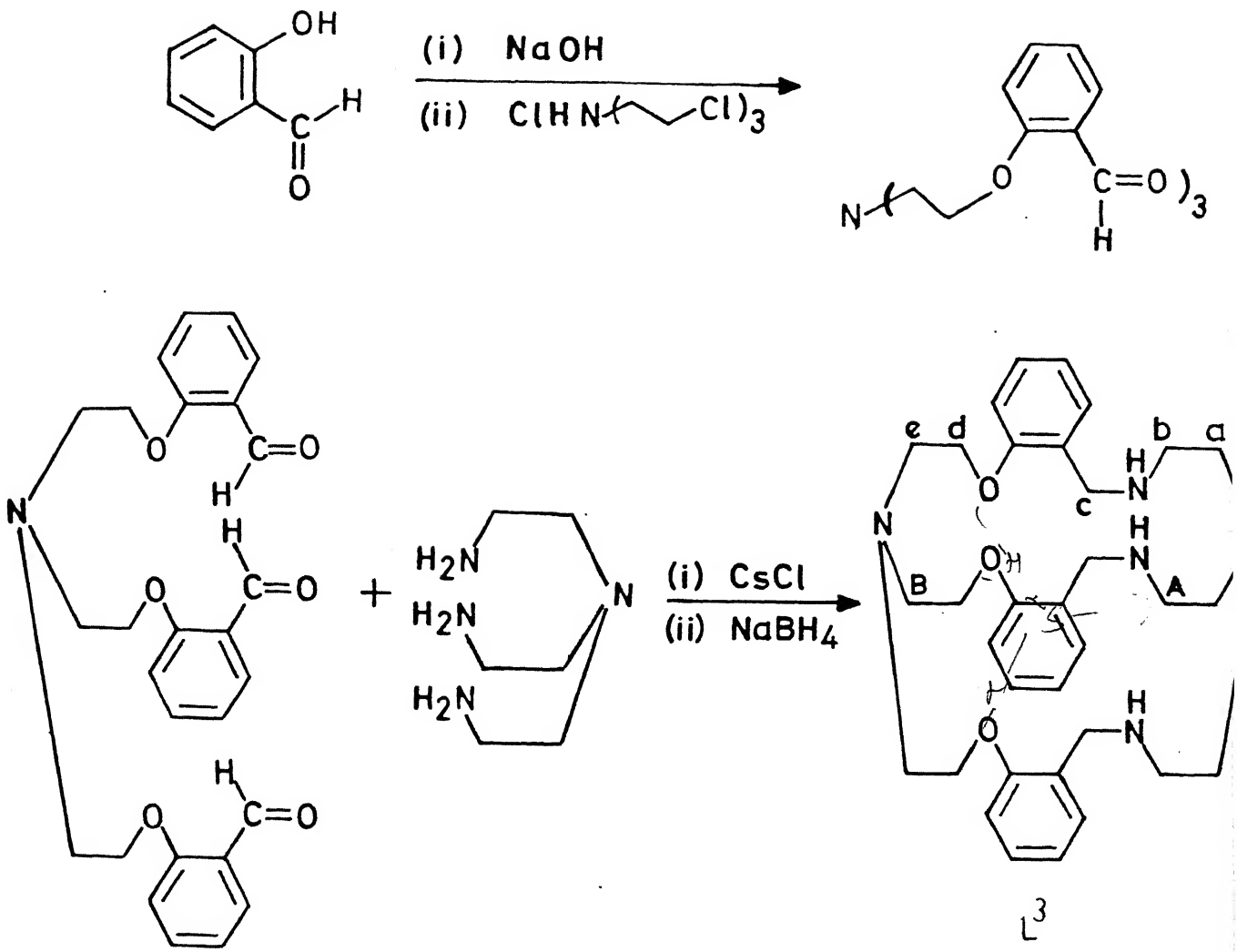

Fig. 5.1 Synthetic scheme for the cryptand, L^3

5.1.3b **Tris{[2-(2-benzaldehyde)oxo]ethyl}amine**

To a solution of salicylaldehyde (0.12 g; 1 mmol) in EtOH (50 ml) was added crushed NaOH (0.16 g; 4 mmol) which dissolved upon stirring at RT for 30 minutes. Tris(2-chloroethyl)amine hydrochloride (0.08 g; 0.33 mmol) was then added to the above solution at RT. A small amount of NaCl deposited almost immediately. To complete the reaction, the mixture was heated under reflux for 2 hr. The product crashed out as a light brown solid when the mixture at ambient temperature was poured into cold water (50 ml). The compound was collected by filtration and purified by recrystallisation from hot EtOH as colourless solid. Yield 80%. m.pt. 84-85°C. ν_{max}/cm^{-1} 1660 (C=O). ^{1}H-NMR (80 MHz, CD_3CN, ppm): 3.4 (t, 3 NCH_2); 4.4 (t, 3 OCH_2); 7.5 (m, 12H, aromatic) and 10.6 (s, 3H, 3CHO). The spectrum is shown in Fig. 5.2.

Analysis: Found C, 69.91; H, 6.02 and N, 3.12%. $C_{27}H_{27}NO_6$ requires C, 70.27; H, 5.90; and N, 3.03%.

5.1.3c **Synthesis of the Cryptand, L^3**

The cryptand, L^3 was synthesised by tripod-tripod Schiff base condensation of the tris{[2-(2-benzaldehyde)oxo]ethyl}amine

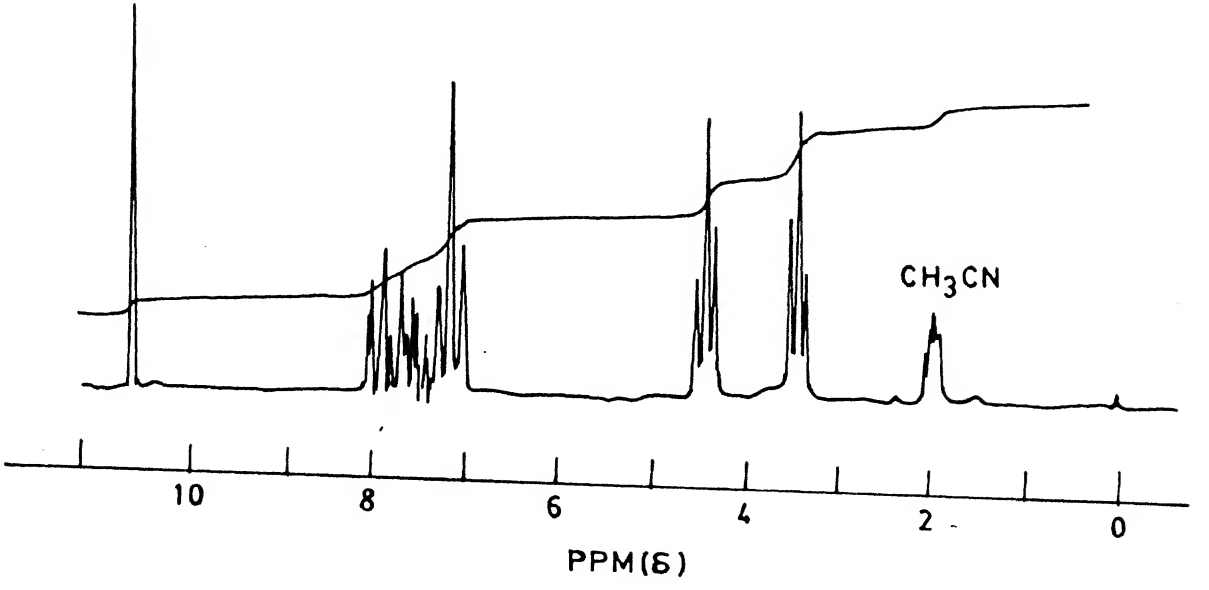

Fig. 5.2 80 MHz ^{1}H-NMR spectrum of the trialdehyde

and tris(2-aminoethyl)amine in presence of Cs(I) ion as the template. In absence of the Cs(I) ion, no pure product could be isolated. The Schiff base, (L^3) being unstable was reduced *in situ* by refluxing with excess $NaBH_4$. The experiment was performed as follows: The tris{[2-(2-benzaldehyde)oxo]ethyl}amine (0.46 g; 1 mmol) and CsCl (0.17g; 1 mmol) were dissolved in MeOH (200 ml) by warming upto 40°C. To this solution was added a solution of tris(2-aminoethyl)amine (0.15 g; 1 mmol) dissolved in MeOH (75 ml) in a dropwise manner over a period of 5 hr while stirring the reaction mixture continuously. The temperature of the reaction solution was maintained at 40°C during addition. After the addition was complete, the reaction mixture was allowed to reflux for 3 hr. Reduction of the Schiff base was achieved by refluxing with excess of $NaBH_4$ for 4 hr. Then, MeOH was removed in a rotary evaporator and the residue shaken with water (20 ml). The desired cryptand was extracted with $CHCl_3$ (2 x 50 ml), the $CHCl_3$ layer dried over anhydrous Na_2SO_4 and finally the $CHCl_3$ was removed to obtain (L^3) in overall 70% yield as a pale yellow oily liquid. It was found to be air-stable and was almost analytically pure.

^{1}H-NMR (80 MHz, $CDCl_3$, ppm): 2.5(m, 12H, a & b); 3.2 (t, 6H, e);

3.6 (s, 6H, c); 4.1(t, 6H, d); 7.1 (m, 12H, aromatic). The spectrum is shown in Fig. 5.3.

^{13}C-NMR (20.1 MHz, $CDCl_3$, ppm): 47.06(3C, a); 48.60(3C, e); 54.37(3C, b); 55.30(3C, c); 67.55(3C, d) and 111.29, 120.63, 127.16, 128.70, 131.33, 156.35 (aromatic). The spectrum is shown in Fig. 5.4.

FAB-mass: m/z = 560 $[L^{3\bullet+}]$ (Fig. 5.5).

5.1.3d Alternate Route to the Synthesis of L^3

The route is shown schematically in Fig. 5.6. This route was followed to study the efficiency of O-C bond formation in the tripod-tripod coupling reaction.

5.1.3e Synthesis of tris(salicylideneamino)ethyl)amine (SALTREN)

This was prepared following a literature procedure [135]. Tren (1.5 g; 10 mmol) in EtOH (25 ml) was added to a stirred solution of salicylaldehyde (3.6g; 30 mmol) in diethyl ether (25 ml). A yellow precipitate crashed out immediately. The reaction mixture was kept at 5^{o}C for 2 hr and then the Schiff base was collected by filtration, washed with diethyl ether and air-dried. Yield 91%. m.pt. 82-83^{o}C (lit. 82-83^{o}C). IR(KBr): 1550cm^{-1}(s), $\gamma_{C=N}$ and $\gamma_{C=C}$.

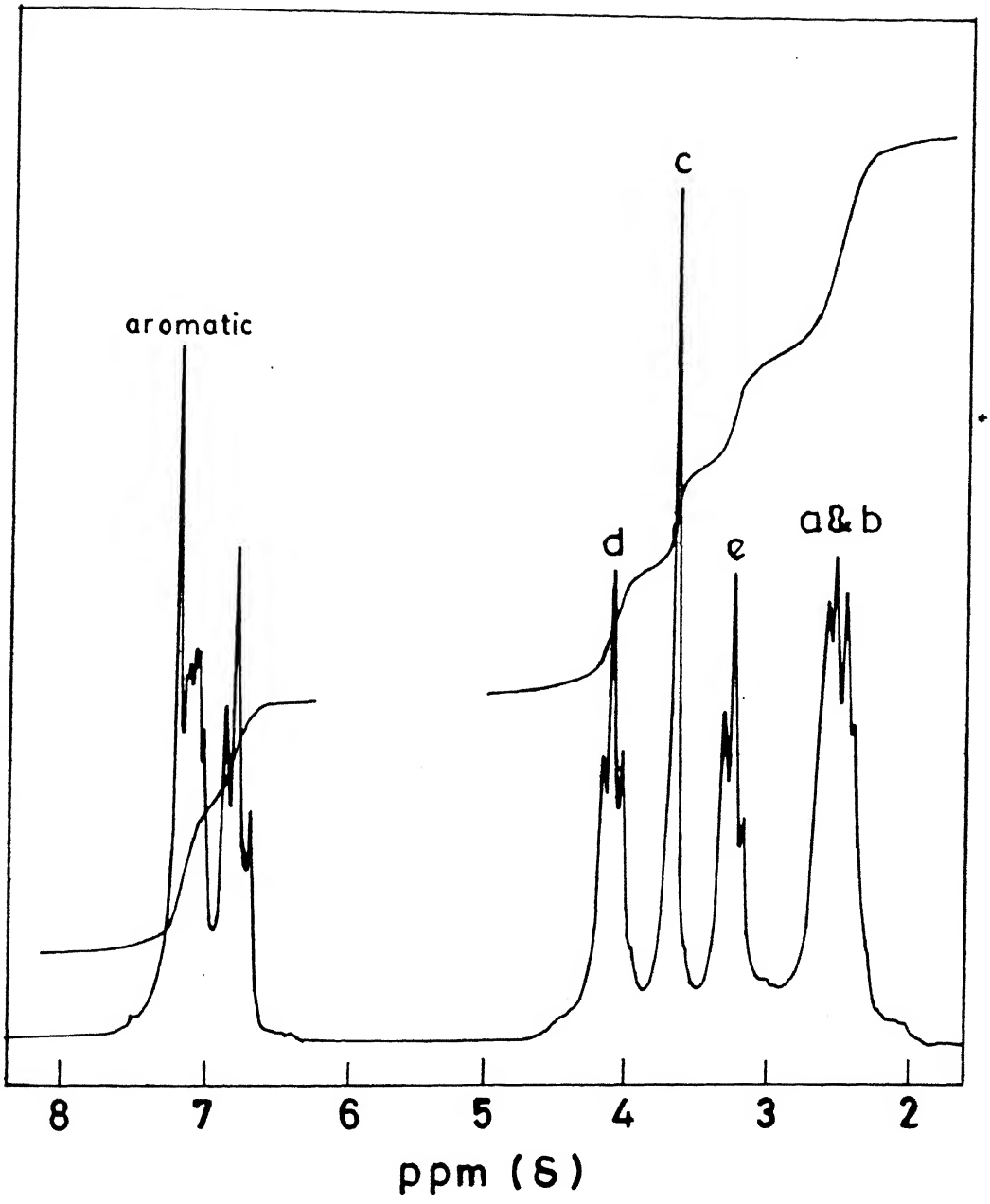

Fig. 5.3 80 MHz ^{1}H-NMR spectrum of the cryptand, L^{3}

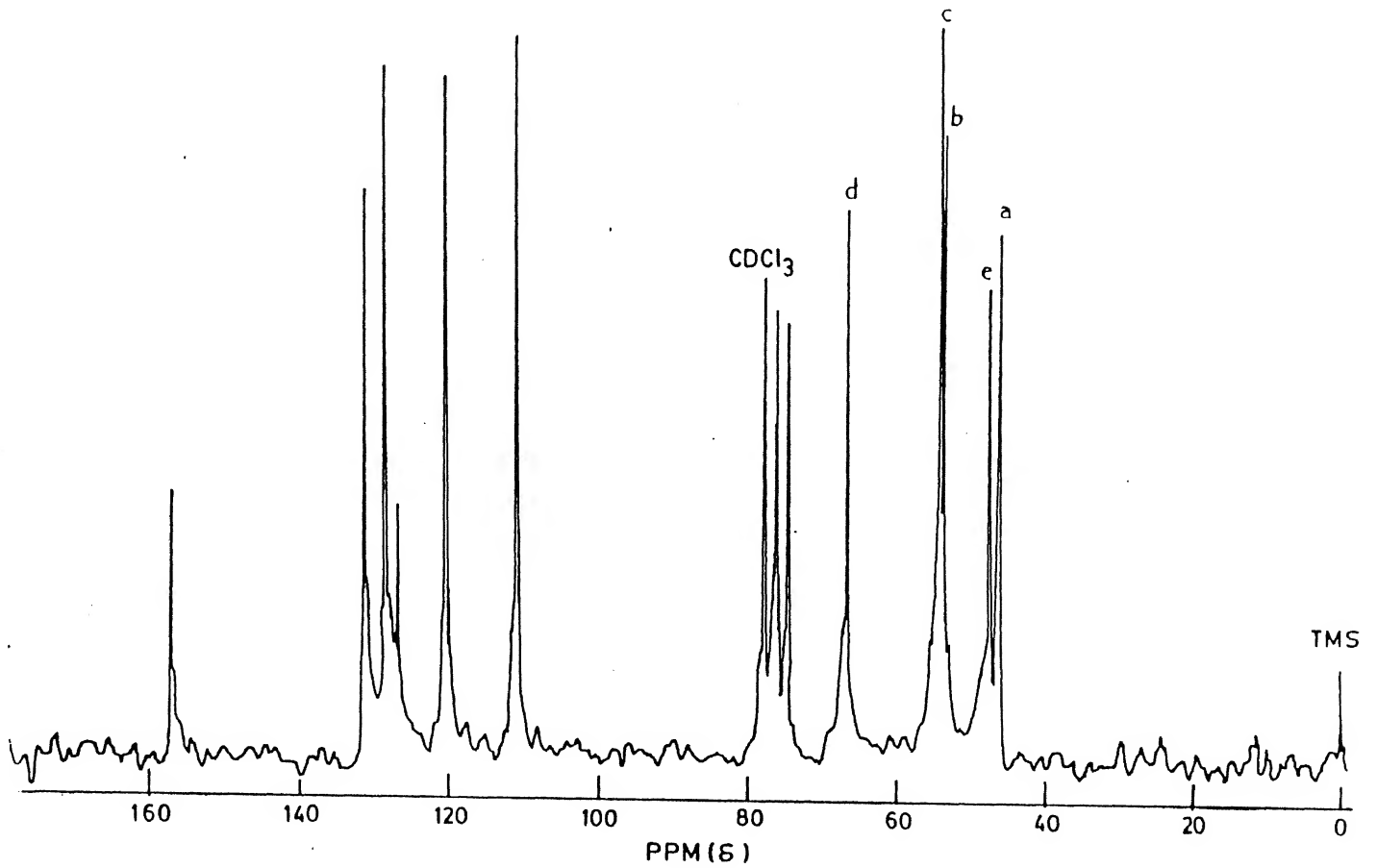

Fig. 5.4 20.1 MHz ^{13}C-NMR spectrum of the cryptand, L^3

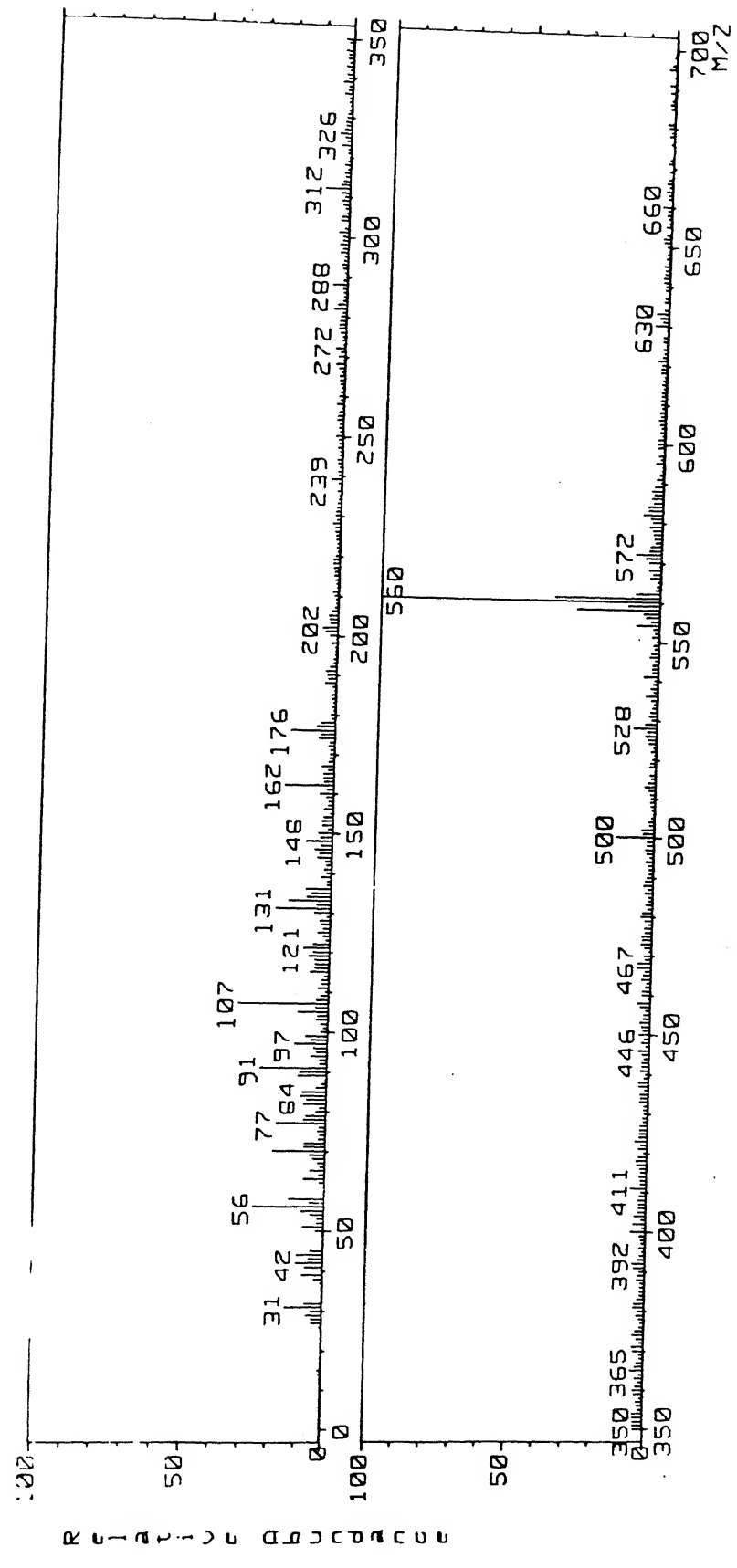

Fig. 5.5 FAB-mass spectrum of the cryptand, L^3

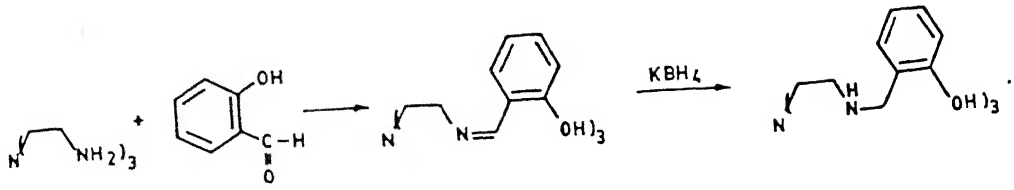

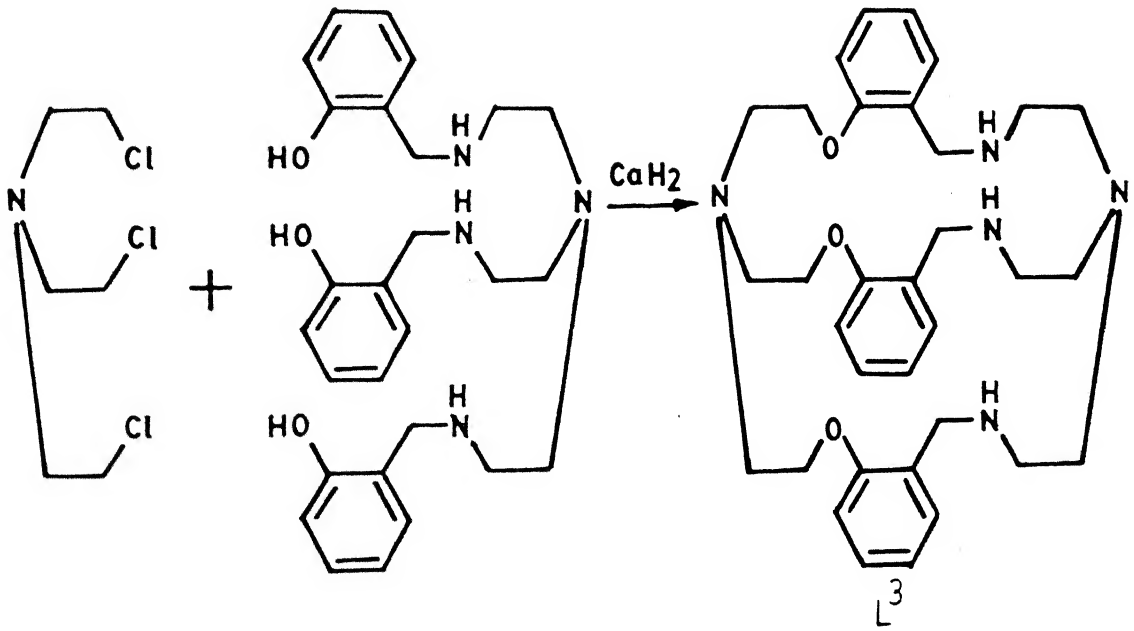

Fig. 5.6 Alternative synthetic scheme for the cryptand, L^3

5.1.3f **Preparation of KBH_4**

It was synthesized following a literature method [136].To a solution of $NaBH_4$ (7.4 g; 20 mmol) in water (13 ml), a solution of KOH (13.3 g; 2.0 mmol) in water (11 ml) was added and stirred for 10 minutes. The white solid that separated was filtered under N_2 and washed with ice cold 95% methanol and dried in vacuum at 80°C. Yield 75.5%. Decomposes at about 500°C.

5.1.3g **Synthesis of tris(((2-hydroxybenzyl)amino)ethyl)amine (reduced SALTREN)**

This was prepared also following the published procedure [135]. $Na_2B_4O_7$ (1.0 g) was added to a solution of saltren (2.3 g; 5 mmol) in methanol (75 ml) and stirred. To this solution, solid KBH_4 (1.06 g; 20 mmol) was added in small portions over 30 minutes. The reaction mixture was stirred for another 2 hr. The solvent was removed under low pressure, the residue treated with a solution of NH_4Cl (5 g) in water (50 ml) and finally the desired compound was extracted with chloroform (3 x 50 ml). The chloroform layer was washed with water and dried over anhydrous Na_2SO_4. The removal of chloroform followed by vacuum-drying afforded a yellow solid. Yield 79%. m.pt. 44-47°C (lit. 45-47°C).

5.1.3h **Tripod-Tripod Coupling of Reduced SALTREN and Tris(2-chloroethyl)amine hydrochloride in Presence of CaH_2**

Reduced SALTREN (0.29 g; 0.5 mmol) was dissolved in THF (300 ml) and to this solution, solid CaH_2 (84 mg; 2 mmol) was added and stirred well at 70°C. Tris(2-chloroethyl)amine hydrochloride (0.12 g; 0.5 mmol) in THF (150 ml) (dissolved by warming) was added dropwise over a period of 5 hrs and resulting mixture was stirred at 70°C for another 12 hr. Then THF was completely removed and the residue obtained is shaken with water (25 ml) and extracted with $CHCl_3$. The chloroform layer was dried over anhydrous Na_2SO_4 and filtered. The filtrate on removal of $CHCl_3$ gave a yellow oily liquid. ^{1}H-NMR (80 MHz, $CDCl_3$) was taken on this sample. However, it was found to be mixture of products that included the desired cryptand. The FAB-mass spectrum showed the presence of the desired cryptand (m/z =560) only as a minor peak.

5.2 **Synthesis of Metal Cryptates**

The cryptand readily forms solid complexes with metal ions like Ni(II), Cu(II) and Zn(II). With Fe(II) and Mn(II) it gives only glassy products which were not probed further in the present research.

5.2.1 **Synthesis of** $[L^3 \subset Zn(II)](ClO_4)_2$, **1**

$[Zn(H_2O)_4](ClO_4)_2$ (0.16 g; 0.5 mmol) in MeOH (20 ml) was slowly added to a stirred solution of the ligand (0.28 g; 0.5 mmol) in MeOH (25 ml) at RT. A white solid precipitated out immediately which was collected by filtration, washed with MeOH and air-dried to obtain the desired product in 70% yield.

^{1}H-NMR (80 MHz, CD_3CN, ppm): 2.85 (s br, 12H, a & b); 3.2 (t, 6H, e); 3.9 (s, 6H, c); 4.3(t, 6H, d) and 7.2 (m,12H, aromatic).

FAB-mass spectrum (Fig. 5.7) for this cryptate showed two prominent peaks around m/z values of 722 and 622 corresponding to the ions formed by the liberation of one and two perchlorate anions respectively.

5.2.2 **Synthesis of** $[L^3 \subset Cu(II)](ClO_4)_2$, **2**

A solution of $[Cu(H_2O)_6](ClO_4)_2$ (0.18 g; 0.5 mmol) in MeOH (15 ml) was added to a stirred solution of (L^3) (0.28 g; 0.5 mmol) in MeOH (30 ml) at RT. A greenish-blue solid precipitated out immediately which was collected by filtration, washed with MeOH (20 ml) and air-dried. Yield 80%.

FAB-mass spectrum (Fig. 5.8) showed two prominent peaks around m/z 721 and 622 like in the case of cryptate, **2**. The peaks correspond to the ions generated by the liberation of one and two

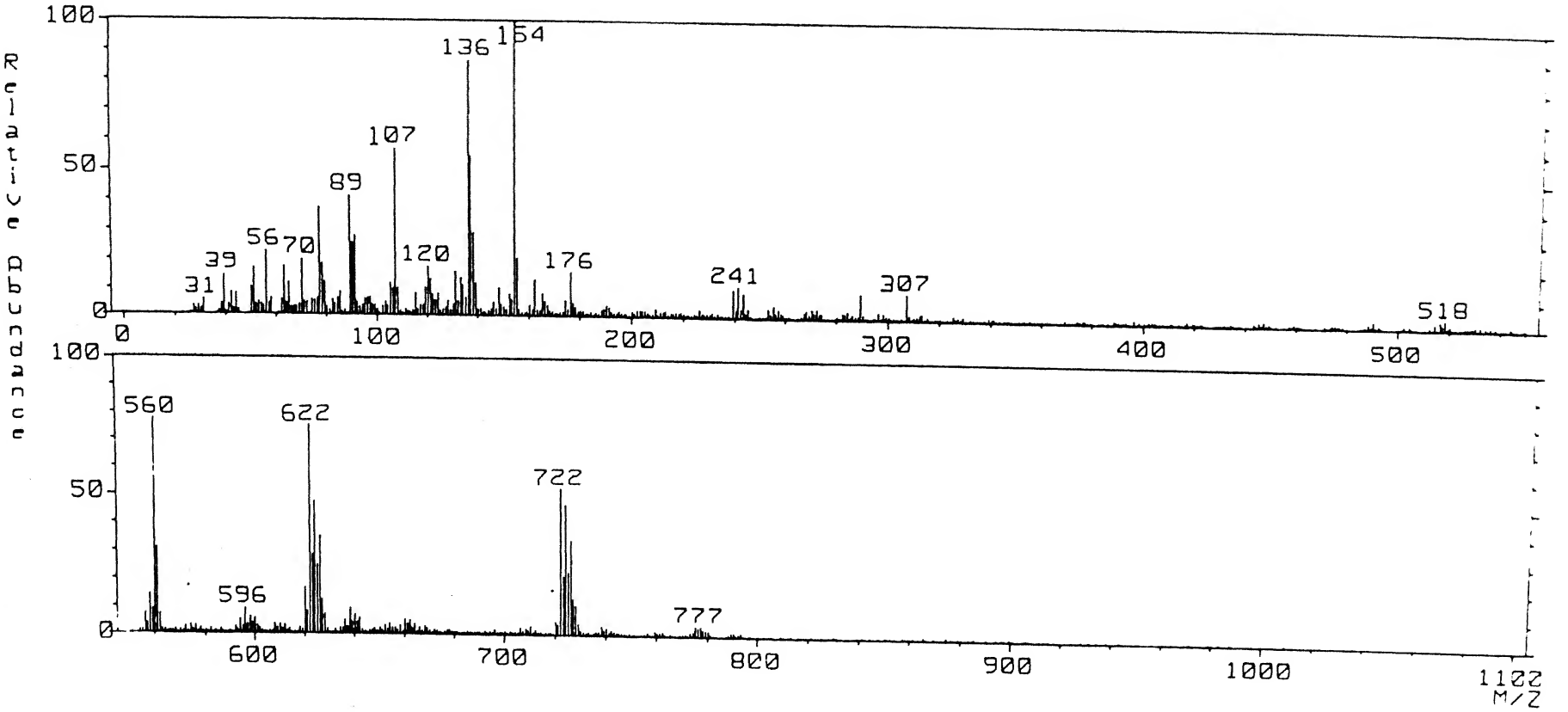

Fig. 5.7 FAB-mass spectrum of the cryptate, **1**

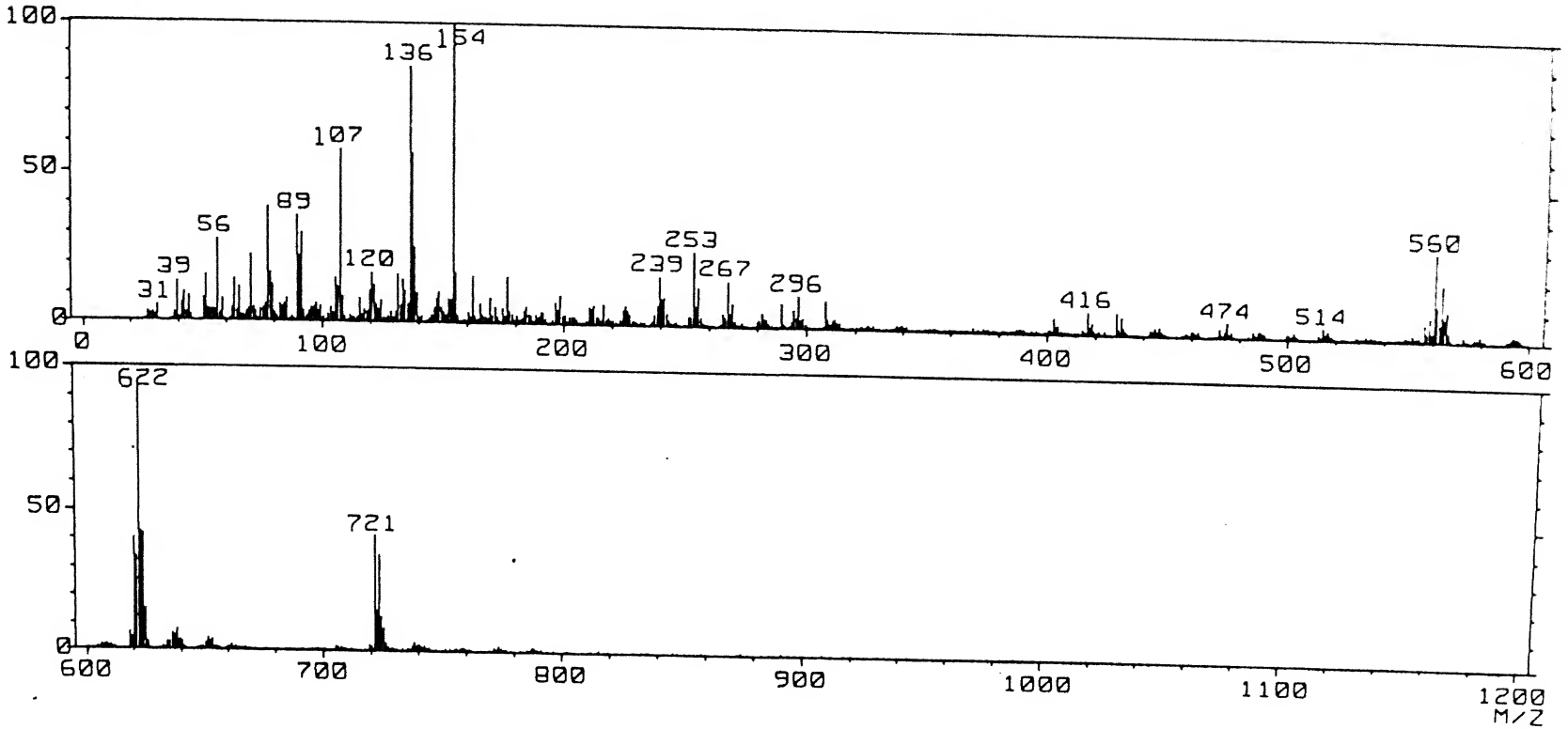

Fig. 5.8 FAB-mass spectrum of the cryptate, **2**

perchlorate ions respectively.

5.2.3 Synthesis of $[L^3_C Ni(II)](ClO_4)_2$, 3

This complex was prepared as above by treating $[Ni(H_2O)_6].(ClO_4)_2$ with L^3) in warm (40°C) MeOH. The complex was obtained as a blue-violet solid in 68% yield upon partial evaporation of the solvent.

FAB-mass spectrum (Fig. 5.9) again showed two prominent peaks around m/z 716 and 616 corresponding to the ions formed by the liberation of one and two perchlorate ions respectively.

5.2.4 Synthesis of $[L^3_C Cu(II)(N_3)](ClO_4)$, 4

Cryptate, **2** (0.21 g; 0.25 mmol) was dissolved in acetonitrile (20 ml) and stirred with a solution of NaN_3 (0.16 g; 0.25 mmol) in water (2 ml). Colour of the solution immediately changed to dark green which on evaporation afforded a dark green solid in 80% yield.

FAB-mass spectrum (Fig. 5.10) showed peaks corresponding to the ions generated by the liberation of the azide group (m/z 723) and then by the liberation of the perchlorate group (m/z 622). The FAB-mass spectral result suggests that the azide group is not very strongly bound to the cryptate.

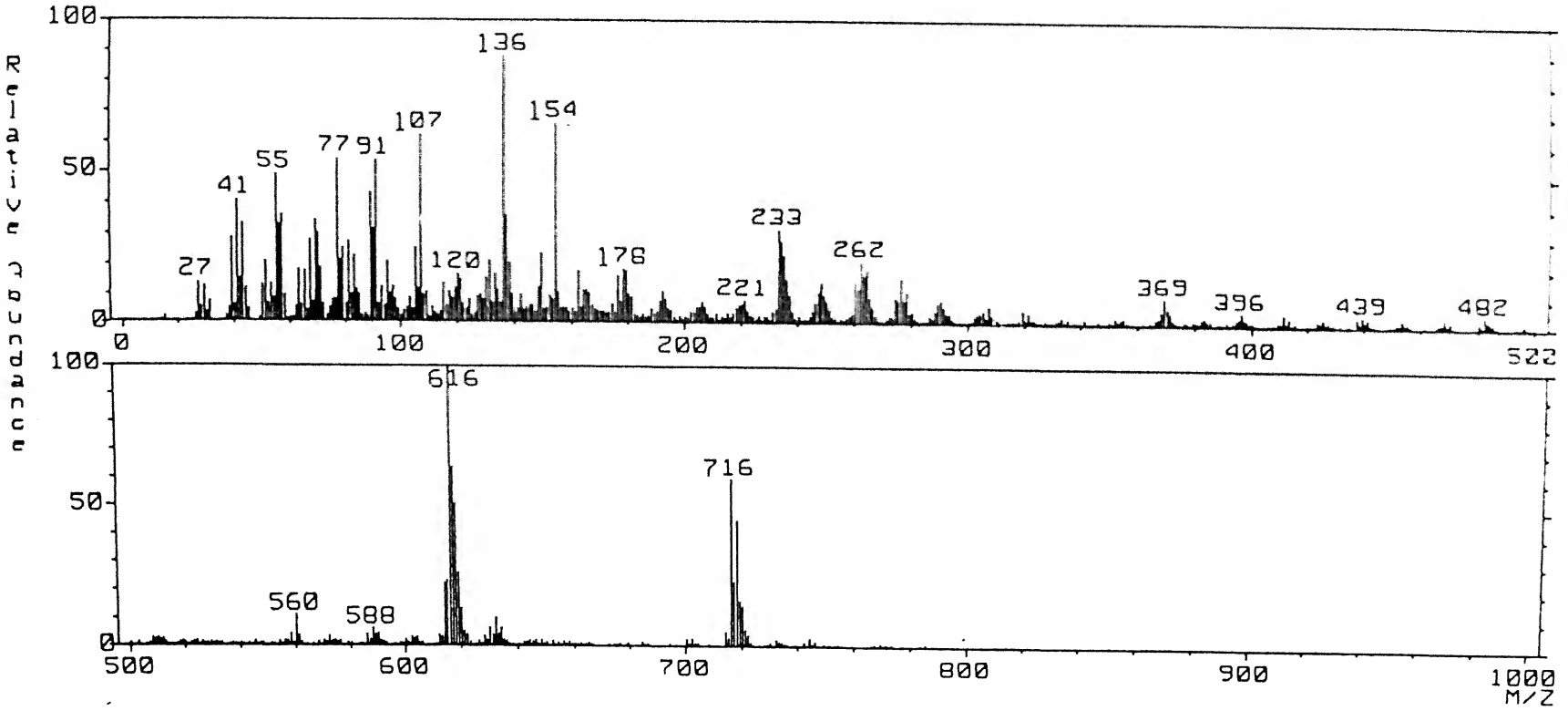

Fig. 5.9 FAB-mass spectrum of the cryptate, 3

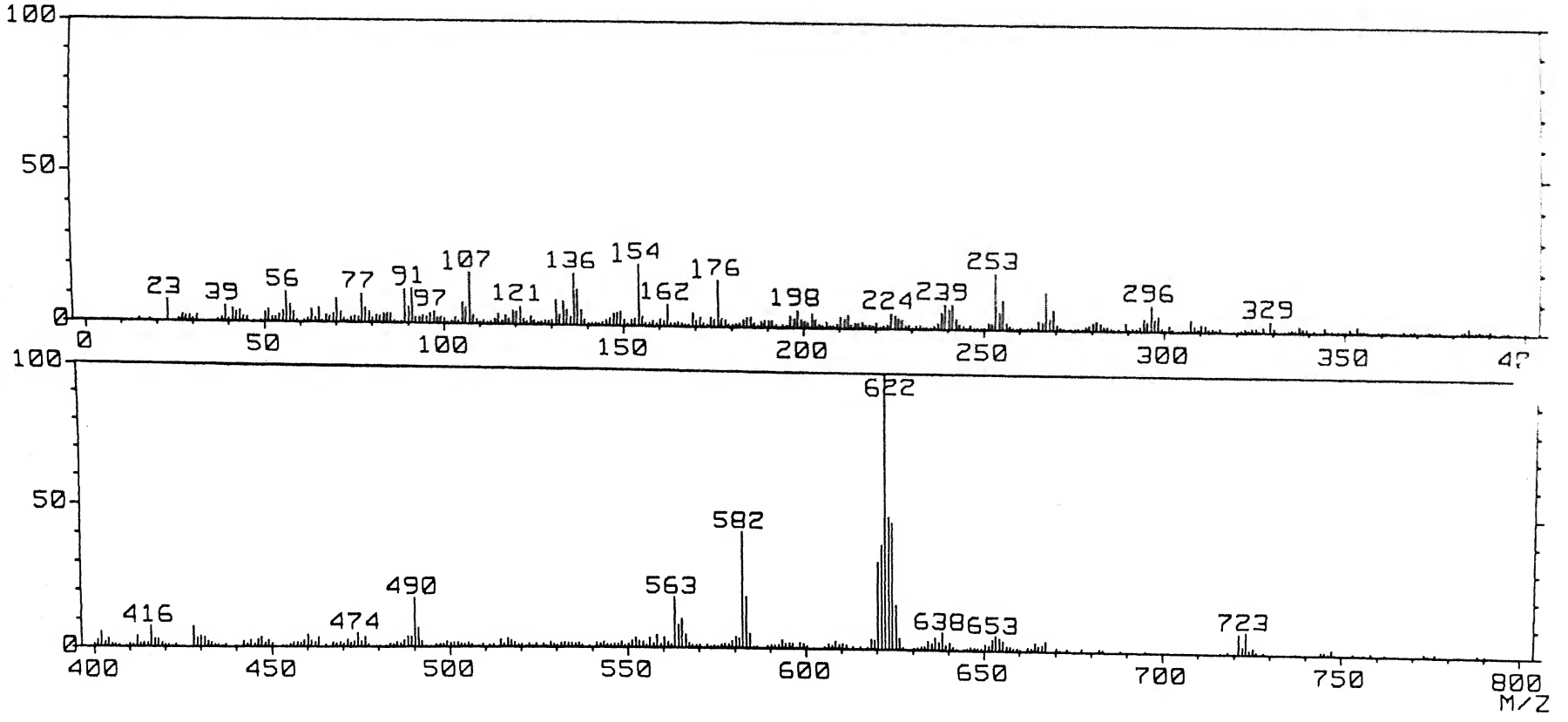

Fig. 5.10 FAB-mass spectrum of the cryptate, **4**

5.2.5 **Synthesis of** $[L^3_C Ni(II)(N_3)](ClO)_4$, 5

Cryptate, 3 (0.21 g; 0.25 mmol) dissolved in warm methanol (35 ml) was stirred with a solution of NaN_3 (0.16 g; 0.25 mmol) in water (2 ml). Colour of the solution changed to blue-purple which yielded blue-purple solid in 73% yield on slow evaporation at RT.

FAB-mass spectrum (Fig. 5.11) like in the case of **4**, showed the peaks due to the ions generated by the liberation of the azide (m/z 716) followed by the perchlorate group (m/z 616).

5.2.6 **Synthesis of** $[L^3_C Cu(II)(N_3)]N_3$, 6

Cryptate **2** (0.21 g; 0.25 mmol) in acetonitrile (35 ml) when treated with a solution of NaN_3 (0.32 g; 0.5 mmol) in water (3 ml) afforded **6** as a dark green solid in 76% yield.

5.2.7 **Synthesis of** $[L^3_C Ni(II)(N_3)]N_3$, 7

This complex was synthesized from the cryptate, **3** as above in aqueous hot MeOH as blue-purple solid in 64% yield.

5.2.8 **Synthesis of** $[L^3_C Cu(II)(H_2S)](ClO_4)_2$, 8

H_2S gas was passed through a solution of **2** (0.42 g; 0.5 mmol) in acetone (15 ml) for 5 minutes at 293 K. The dark green solution which formed, gave dark green solid on slow evaporation

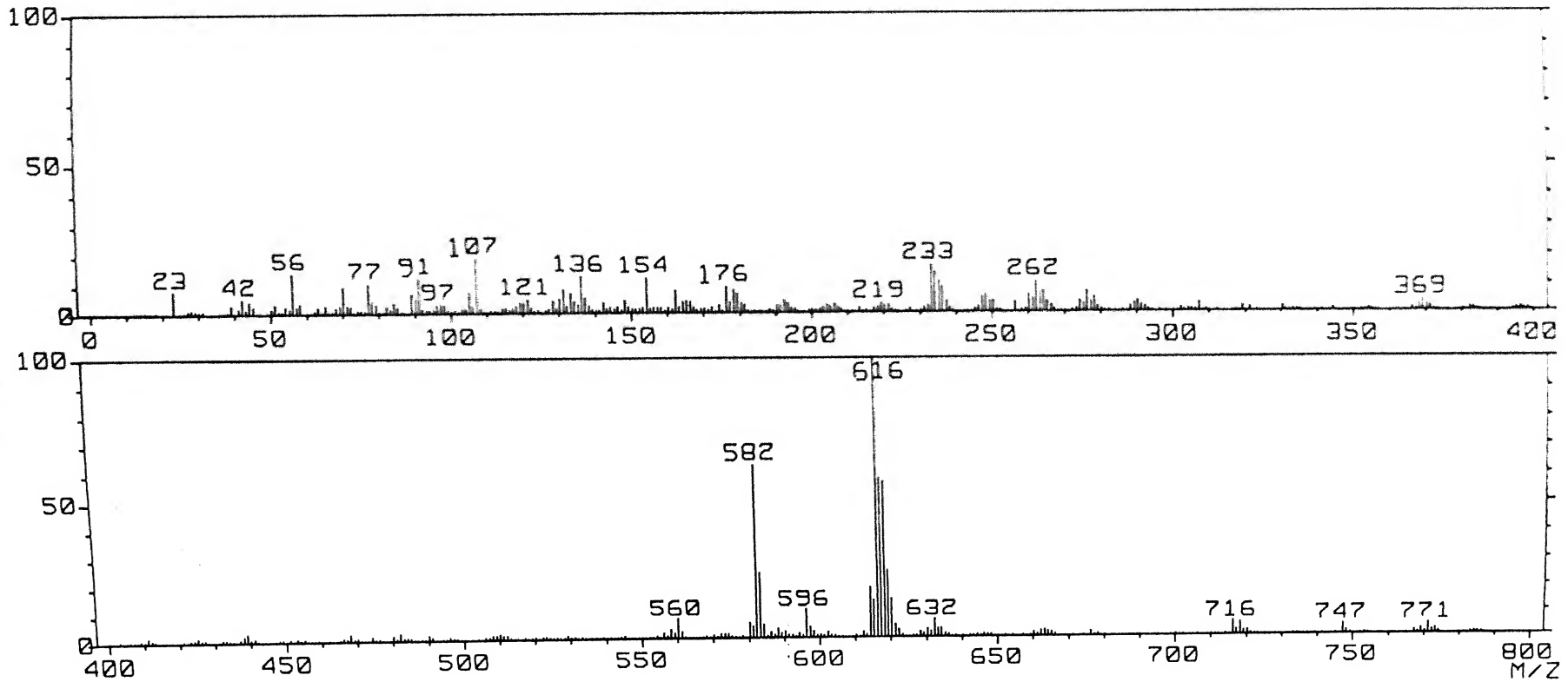

Fig. 5.11 FAB-mass spectrum of 5

in about 60% yield.

FAB-mass spectrum (Fig. 5.12) showed three peaks due to the ions generated by the liberation of one perchlorate (m/z 762), liberation of two perchlorates (m/z 660) and finally liberation of H_2S (m/z 622). The base peak corresponded to the free ligand. $CuL^3(H_2S)+2H^+$; 662, CuL^3; 560, L^3.

Elemental analyses for the cryptates are collected in Table 5.1.

5.3 **Results and Discussion**

The hetero-ditopic cryptand L^3 was prepared by tripod-tripod Schiff base condensation of tren and trialdehyde in presence of Cs(I) ion as the template followed by reduction with $NaBH_4$. The Schiff base was highly unstable and so it was reduced <u>in situ</u> with $NaBH_4$. The reaction is very facile as evident from the 70% yield of the cryptand. The two tripod units are ideally oriented in presence of Cs(I) ion for the coupling reaction. In the absence of Cs(I) ion, no product of definite composition could be isolated. This clearly indicates the vital role of Cs(I) ion in this reaction. It is of importance to note that the product isolated was analytically pure. The ^1H NMR (80 MHz) spectrum (Fig. 5.3) shows a multiplet for the protons on carbons **a** and **b** at δ 2.5 . The protons on **c** appear as singlet at δ 3.9. The

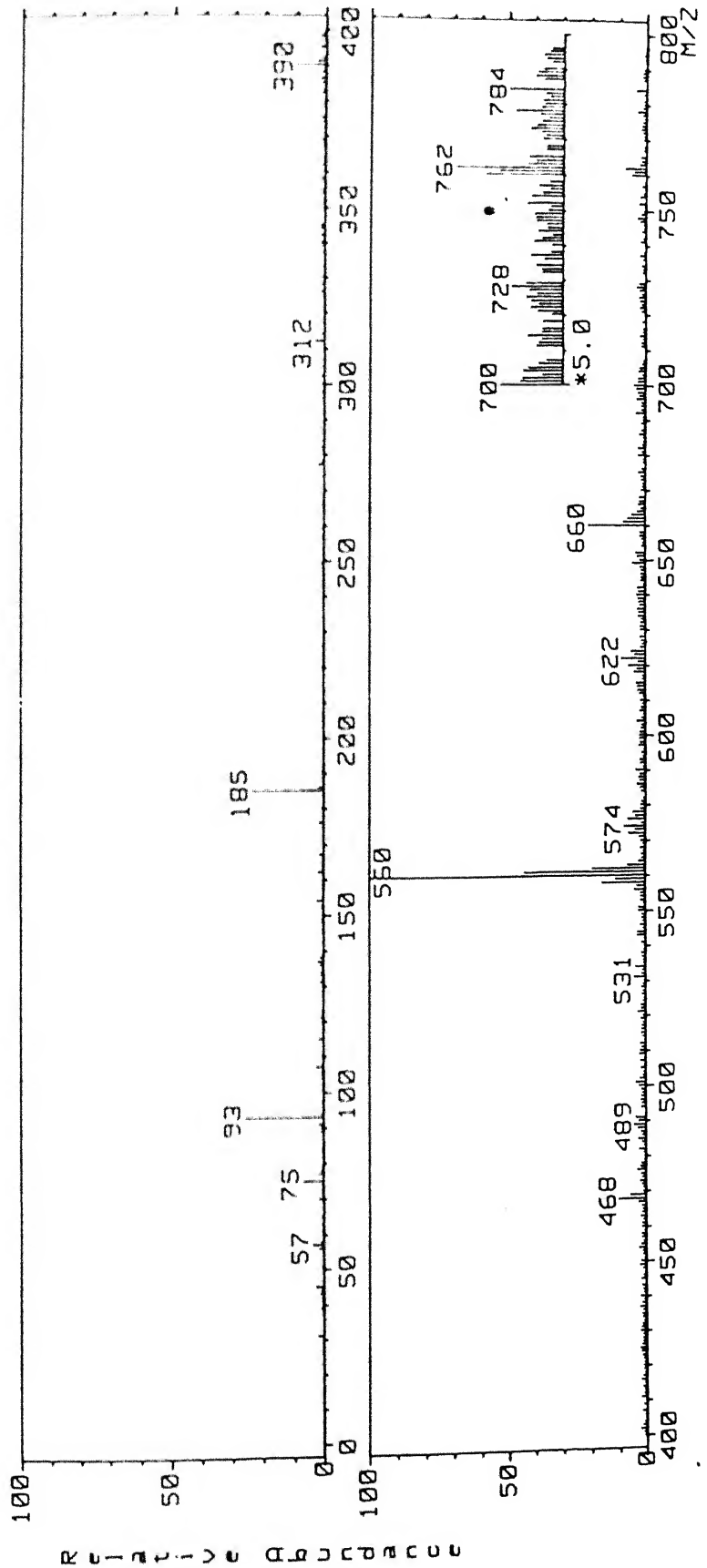

Fig. 5.12 FAB-mass spectrum of 8

protons on carbon **d** and **e** appear as triplets at δ 3.8 and 4.1. The aromatic protons appear as multiplets at δ 7.5. The ^{13}C-NMR spectrum (Fig. 5.4) shows the five aliphatic resonance peaks at 47.06, 48.60, 54.37, 55.30, 57.55 and aromatic resonance peaks at 111.29, 120.63, 127.16, 128.70, 131.33 and 156.35 δ. These spectral results indicate the presence of C_3 symmetry in the molecule. The FAB-Mass spectrum shows the base peak at M/Z 560 corresponding to the molecular ion $[L^3]^+$.

The cryptand has two receptor sites with N_4 and NO_3 donor sets. The donor sets are bridged by benzyl groups. This should provide rigidity to the donor sites owing to the flattened nature of the aromatic groups and the restricted rotation of the bonds in the benzyl moiety. The N_4 donor set can easily form complexes with transition metal ions which has the tendency to form four coordinate complexes. Molecular modelling studies show that the N_4 donor set describes a distorted tetrahedral geometry. Due to the ligand structure, the N_4 donor set can impose this distorted tetrahedral geometry on to the metal ions. The other end which has NO_3 donor set are not strong donors for transition metal ions because of the poor donor ability of the ethereal oxygens. Characterisation of the cryptates is described next.

5.3.1 {Zn(II), 1}, {Cu(II),2} and {Ni(II), 3} cryptates

The cryptand readily forms mononuclear complexes with Ni(II), Cu(II) and Zn(II) ions as their perchlorate salts. They are stable in air and soluble in common organic solvents. Molecular conductivity data (Table 5.1) of the complexes in MeCN (ca. 1 x 10^{-3} M) at RT correspond [86] to 1:2 electrolytes. Complexes 1-3 exhibit a strong and broad peak at 1100 cm^{-1} where the free ligand absorbs only weakly. This peak is due to the presence of ionic perchlorates [100]. Perchlorate anion is a poor donor for transition metal ion. Besides, the perchlorate group should not be able to penetrate the cavity of the cryptand and make direct bonds with the metal ion inside.

Electronic spectral results of the complexes in acetonitrile at RT are presented in Table 5.2 while the spectra of 2 and 3 are shown in Figs. 5.13a and 5.13b respectively. The free ligand or the Zn(II)-cryptate (1) does not absorb at wavelengths longer than 280 nm. However, at higher energies, both exhibit strong absorptions.

The band positions for any of the Cu(II)-complexes do not change upon changing the solvent from MeOH to better coordinating MeCN indicating no solvent coordination with the metal ions. Electronic absorption spectrum for the complex $[L^3\ Cu(II)](ClO_4)_2$

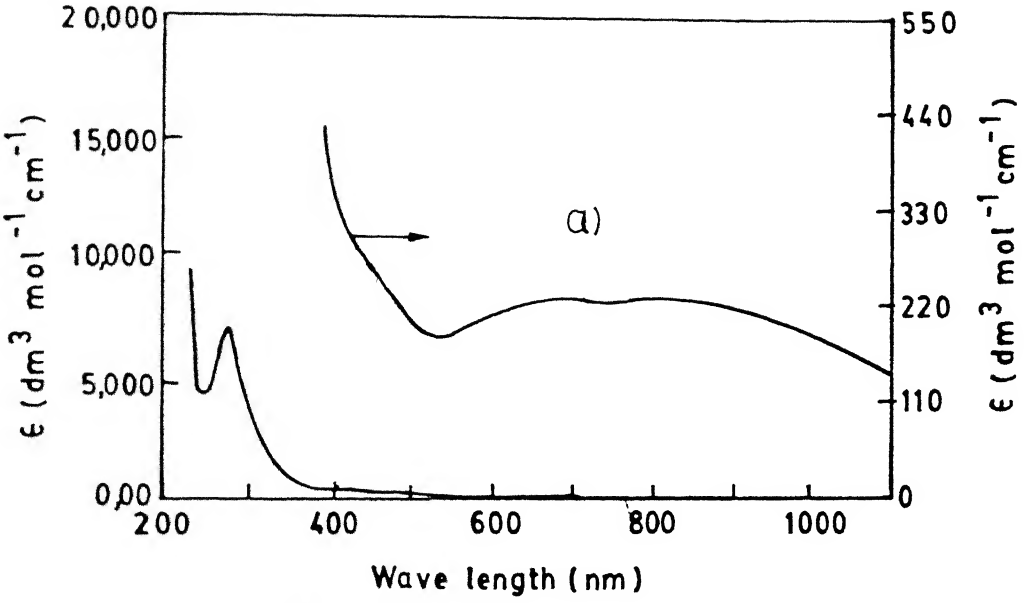

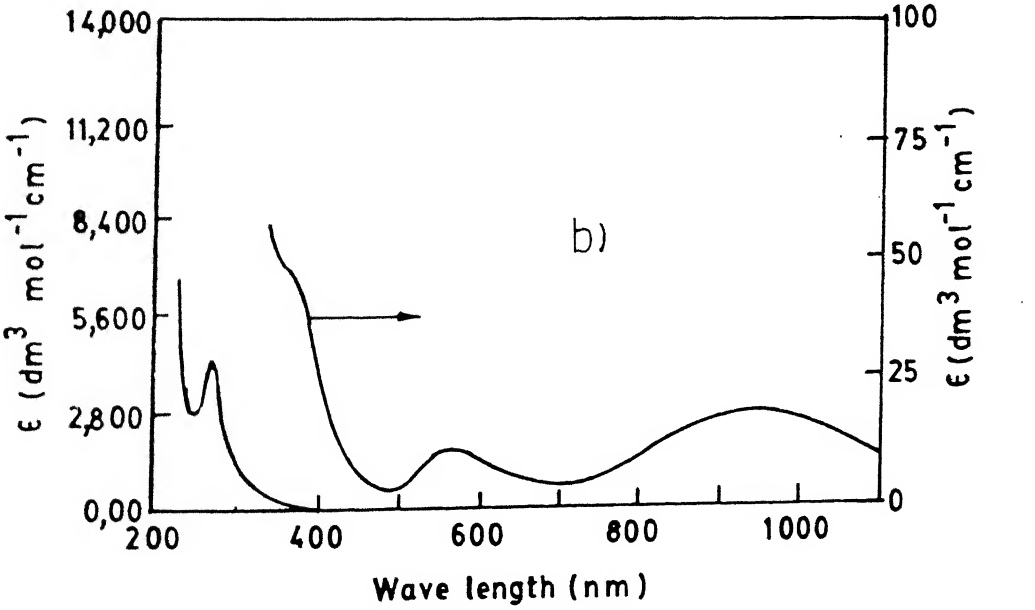

Fig. 5.13 Electronic absorption spectra of 2 (a) and 3 (b) in acetonitrile

(2), is expected to be simple consisting of the ligand field bands in addition to one LMCT transition from σ(N)--> Cu(II). The number as well as positions of the ligand field bands are quite sensitive [137] to the coordination geometry. As the geometry distorts from planarity towards tetrahedral, the overall splitting of the d-orbital energy levels will decrease leading to red-shifts for the d-d bands. For a D_{2d} Cu(II) complex, three d-d absorptions are expected [138]. In cryptate 2, the ligand field band positions are significantly red-shifted compared to those with known square planar CuN_4 chromophores [139] and agrees well with those observed with an x-ray crystallographically characterised [140] pseudotetrahedral CuN_4 complex with the geometrically constraining bidentate ligand, 2,2'-bis(2-imidazolyl)biphenyl. Other pseudotetrahedral CuN_4 complexes also exhibit [140] similar ligand field transitions. The LMCT transition of σ-symmetry involving a primary amine and Cu(II) appears at about 240 nm [91]. Alkylation of the amine lowers its ionization potential and causes red-shift of this transition. Therefore, in 2, the strong peak at 275 nm is assignable to this transition. As the free ligand or the Zn(II)-complex absorbs slightly at 275 nm, this peak should be mixed σ(N) --->Cu(II) and

ligand localized transitions.

The Ni(II)-cryptate **3**, shows three ligand field bands (Table 5.2) with low intensities in acetonitrile. The positions of these bands do not shift noticeably upon changing to a solvent with different coordinating ability like methanol. The perchlorate anion, having a large size cannot enter the cavity to make direct bond(s) with the Ni(II) ion. Therefore, The Ni(II) ion can either be hexa-coordinated to N_3O_3 donor set being in the middle of the cavity or can be tetracoordinated to N_4 donor set at the tren-end. Pseudotetrahedral NiN_4 complexes are rare in the literature [140,141]. The structurally characterized [140] pseudotetrahedral NiN_4 chromophore shows three d-d bands at 770, 640 and 470 nm. Another pseodotetrahedral NiN_4 complex [141] shows ligand field absorptions at 1170, 940, 613 and 560 nm. If ligand field band positions are any indication, the coordination geometry around Ni(II) in **3** should then be pseudotetrahedral rather than distorted octahedral. The LMCT transitions involving the nitrogens and Ni(II) should occur [133] at higher energies compared to those involving Cu(II). Hence, these transitions will be mixed with the intra-ligand transitions.

The effective magnetic moment (μ_{eff}/μ_B) for the Cu(II)-complex **2** after diamagnetic corrections is found to be 1.97 at

301 K. This value is consistent with the discrete, mononuclear formulation for the complex. Other pseudotetrahedral CuN_4 complexes [140] show RT magnetic moment values in the same range. For a tetrahedral Ni(II) complex, the ground term is $^3T_1(F)$ which has significant orbital angular momentum so that a complex having the perfect T_d symmetry, should show [142] an effective magnetic moment of 4.2 at RT. Distortion from the ideal T_d symmetry causes further splitting of the orbital degeneracy. As a consequence, the effective magnetic moment value decreases. Thus, for pseudotetrahedral complexes [143] the observed values lie in the range, 2.7-3.5 at RT. The x-ray crystallographically characterised NiN_4 complex [140] where the dihedral angle is 87.6° (a dihedral angle of 90° corresponds to perfect tetrahedral geometry) gives the magnetic moment of 3.5 at RT. For 3, this value is 2.89 at RT suggesting the coordination symmetry to be quite distorted from T_d.

The EPR spectra of the Cu(II)-cryptate was recorded in the solid state as well as in acetonitrile (ca. 1×10^{-3} M) both at 298 and 77 K. The data are presented in Table 5.3 while the solution spectra are shown in Fig. 5.14. The cryptate displays a broad signal with g_{av} = 2.07 in the solid state at 298 K which

sharpens somewhat on cooling to 77 K. Thus, the pure solid sample is not magnetically dilute to exhibit resolved ESR spectra indicative of its stereochemistry. The solid-state spectra are, therefore, not shown; only the data are presented. In MeCN solution at 298 K, it exhibits an axial spectrum (Fig. 14a) characteristic of a Cu(II)-complex with the $d_{x^2-y^2}$ ground state. The characteristics of the RT spectrum are: not so high $g_{\parallel}$ and very low $A_{\parallel}^{Cu}$ values. The $g_{\parallel}$ value of 2.12 is, however, within the limit for a pseudotetrahedral CuN_4 complex [102]. The $A_{\parallel}^{Cu}$ value (61×10^{-4} cm^{-1}) is the smallest observed so far for a CuN_4 complex and matches quite closely with the value [37] obtained on metalloproteins like plastocyanin, azurin etc. For tetragonal geometry the expressions for $g_{\parallel}$ and $g_{\perp}$ are [144]

$$g_{\parallel} = g_e + -8\xi / \Delta E_{xy} \quad \text{and}$$
$$g_{\perp} = g_e + -2\xi / \Delta E_{xz,yz} \qquad (5.1)$$

E_{xy} is the energy difference between d_{xy} and $d_{x^2-y^2}$(ground state); similar for $E_{xz,yz}$; ξ is the one electron spin-orbit coupling parameter. The hyperfine couplings are expressed as:

$$A_{\parallel} = P_d[-\chi -4/7\alpha^2 + (g_{\parallel}-2)+3/7(g_{\perp}-2)] \quad \text{and}$$
$$A_{\perp} = P_d[-\chi +2/7\alpha^2 + 11/14(g_{\perp} -2)] \qquad (5.2)$$

where χ is the contribution from the indirect Fermi contact, and the second term is the anisotropic dipolar contribution; P_d is a

constant which is ca. 350×10^{-4} cm^{-1} for the free copper ion. As these equations indicate, both $g_{||}$ and $A_{||}$ values are dependent on the ligand field strength; specially in the equatorial plane. As the geometry distorts towards tetrahedral, $g_{||}$ value tend to increase while the $A_{||}$ value decreases sharply. The ligand field strength here is low due to distortion of the coordination geometry towards tetrahedral (D_{2d}) which accounts for the observed $g_{||}$ and $A_{||}^{Cu}$ values. In acetonitrile glass (77 K), the signal is still axial (Figure 14b) and the g values change slightly although the parallel hyperfine coupling increases substantially ($A_{||}^{Cu} = 93 \times 10^{-4}$ cm^{-1}). This is attributable to the conformational changes in the ligand superstructure upon cooling, resulting in D_{2d} flattening of the coordination geometry.

Electron transfer properties of the complexes 2 and 3 were probed by cyclic voltammetry at RT on dinitrogen flushed solutions. Neither of the complexes show any cyclic responses in the region, +1.0 to -1.0 V. Only ill-defined peaks are found in the forward scan which disappear in the reversed scan. However, when scanning the negative side, a sharp peak is observed near -0.25 V in case of the Cu(II)-cryptate. The shape and nature of

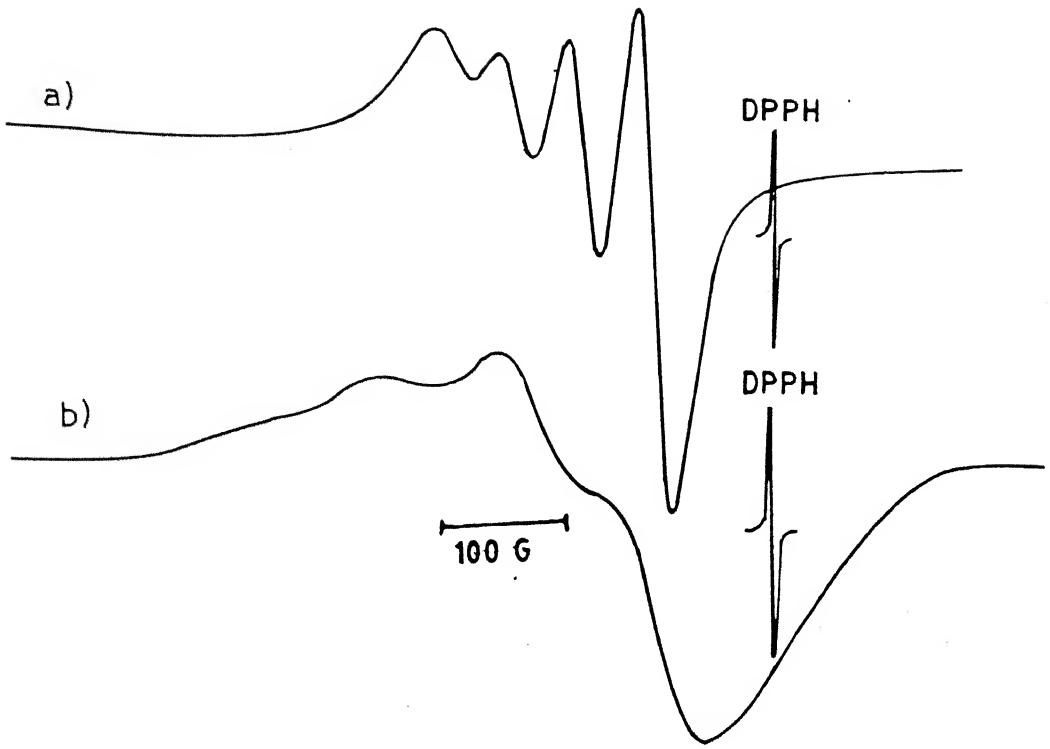

Fig. 5.14 Solution EPR spectra of 2 at (a) 298 K and (b) 77 K in acetonitrile

this peak is attributable to the oxidation of metallic copper deposited at the electrode [99]. The absence of any cyclic response in the voltammograms of either complex is due to the rigidity of the donor atoms' topology. However, rigidity of the N_4-donor set does not allow its spatial rearrangements upon reduction or oxidation of the metal-ligand ensemble. Besides, the strong -donating amino nitrogens favour +2 state over +1 state. Both of these lead to irreversibility of the cyclic redox processes.

5.4. Secondary Recognition by the Cu(II)- and the Ni(II)-Cryptates Towards N_3^- and H_2S

5.4.1 Recognition Towards the Azide Group

Both the cryptates **2** and **3** readily reacts with the azide anion at RT. Thus, when allowed to react with NaN_3 in 1:1 molar equivalents, one of the perchlorates is replaced forming complexes $[L^3C\,Cu(II)(N_3)](ClO_4)$ (**4**) and $[L^3CNi(II)(N_3)](ClO_4)$ (**5**). When allowed to react with two equivalents of NaN_3, both the perchlorates are replaced by N_3 to form $[L^3C\,Cu(II)(N_3)]N_3$ (**6**) and $[L^3C\,Ni(II)(N_3)]N_3$ (**7**). The molar conductance values for these complexes lie in the range, 140-150 $ohm^{-1}cm^2mol^{-1}$ in acetonitrile that correspond to the 1:1 electrolytic nature of the complexes.

These data also indicate that the azide group is directly bonded to the metal ion. The azide group cannot be strongly bonded to the metal ion in these complexes as the FAB-mass data given in the experimental section indicate. Similar observation has been reported in the literature [55] for a dicopper cascade complex with the azide ion where this ion is proposed to be coordinated simultaneously to both the Cu(II) ions. However, in the FAB-mass spectrum the molecular ion peak is not observed.

The $_{asym}(N_3)$ stretching vibrations in **4** and **5** occur at 2060 and 2065 cm^{-1} which are blue shifted compared to the free azide group (for NaN_3 this value is 2040 cm^{-1}). This is an indication [145] that the azide group is directly bonded to the metal ion in each complex. Two terminally bonded azide groups present in $[\{Ni(pepci)(N_3)_2(N_3)_2\}_2]$ (pepci = N-(2-pyridine-2-ylethyl)pyridine-2-carbaldimine) [146] and in $[\{Ni(terpy)(N_3)_2(N_3)_2\}_2]$ (terpy = 2,2:6,2-terpyridine) [147] show $_{asym}(N_3)$ at 2050 cm^{-1}. Both (**4**) and (**5**) also exhibit a strong and broad peak at 1100 cm^{-1} due to the presence of an ionic perchlorate [100] group. Two $_{asym}(N_3)$ stretching frequencies are observed in the infrared spectrum of either **6** (2060 and 2042 cm^{-1}) or **7** (2065 and 2041 cm^{-1}) indicating the presence of both

ionic and coordinated azide groups.

The electronic spectral data for the azide complexes (Fig. 5.15) are given in Table 5.2. No noticeable differences exist between the complexes **4** and 6 or between **5** and **7**. So, the electronic spectral characteristics of only **4** and 5 are discussed here. The strong binding of the azide group to Cu(II) in **4** is revealed by the noticeable changes in the d-d band positions and appearance of a new band at 390 nm (Table 5.2). However, the d-d band positions are quite different from those obtained on trigonal bipyramidal (TBP) $[Cu(tren)X]^{n+}$ [98] and $[Cu(ntb)X]^{n+}$ [93] (ntb = tris(2-benzimidazolylmethyl)amine; X = NCS^- , NH_3 etc, where n= 1 or 2) complexes. This indicates the overall symmetry to be different from TBP at RT which will be the case if the entire azide group does not enter the cavity and the bridgehead(N)-Cu(II)-(N_3^-) bonding is not coaxial. The band at 390 nm is assignable [48,96b&c] to the charge transfer transition involving a terminally bound azide group and Cu(II) ion.

The data in Table 5.2 indicate that the band positions for the ligand field as well as the charge transfer transitions in the complexes 5 and 7 shift only slightly with respect to the parent complex, 3. Be it as it may, the spectral positions do not conform [148] to the TBP coordination geometry around Ni(II).

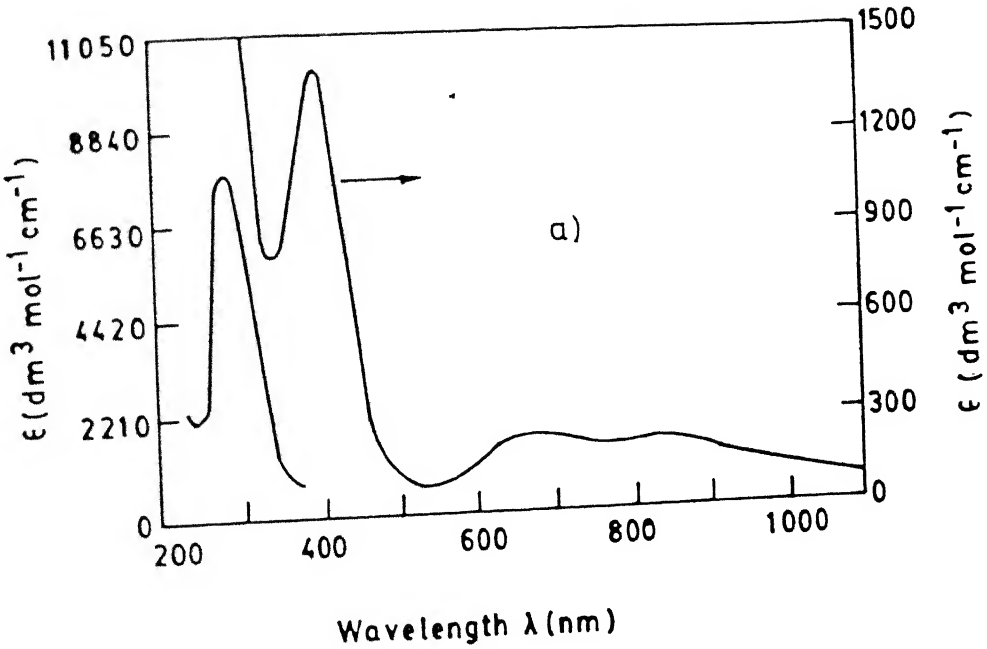

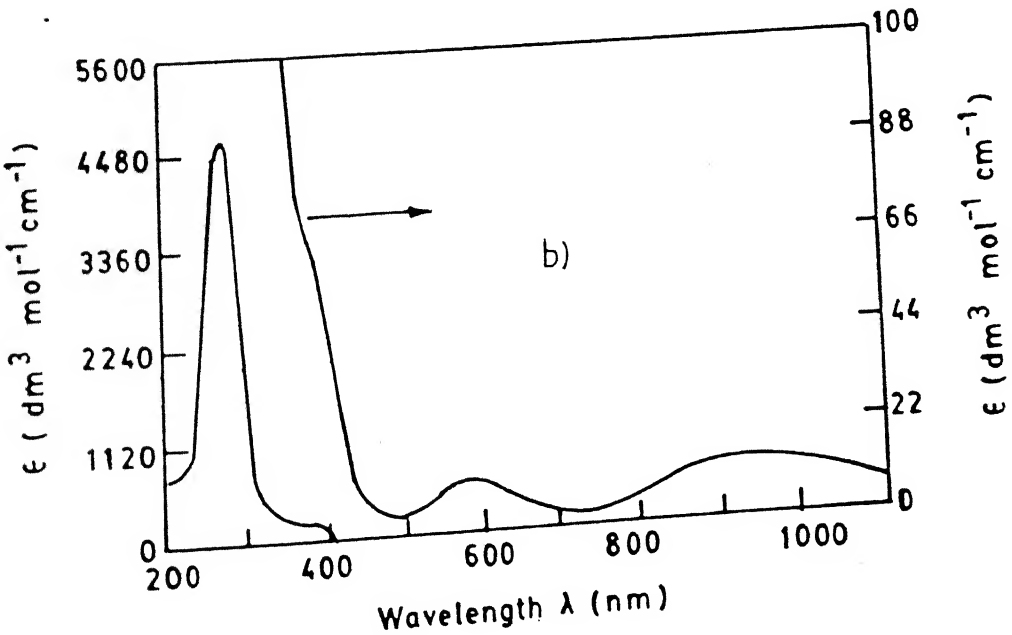

Fig. 5.15 Electronic absorption spectra of **4** (a) and 5 (b) in acetonitrile

The effective magnetic moment (μ_{eff}/μ_B) values for the azide complexes at 301 K are given in Table 5.3. The data for the Cu(II)-complexes are consistent with discrete, mononuclear formulations for these complexes. For the Ni(II)-complexes, the data are quite different from either high- or low-spin Ni(II)-complexes having TBP coordination [148] geometry.

All the EPR spectral data for **4** and **6** are given in Table 5.3 while only the solution spectra of **4** are shown in Fig. 5.16. Both show broad signals near g_{av}= 2.09 in the solid state at 298 or 77 K. On the other hand, in MeCN solution each exhibits a significantly rhombic signal at 298 K. Both the **g** and the **A** values are quite different from those of **2** and agrees [93] somewhat with trigonal bipyramidal $[Cu(ntb)X]^{n+}$ (X= NCS^-, NH_3, N_3 etc, where n=1 or 2) complexes. On cooling to 77 K, the spectrum changes to a 8-line spectrum quite similar to that obtained [93] with the TBP complex, $[Cu(ntb)N_3]N_3$ at 77 K. This is due to conformational changes in the ligand which in turn, enforces the coordination geometry of the CuN_5 chromophore towards TBP. An X-ray structure is available (<u>vide infra</u>) of the cryptand, L^3 where one H_2O molecule is included inside the cavity. This structure shows that the cryptand can undergo significant

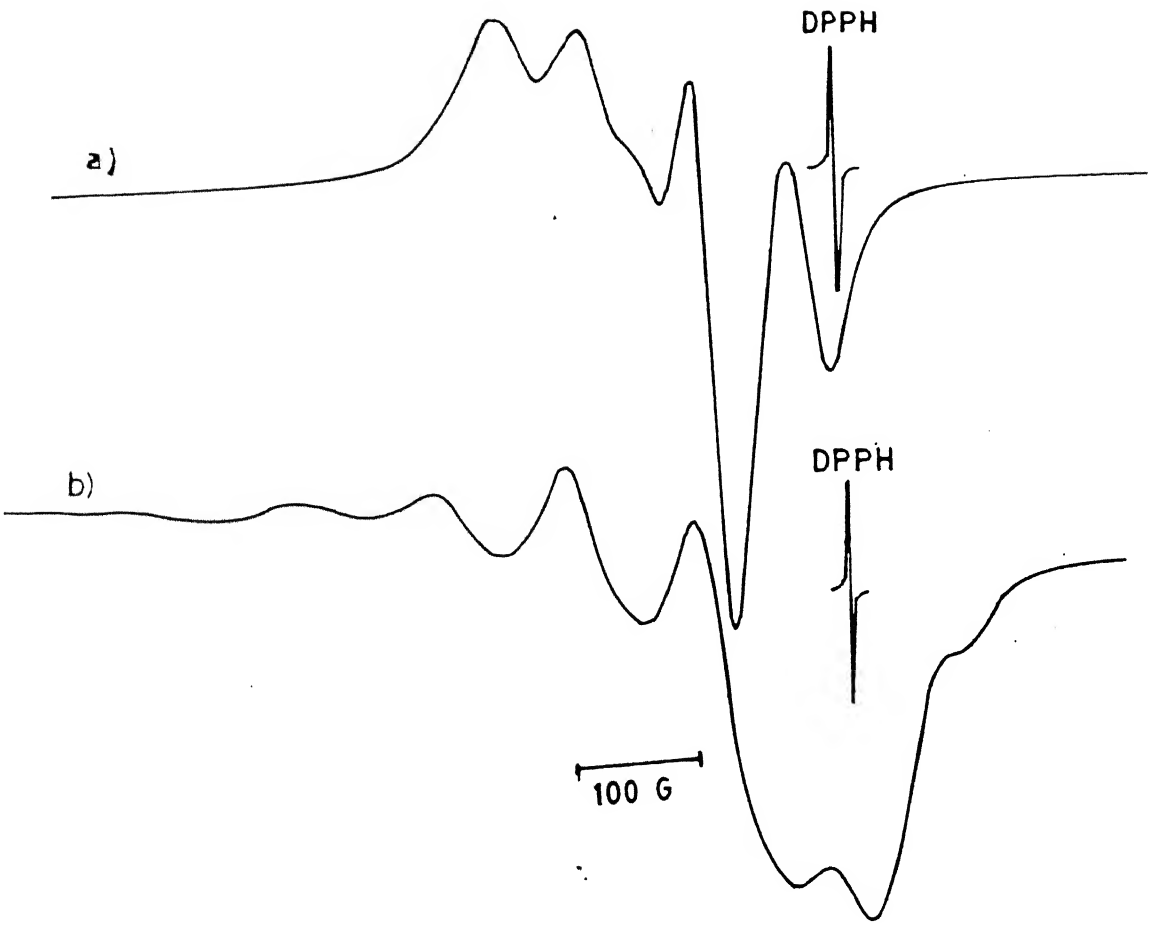

Fig. 5.16 Solution EPR spectra of **4** at (a) 298 K and (b) 77 K in acetonitrile

conformational changes.

Electron transfer properties of the complexes were probed by cyclic voltammetry at 298 K. None of the Cu(II)- or Ni(II)-azide complexes show any cyclic response in the region, +1.0 to -1.0 V. Only ill-defined peaks are found in the forward scan which disappear in the reversed scans. However, when scanning the negative side, a sharp peak is observed near -0.25 V in case of each of the Cu(II) complexes on scan-reversal from -1.0 V. The shape and nature of this peak is attributable [99] to the oxidation of metallic copper deposited at the electrode. This behaviour of the Cu(II) complexes are quite similar to the parent Cu(II)-cryptate.

5.4.2 Recognition Towards H_2S Molecule

Cryptate **2** forms a dark green solid when H_2S gas is passed through the solution of the cryptate in acetonitrile at RT. The complex is stable in air and is the first known Cu(II) bonded to H_2S. In solutions, however, it decomposes to a brown mass in about 5 days. The Ni(II)-cryptate, **3** does not give a product of definite composition with H_2S.

The FAB-Mass spectrum (Fig. 5.12) of the cryptate shows peaks at M/z 762, 660, 622 and 560 corresponding to the fragments

formed due to the release of one, two perchlorates, H_2S and the Cu(II) ion. The IR spectrum of the cryptate shows a weak band at 2565 cm^{-1} indicating the presence of H_2S molecule. This band occurs at slightly lower frequency (2560 cm^{-1}) for a tungsten complex [149]. Also a strong and broad peak appears near 1100 cm^{-1} attributable to the ionic perchlorates. The molar conductivity at 298 K in acetonitrile is 227 $ohm^{-1}cm^{2}mol^{-1}$ that corresponds to a 1:2 electrolyte.

In the elctronic spectrum (Fig. 5.17), a new band appears at 430 nm which is absent in the parent cryptate (2). Electronic spectral studies have been made on Ru(II) complexes having H_2S bonded to the metal ion [150]. These complexes show a low-energy band (430 nm) which is not present in the parent complexes. This band has been attributed to the LMCT transition involving H_2S and Ru(II). The 460 nm band in the present cryptate is similarly assigned. The strong band at 275 nm is assigned to σ(N)----> Cu(II) LMCT transition like in the case of the parent cryptate (vide supra). The cryptate exhibits ligand field transitions as a broad envelop centering at 865 nm.

The room temperature effective magnetic moment (μ_{eff}/μ_B) is 1.9 which corresponds to a discrete mononuclear Cu(II) complex. The EPR spectrum of the cryptate in solid state gives a broad

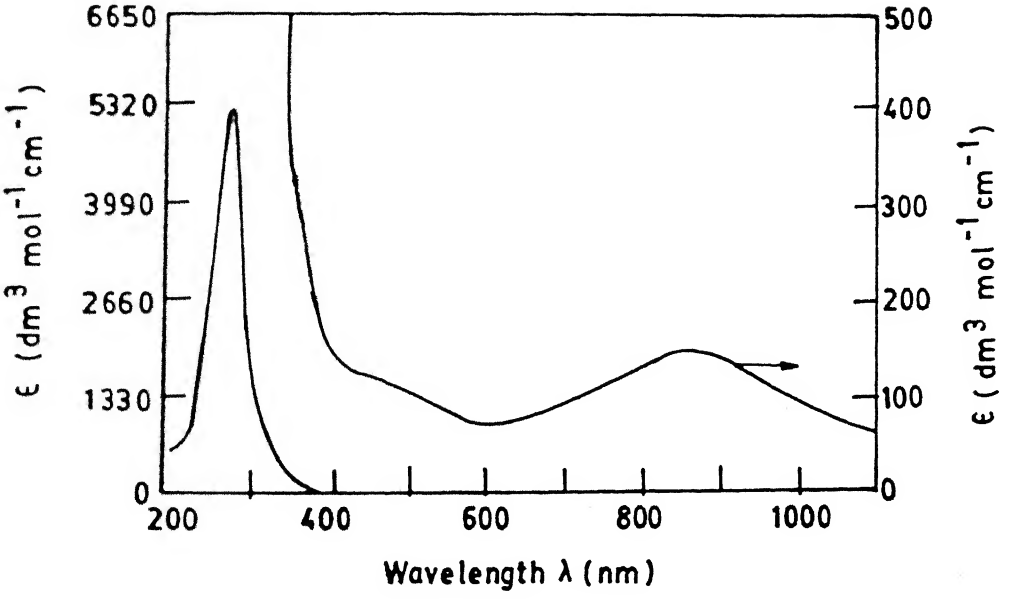

Fig. 5.17 Electronic absorption spectrum of **8** in acetonitrile

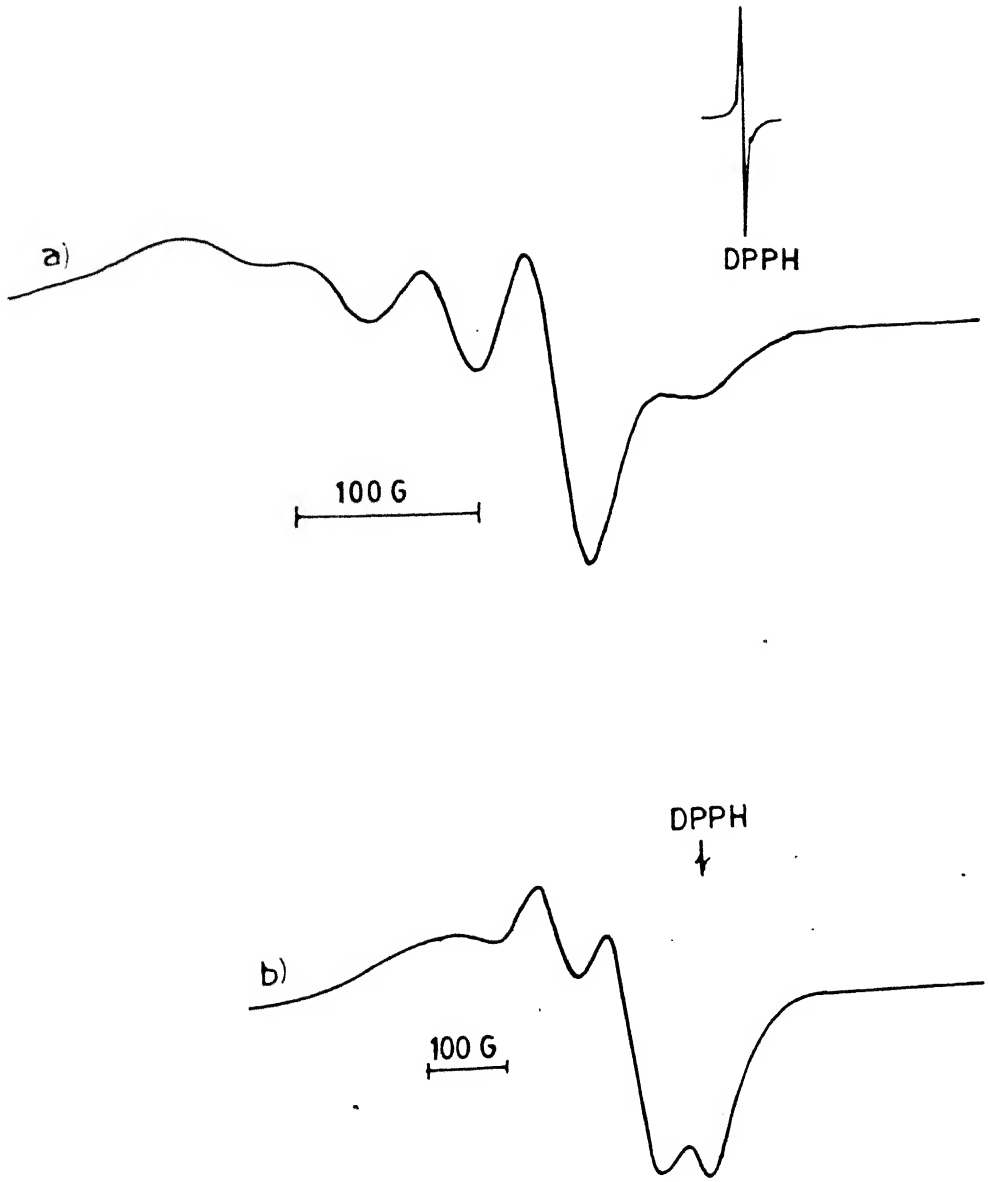

Fig. 5.18 Solution EPR spectra of 8 at (a) 298 K and (b) 77 K in acetonitrile

signal around $g_{av} = 2$, both at 198 and 77 K. The spectrum in acetonitrile (Fig. 5.18) at 298 K is slightly rhombic in nature with the g values; $g_1 = 2.13$, $g_2 = 2.07$ and $g_3 = 2.03$ while the $A_{||}$ value is 60×10^{-4} cm^{-1} (which is same as the value obtained on the parent cryptate). Thus the $A_{||}$ value does not change upon further coordination by H_2S. At 77 K, the spectrum (Fig. 5.18) is still rhombic. However, the $A_{||}$ value increases significantly to $103 \times 10^{-4} cm^{-1}$ while the g values change to a very small extent. The change in A value is due to conformational changes in the cryptand as in the case of **2**.

SECTION B

This section describes the synthesis of the hetero-ditopic receptor with naphthalene bridges (Fig. 5.19). This study is undertaken to probe the rigidity factor at donor atoms on varying the bridging unit from benzene rings to naphthalene rings. Also, the naphthalene groups should have more pronounced layer effects. The complexation with Zn(II), Cu(II) and Ni(II) has been probed and a successful air stable H_2S complex of Cu(II) has been studied. The ligand was prepared (shown schematically in Fig. 5.19) by tripod-tripod Schiff base condensation of tren and the

trialdehyde, in presence of Cs(I) ion followed by reducion with $NaBH_4$.

5.5 Synthesis of the Cryptand, L^4

The synthetic route is shown schematically in Fig. 5.19. The method is quite similar to the one adopted for the synthesis of L^3.

5.5.1a Synthesis of tris(2-chloroethyl)amine hydrochloride

This compound was prepared as mentioned in the **Section A.**

5.5.1b Synthesis of the trialdehyde

Potassium salt of 2-naphthol-1-carbaldehyde was prepared by shaking 2-naphthol-1-carbaldehyde (0.34 g; 2 mmol) in ethanol (50 ml) with KOH (3.4 g; 6 mmol) at RT for 20 minutes. To the resulting dark brown solution, solid tris(2-chloroethyl)amine hydrochloride (0.48 g; 2 mmol) was added and the mixture was refluxed with stirring for 3 hr. The dark brown solution obtained was allowed to cool to RT and then poured into water (100 ml). The oily mass settled at the bottom of the flask was separated out by decanting off the solution above followed by extraction with $CHCl_3$ (50 ml). The chloroform layer was treated with decolorizing charcoal and concentrated to 15 ml. To this

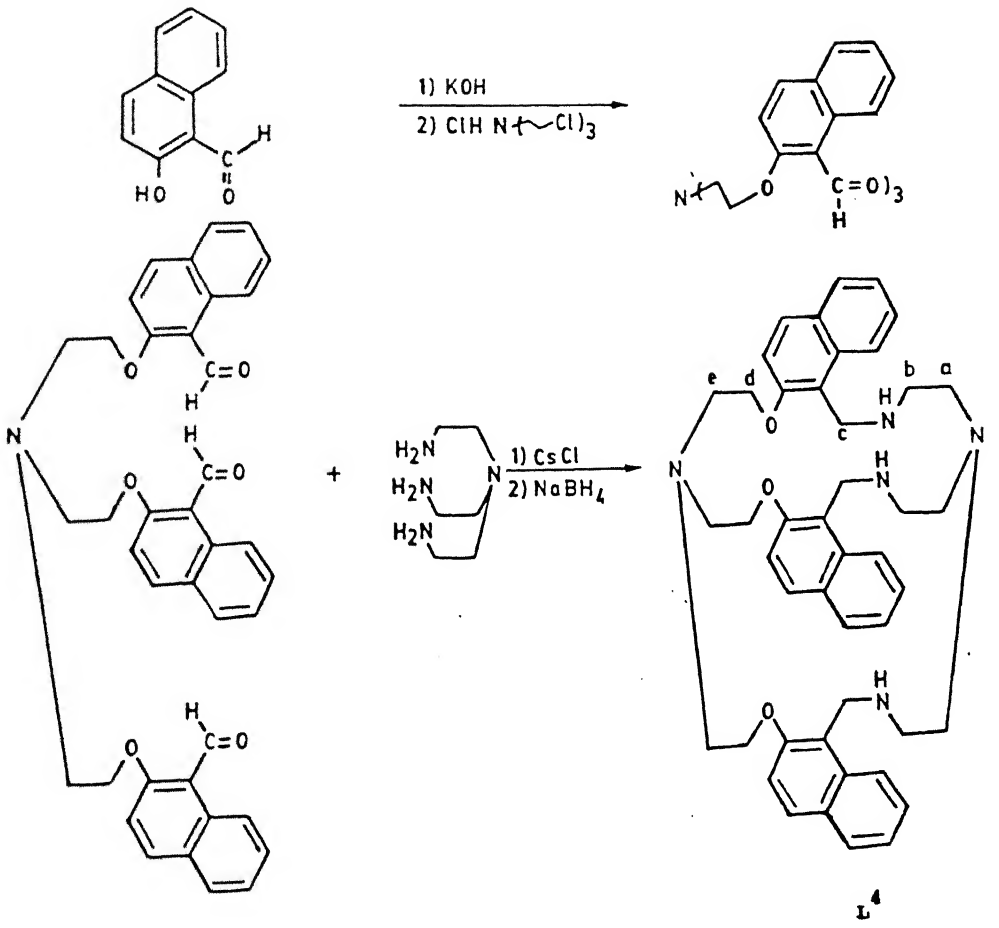

Fig. 5.19 Synthetic scheme for the cryptand L^4

solution methanol (50 ml) was added and the solid separated was collected by filtration, washed with methanol and air-dried. The entire operation was carried out in the dark. Yield 60%. m.pt. 138-140^{o}C.

IR(KBr): A strong peak was observed at 1660 cm^{-1} attributable [83] to the presence of the aldehyde groups.

^{1}H-NMR (80 MHz, $CDCl_3$, ppm): 3.2(t, 6H, NCH_2); 4.3(t, 6H, OCH_2); 7.5(m, 18H, aromatic) and 10.9 (s, 3H, CHO). The spectrum is shown in Fig. 5.20.

5.5.1c Synthesis of the cryptand L^4

The trialdehyde (0.61 g; 1 mmol) and CsCl (0.17 g; 1 mmol) were dissolved in a mixture of MeOH (150 ml) and THF (50 ml) at 40^{o}C. To this warmed and stirred solution, was added a solution of tren (0.15 g; 1 mmol) in MeOH (150 ml) over a period of 5 hr under argon atmosphere. The temperature of the reaction was maintained at 40^{o}C. The solution was allowed to stir for another 3 hr at 40^{o}C. To the Schiff base thus formed, solid excess $NaBH_4$ (0.24 g) was added in portions and the solution was refluxed for 4 hr. The brown residue obtained, after removal of the solvents was shaken with water (30 ml) and extracted with CH_2Cl_2 (2 x 50 ml). The dichloromethane layer was dried over anhydrous Na_2SO_4

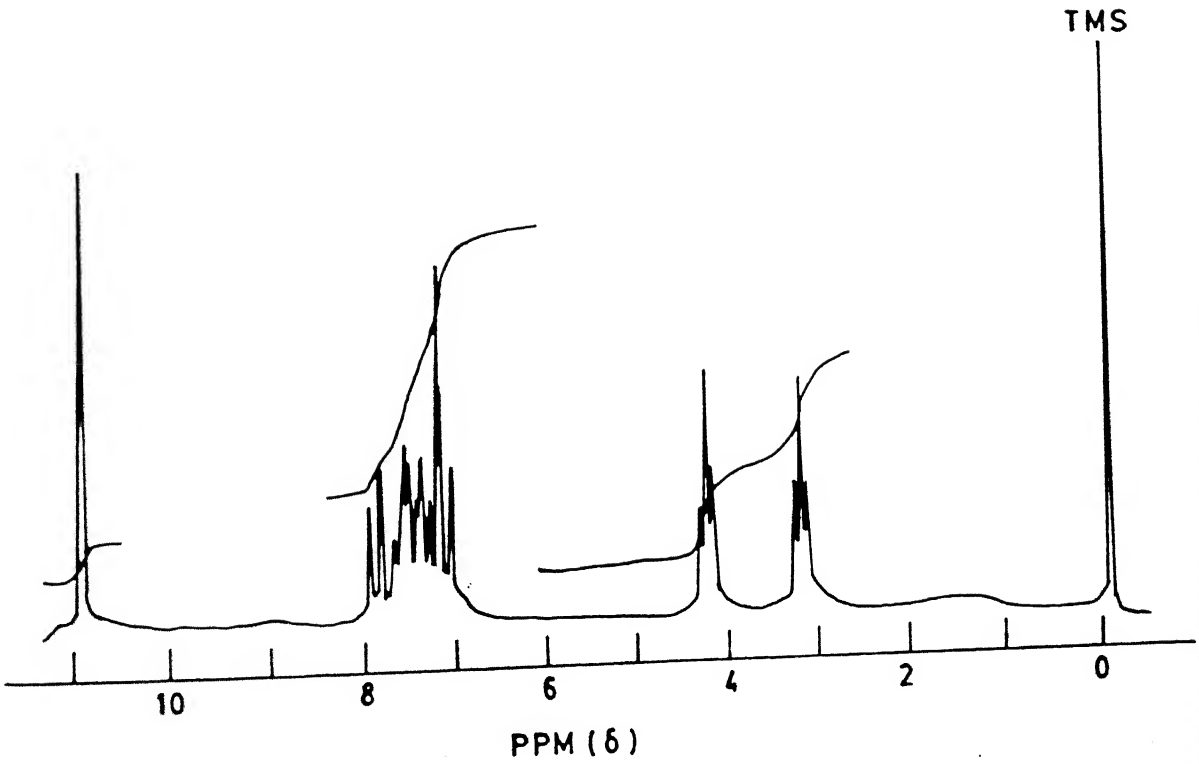

Fig. 5.20 80 MHz ^{1}H-NMR spectrum of the trialdehyde

and the brown solution was treated with activated charcoal and finally upon the removal of dichloromethane a brown oily liquid was obtained. This was purified by column chromatography over neutral alumina. The impurities were eluted with a chloroform:hexane (1:1) mixed solvent system. The pure product was eluted with chloroform:methanol (2:1). Upon removal of the solvents a light brown solid is obtained in 43% yield. The compound decomposes at 130°C.

^{1}H-NMR (400 MHz, $CDCl_3$, ppm): 2.4(t, 6H, a); 2.7(s, 6H, b); 3.4 (s, 6H, e); 4.2(s, 6H, c); 4.3(t, 6H, d) and 7.6(m, 18H, aromatic). The spectrum is shown in Fig. 5.21.

FAB-mass: m/z 710 $[L^4]^+$ (crude product).

FAB-mass: m/z, 732 $[H_4L^4 + H_2O]^+$ and 710 $[L^4]^+$ (purified product). The spectrum is shown in Fig. 5.22.

As the data above indicate, the FAB-mass spectrum of the crude product showed the free cryptand as the molecular ion peak. However, FAB-mass of the purified product by column chromatography, showed the presence of one water molecule inside the cavity of the cryptand.

5.5.2 Synthesis of Cryptates with Ni(II), Cu(II) and Zn(II) ions

The cryptand L^4 exhibits excellent coordination properties

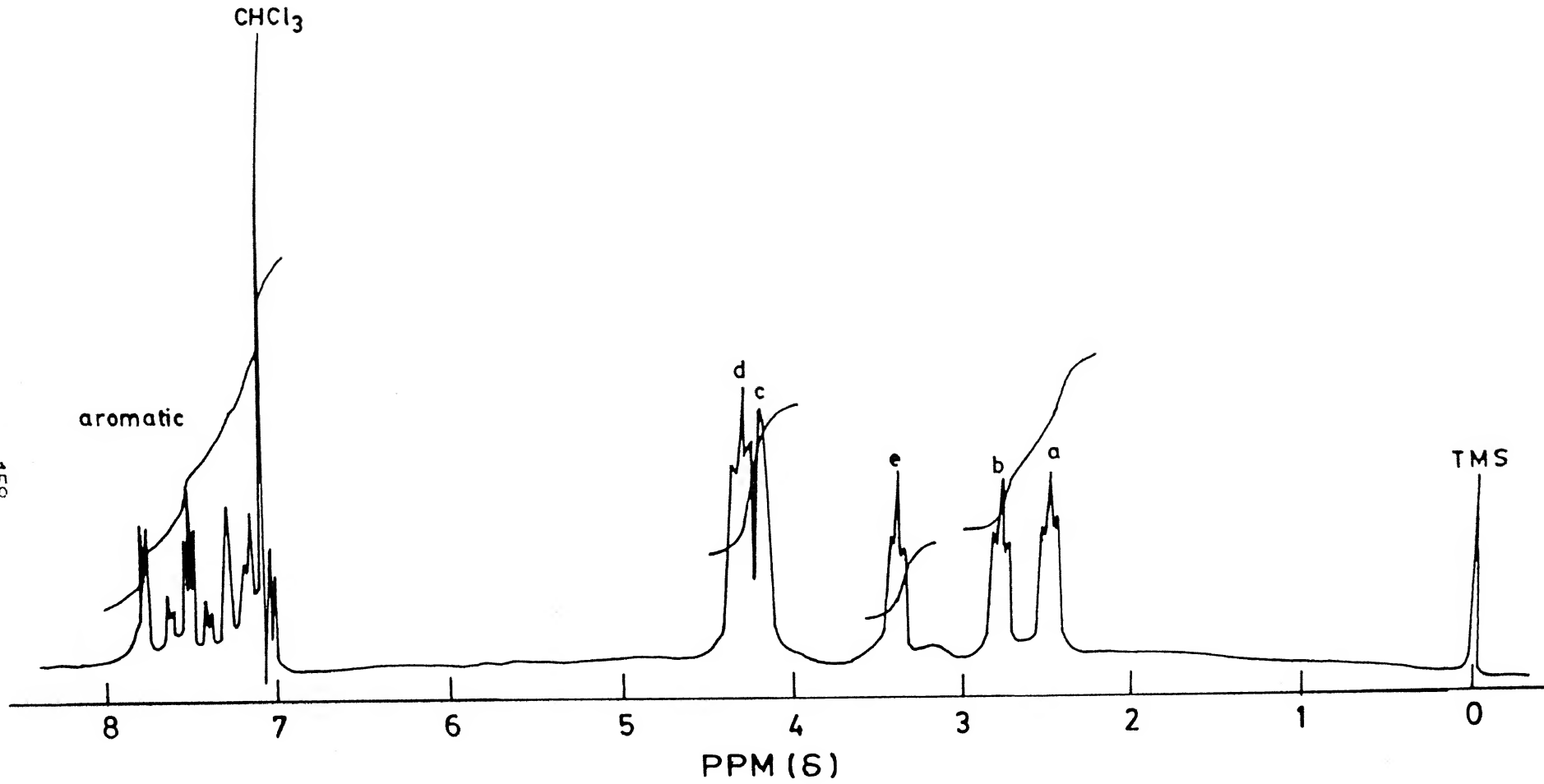

Fig. 5.21 400 MHz ^{1}H-NMR spectrum of the cryptand, L^{4}

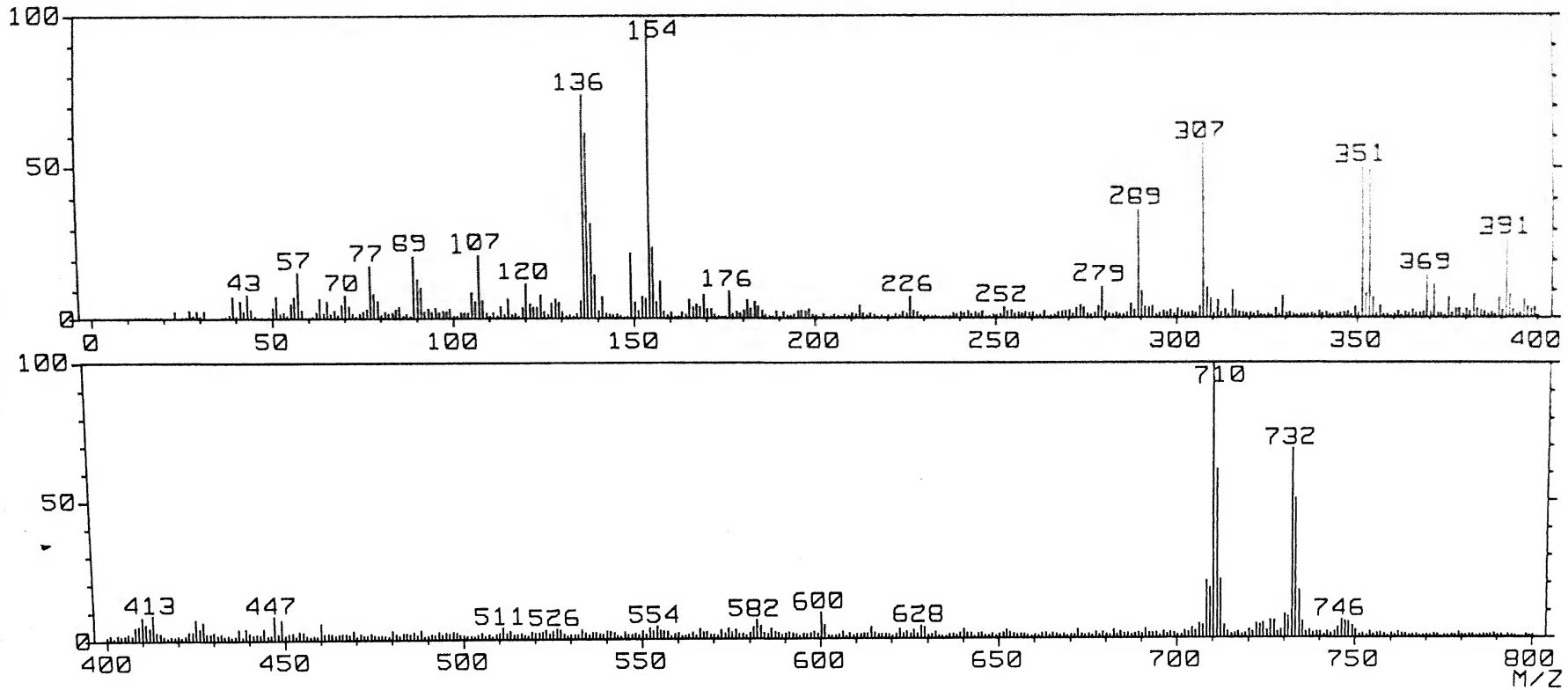

Fig. 5.22 FAB-mass spectrum of the cryptand, L^4

and forms complexes with metal ions as well as neutral molecules. All the complexation reactions were carried out in the dark.

5.5.2a Synthesis of $[L^4_C Zn(II)](ClO_4)_2$, 9

To the cryptand (0.35 g; 0.5 mmol) in methanol (10 ml), $Zn(ClO_4)_2.4H_2O$ (0.17 g; 0.5 mmol) in methanol (10 ml) was added and stirred for 10 minutes. The colorless solid crashed out was filtered out, washed with methanol and air-dried. Yield 80%.

The FAB-mass spectrum (Fig. 5.23) showed three peaks at m/z 874, 780 and 710 corresponding to the ions generated by the liberation of one perchlorate, two perchlorates and the metal ion respectively.

5.5.2b Synthesis of $[L^4_C Cu(II)](ClO_4)_2$, 10

To a stirred solution of the cryptand (0.35 g; 0.5 mmol) in methanol (10 ml), $[Cu(H_2O)_6](ClO_4)_2$ (0.18 g; 0.5 mmol) in methanol (10 ml) was added whereupon a greenish-blue solid crashed out. This was collected by filtration, washed with cold methanol and air-dried. Yield 85%.

FAB-mass spectrum (Fig. 5.24) showed two peaks at m/z 873 and 772 corresponding to the ions generated by the liberation of one and two perchlorates respectively.

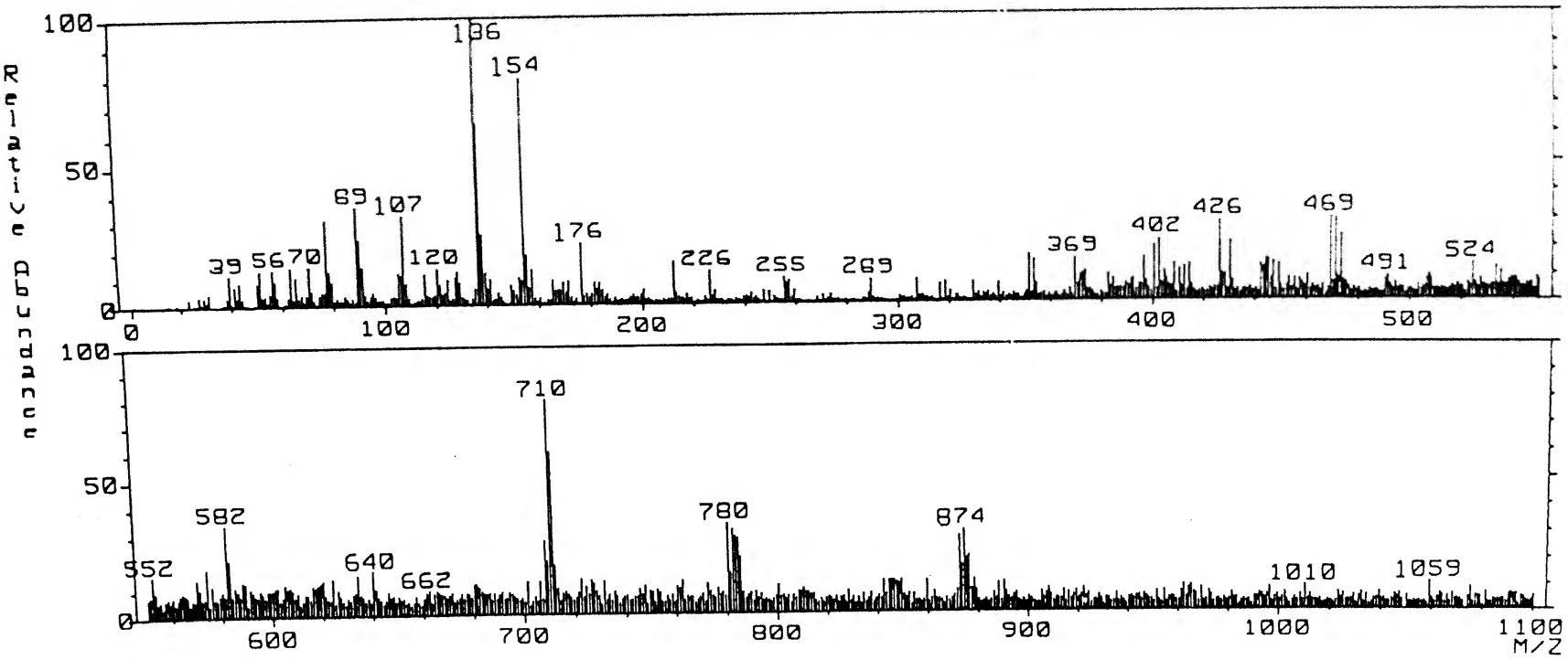

Fig. 5.23 FAB-mass spectrum of 9

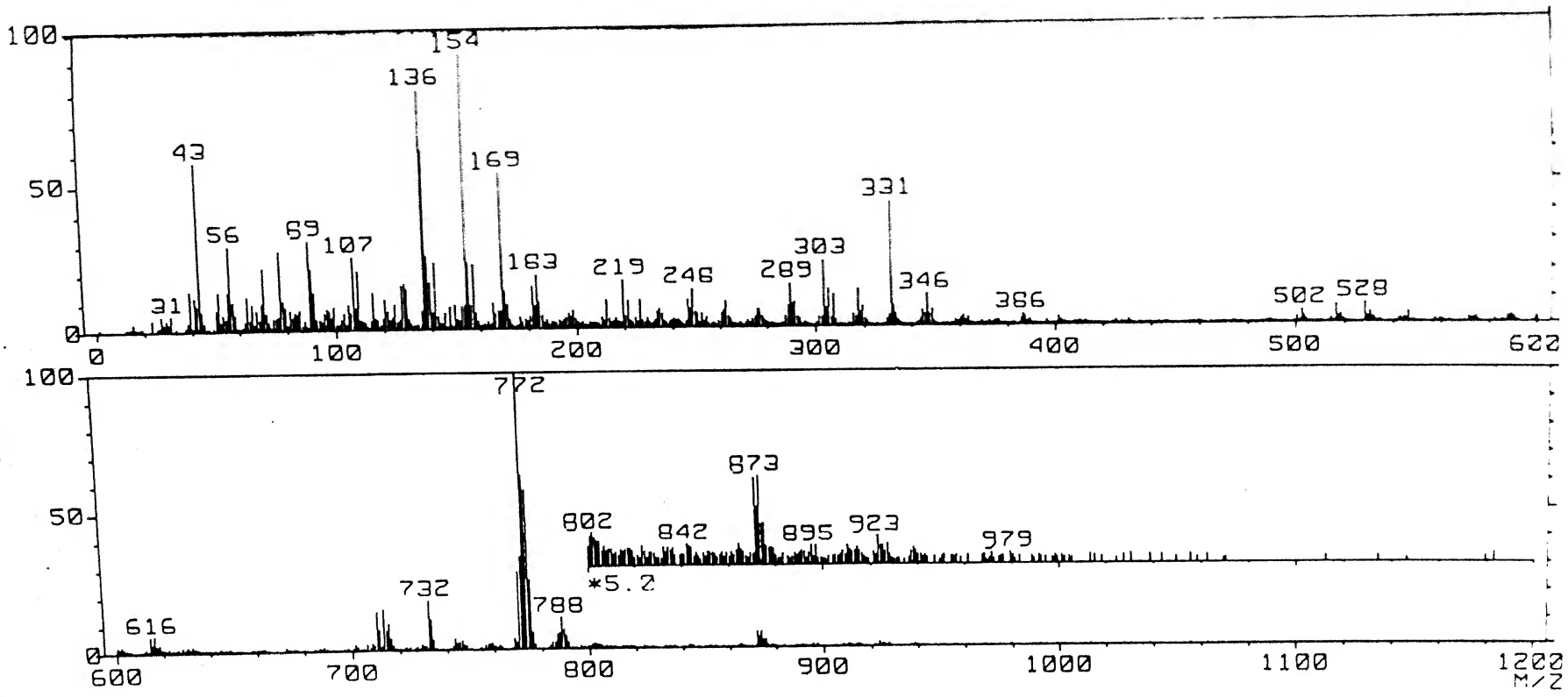

Fig. 5.24 FAB-mass spectrum of 10

5.5.2c **Synthesis of $[L^4 \subset Ni(II)](ClO_4)_2$, 11**

A solution of $[Ni(H_2O)_6](ClO_4)_2$ (0.18 g; 0.5 mmol) in methanol (10 ml) was added to a solution of the cryptand (0.35 g; 0.5 mmol) in methanol (15 ml) and stirred for 15 minutes. Slow evaporation of the solution afforded a blue solid which was collected by filtration, washed with methanol and air-dried in 60% yield.

5.5.2d **Synthesis of $[L^4 \subset Cu(II)(H_2S)](ClO_4)_2$, 12**

To a solution of $[CuL^4](ClO_4)_2$ (0.44 g; 0.5 mmol) in acetone (25 ml), H_2S gas was passed for 5 minutes. The resulting green solution was filtered and allowed to evaporate at RT which afforded a green solid. The solid was filtered out, washed with cold methanol (5 ml) and dried in a dessicator. Yield 68%. FAB-mass spectrum (Fig. 5.25) showed two peaks at m/z 873, 772 that correspond to the liberation of one and two perchlorates respectively.

5.6 Results and Discussion

The cryptand L^4 forms readily in 43% yield in presence of Cs(I) ion as the template. The tripod-tripod Schiff base condensation is less efficient compared to the one described in

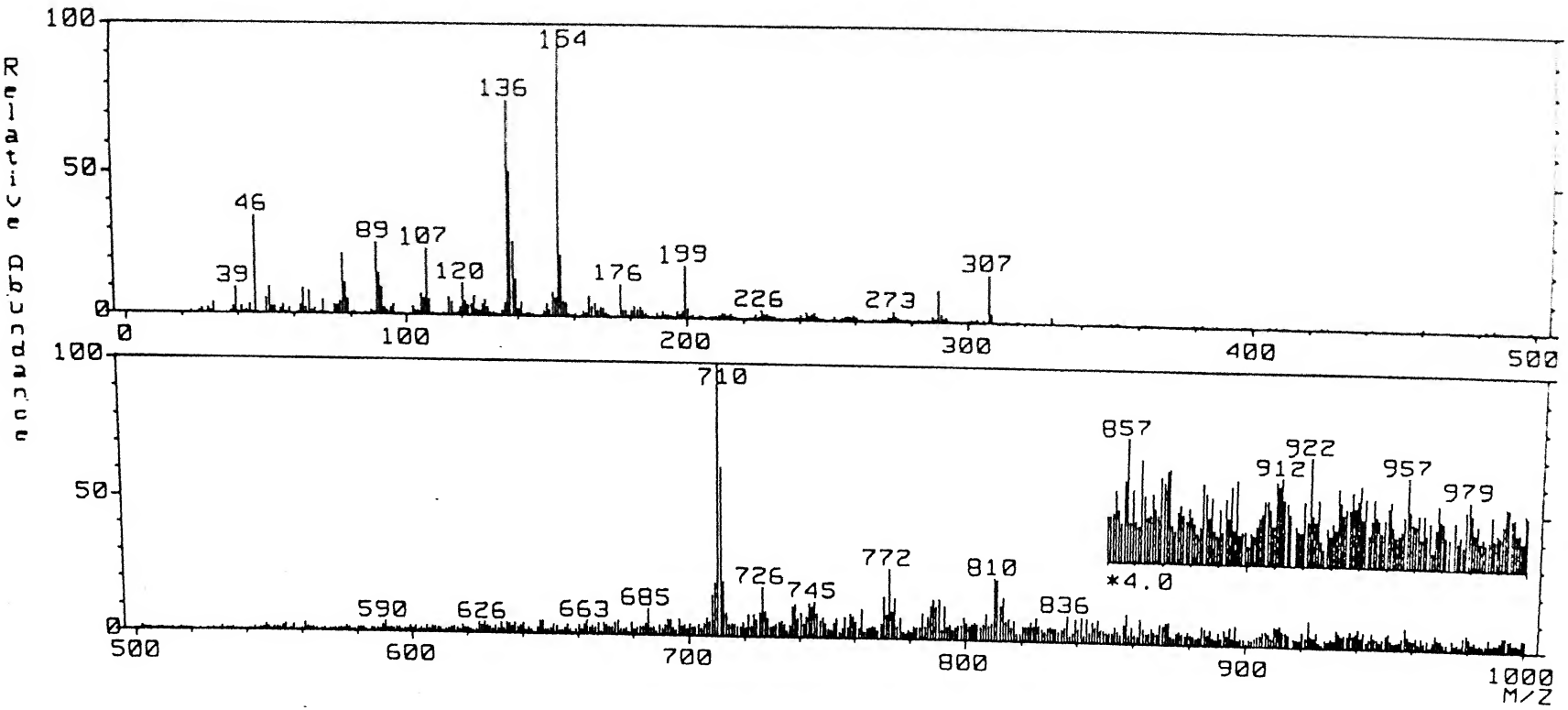

Fig. 5.25 FAB-mass spectrum of 12

Section A. This might be due to the heavier arms of the trialdehyde that affect the positioning of the reactive groups in a proper manner for the reaction to take place. The reaction also takes place smoothly in 36% yield using Rb(I) ion as the template.

The ligating properties of the cryptand L^4 towards the metal ions Zn(II), Cu(II), and Ni(II) have been shown by the isolation of the cryptates as described above. The cryptand forms mononuclear cryptates with these metal ions. Mononuclear cryptate was isolated in the solid state, when the cryptand was treated with one or more equivalents of the metal perchlorate salts in alcoholic medium. Dinuclear cryptates could not be isolated under any circumstances. This result indicates that the three metal ions recognize only one of the two available receptor sites. The IR spectrum of each cryptate as the perchlorate salt shows a strong and broad peak at 1100 cm^{-1} indicating the presence of ionic perchlorates. Like in the case of the cryptand, L^3, the perchlorate anion cannot enter the cavity and/or make direct bond with the metal ion inside. The molar conductivity data (Table 5.4) of the complexes (ca. $1x10^{-3}$ M) at 298 K correspond to 1:2 electrolytic nature of the cryptates thus indicating the

formulations as $[M(II)L4](ClO_4)_2$ [M(II) = Ni(II), Cu(II) and Zn(II)]. The FAB-mass data (experimental section) are also consistent with this formulation.

The donor atoms for L^4, being similar to the previous cryptand (L^3), the spectral properties of the Cu(II)- and the Ni(II)-cryptates should depend upon the topology of the donor set. Hence, to probe any possible differences, the two cryptates were subjected to a number of physicochemical studies.

The electronic spectral results are given in Table 5.5 and the spectra are shown in Figs. 5.26 - 5.28. The Zn(II)-cryptate absorbs (Table 5.5) strongly upto 330 nm which is due to the intra - ligand absorptions. The electronic absorption spectrum of $[L^4 \subset Cu(II)](ClO_4)_2$ shows two ligand field bands at 800 and 690 nm. If the metal ion is assumed to recognize the end providing the N_4 donor set, then these band positions are considerably red-shifted compared to those of square planar CuN_4 chromophores indicating distortion towards tetrahedral geometry in the present case. Comparing these band positions with those obtained on the $[L^3 \subset Cu(II)](ClO_4)_2$ (Table 5.2), the geometry around Cu(II) should be very similar in both the cases. The LMCT transition involving amino nitrogens and Cu(II) should occur at wavelengths shorter than 300 nm. However, since L^4 absorbs

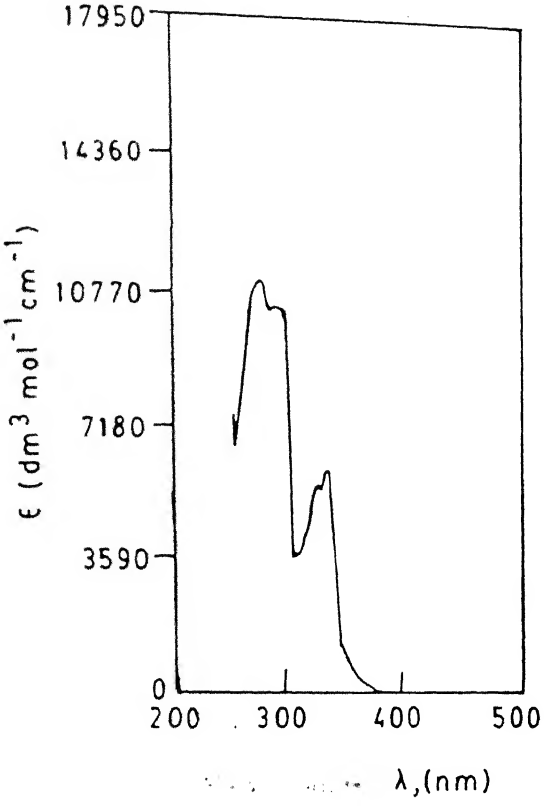

Fig. 5.26 Electronic absorption spectrum of **9** in acetonitrile

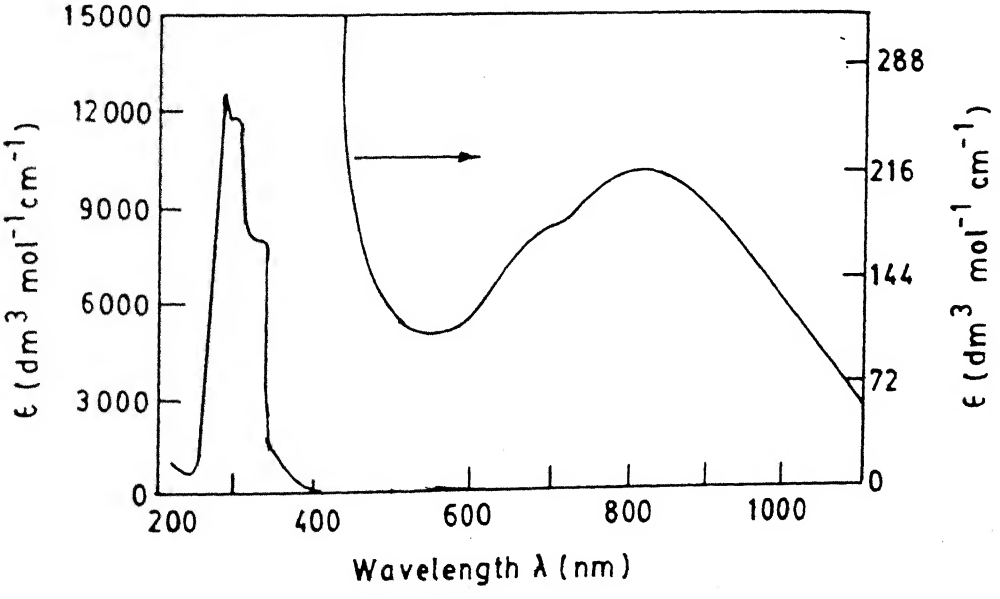

Fig. 5.27 Electronic absorption spectrum of **10** in acetonitrile

strongly in this region, no conclusion can be drawn regarding the position of the σ(N)-->Cu(II) LMCT transition.

The mononuclear Ni(II)-cryptate, like $[L^3C\,Ni(II)](ClO_4)_2$, shows three weak bands at 960, 575 and 375 nm. Again, these band positions are similar in both the cases indicating nearly the same distorted tetrahedral coordination geometry around Ni(II).

The Cu(II) cryptate gives an effective magnetic moment number (μ_{eff}/μ_B) of 2.02 at 301 K indicating a discrete mononuclear Cu(II) complex. The value for the Ni(II)-cryptate is 3.07 . In the case of perfect tetrahedral Ni(II) complex, the effective magnetic moment number lies close to 4.2. The value of 3.07 shows that the Ni(II) atom is present in a pseudotetrahedral geometry like in the case of the cryptate with L^3.

The EPR spectrum of Cu(II)-cryptate in the solid state shows a broad signal with g_{av} = 2.08 at 298 K. At 77 K, the signal sharpens with g_{av} = 2.07. The spectra are typical of magnetically concentrated systems and are not indicative of the solid-state stereochemistry of the cryptate. The EPR spectrum (Fig. 5.29) in acetonitrile solution at 298 K shows an axial spectrum corresponding to the $d_{x^2-y^2}$ ground state. The $g_{||}$ value of 2.13 lies within the limit for a pseudotetrahedral CuN_4 complex. The $A_{||}$

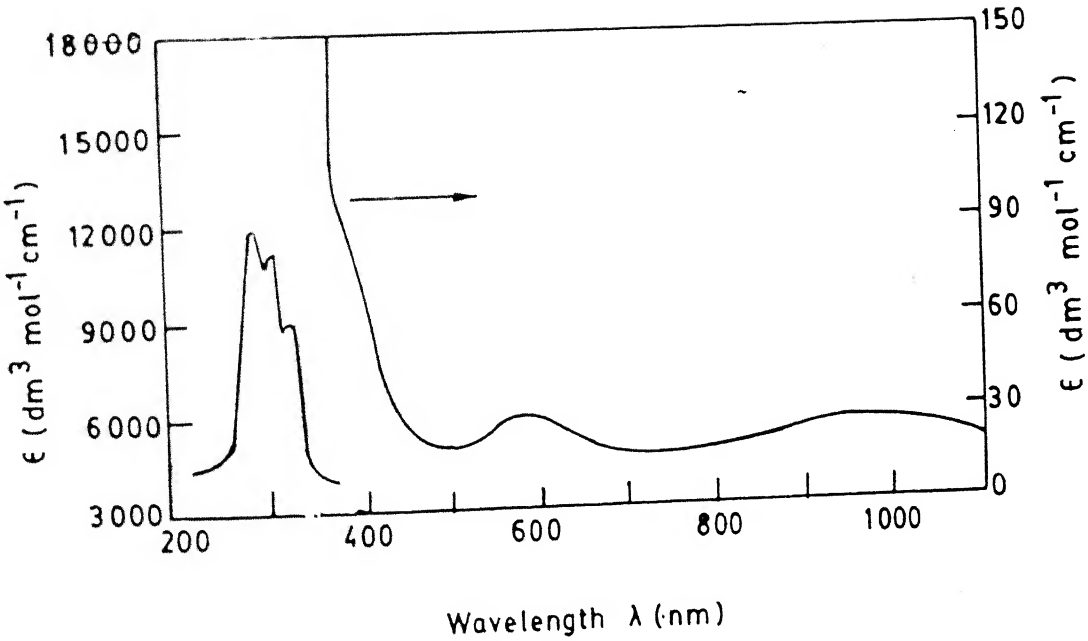

Fig. 5.28 Electronic absorption spectrum of **11** in DMF

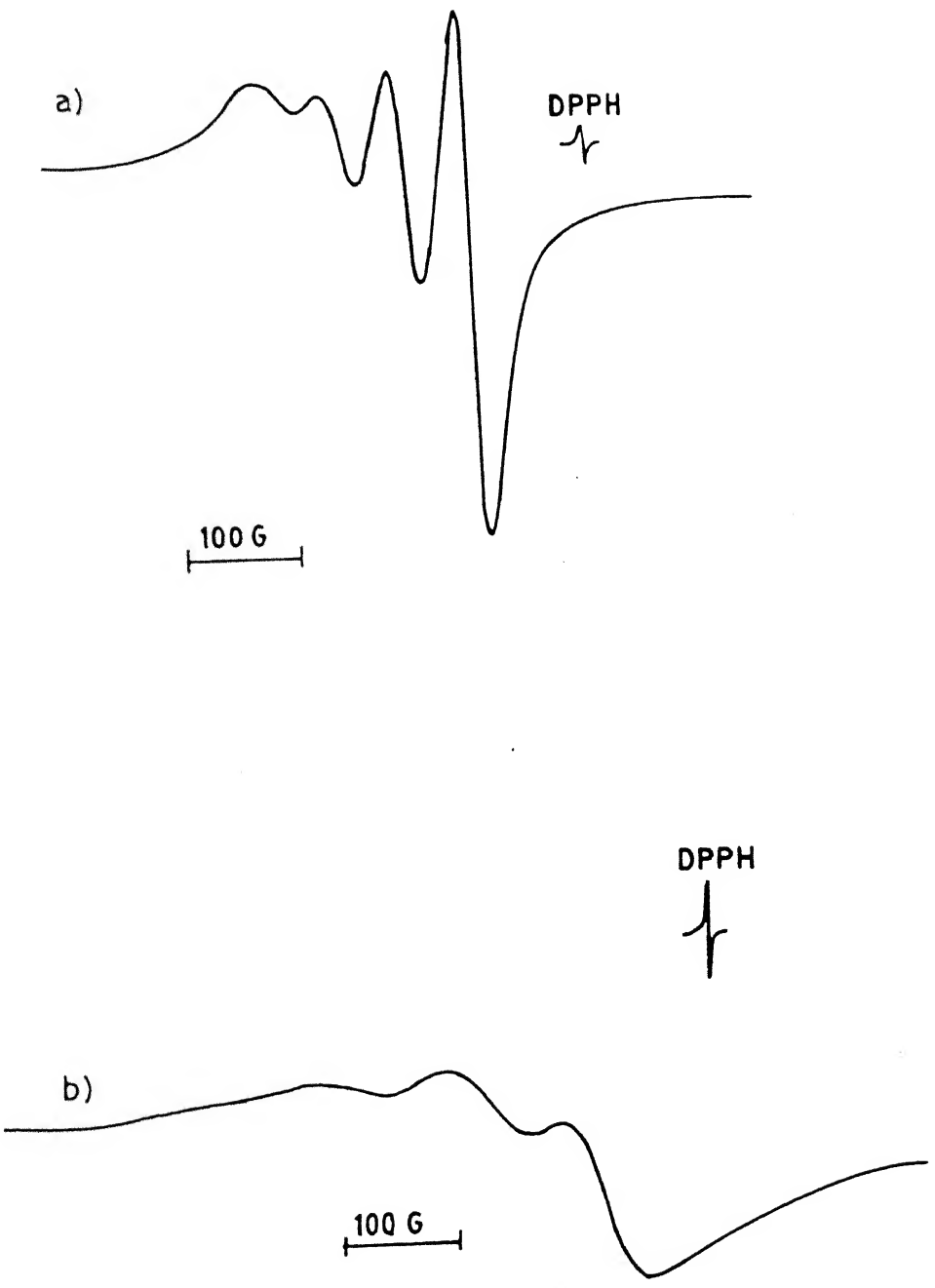

Fig. 5.29 Solution EPR spectra of 10 at (a) 298 K and (b) 77 K in acetonitrile

value of 60 x 10^{-4} cm^{-1} is very small and almost the same with that obtained on the Cu(II)-cryptate of L^3. Like in the previous case, this value closely matches with those exhibited by the active sites of copper blue proteins. On cooling to 77 K, the g values do not change significantly while the $A_{||}$ value increases significantly to 94 x 10^{-4} cm^{-1}. This is attributed to the flattening of the coordination geometry around the metal ion.

5.7 Secondary recognition of the Cu(II)-cryptate (10) by H_2S

The cryptate, 10, readily accepts a molecule of H_2S and the resulting H_2S complex is found to be air-stable.

The IR spectrum of the cryptate shows a band at 2557 cm^{-1} indicating [150] the presence of H_2S molecule. Besides, the strong and broad peak centering around 1100 cm^{-1} which is attributable to the ionic perchlorates is also seen. The molar conductance in CH_3CN is 215 $ohm^{-1}cm^2mol^{-1}$ and corresponds [86] to a 1:2 electrolyte.

The electronic spectrum of the cryptate shows a well-defined band (Fig. 5.30) at 450 nm which is absent in the parent cryptate. No Cu(II)-S(H_2S) complex has been characterised. However, other transition metals bonded to H_2S has been probed by UV-Vis spectroscopy where the LMCT transition involving H_2S and

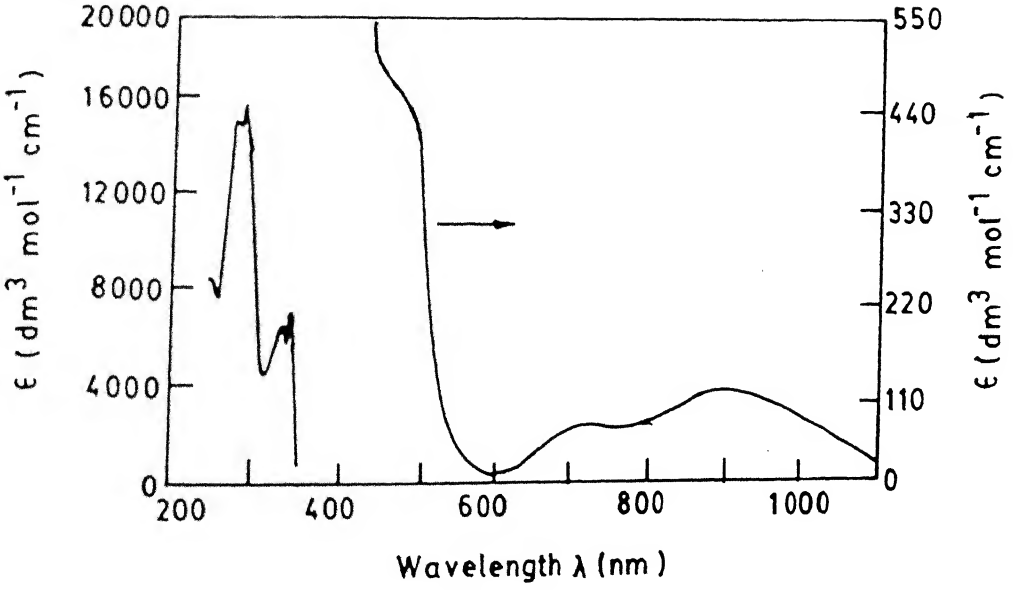

Fig. 5.30 Electronic absorption spectrum of **12** in acetonitrile

the metal ion appears in the region 450-500 nm as a well defined but weak band. Therefore, the band that appears at 450 nm is attributable to the (H_2S)-->Cu(II) LMCT transition. The ligand field bands show appreciable red-shifts (Table 5.5) compared to the parent Cu(II)-cryptate indicating changes in the coordination geometry as a result of the H_2S coordination.

The effective magnetic moment number (μ_{eff}/μ_B) for this cryptate is found to be 2.09 at 301 K showing a discrete mononuclear Cu(II) complex.

The EPR spectrum of the solid sample (Fig. 5.31) at 298 K is anisotropic in nature at g_{av}= 2.07. The solid sample at 77 K gives an axial spectrum. The CH_3CN solution at 298 K shows an ill-defined four-line signal (Fig. 5.31) with g_{av} = 2.07 and A_{av} = 65 x 10^{-4} cm^{-1}. At 77 K, the signal is highly rhombic with the values: g_1 = 2.17, g_2 = 2.07, g_3 = 2.03. The hyperfine coupling is not well-resolved. Thus, EPR results indicate a distorted geometry for the Cu(II) ion that is different from the parent cryptate.

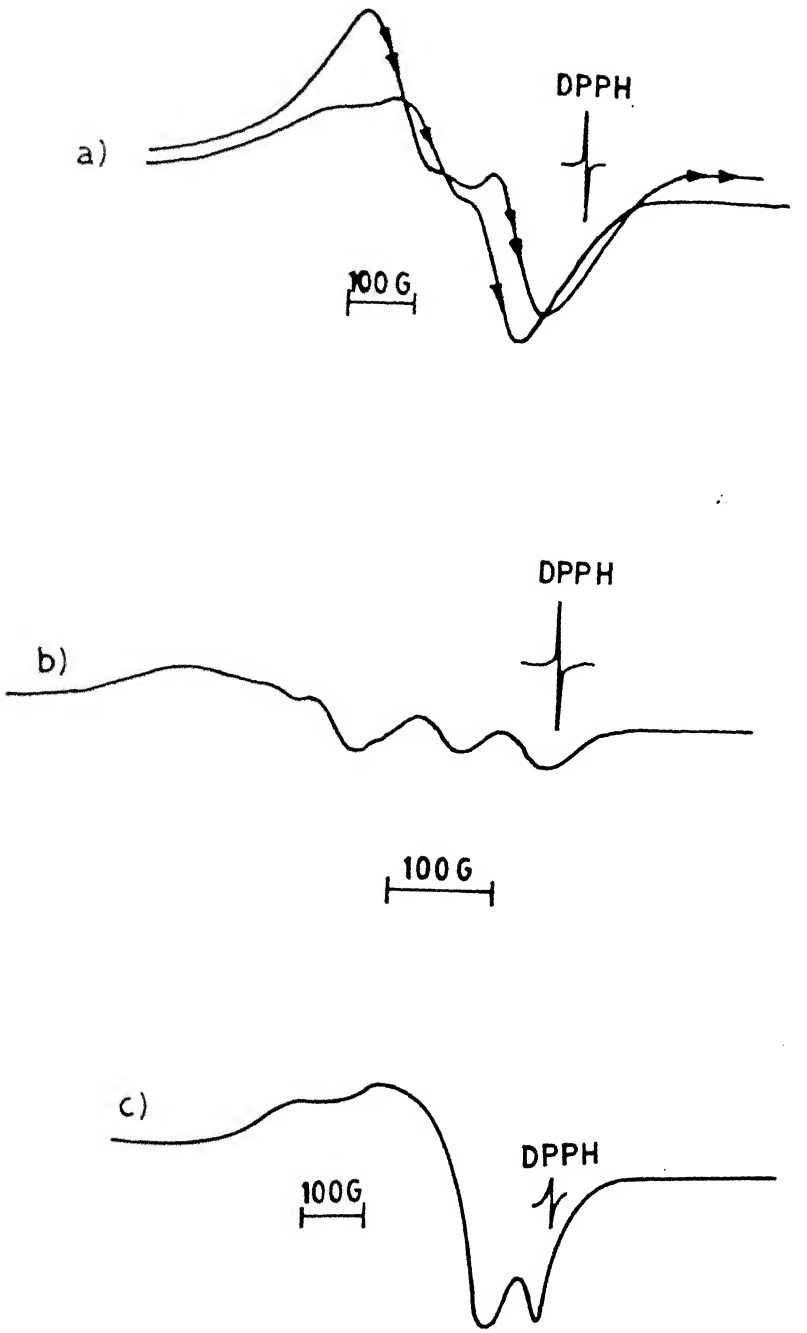

Fig. 5.31 EPR spectra of the cryptate, **12**: (a) solid-state at 298 K (double arrow) and 77 K (single arrow); (b) in acetonitrile at 298 K; (c) in acetonitrile at 77 K

SECTION C

Cryptands can strongly bind neutral molecules. The attractive or binding forces [4,59] are mainly hydrogen bonding, acid to base interactions, dipole-dipole, van der Waals forces, etc. Crown ethers are known [151] to dissolve water in chloroform by complexing water inside the cavity. The neutral water molecule is held by hydrogen bonding between the hydrogen of water molecule and oxygen of the crown ether ring. Cryptands [2.2.2], [2.2.1] and [2.1.1] with the donor sets, N_2O_6, N_2O_5 and N_2O_4 respectively, encapsulate a water molecule inside the cavity [152]. A diprotonated macrotricyclic cryptand describing a spherical topology of the donor atoms is known to form a tetrahedral array of hydrogen bonding with a water molecule as studied by NMR techniques [13]. Natural antibiotics have been shown [7] to complex water molecules by hydrogen bonding when they are free of metal ions. This complexation is believed to assist in the metal ion complexation by influencing the hydration shell of the metal ion.

This section describes the complexation of water by the cryptands, L^3 and L^4. One of the complexes with water inside the cavity could be isolated in single crystal forms suitable for X-

ray structure determination. The molecular and crystal structure of this complex is described. Other complexes are studied by FAB-mass spectroscopy.

5.8 Synthesis of the water inclusion complex, 1

The water inclusion complex, **1**, was obtained in a serendipitous manner. In order to probe the molecular recognition properties of the cryptand, L^3, it was allowed to react with ethylenediammonium, hydroxylammonium and methylammonium cations. However, it was found that these cations can not enter the cavity apparently due to their sizes. Instead, with ethylenediammonium dication in methanol, the water inclusion complex, **1** was isolated. In what follows next, the steps leading to the formation of the complex, 1 are described.

5.8.1a Preparation of ethylenediammonium dithiocyanate

This was prepared following a literature method [153]. A solution of KSCN (0.195 g; 2 mmol) in water (10 ml) was added to a solution of ethylenediamine dihydrochloride (0.13 g; 1 mmol) in water (5 ml) and stirred for 10 minutes. The solution was filtered and allowed for slow evaporation at RT which afforded colorless crystals of the product in 80% yield. m. pt. 202^0C.

5.8.1b **Synthesis of $[H_2L^3 \subset H_2O]^{2+}$. 2 SCN^-.2H_2O, 1**

To the cryptand (0.28 g; 0.5 mmol) in methanol (25 ml), solid ethylenediammonium dithiocyanate (0.09 g; 0.5 mmol) was added and stirred for 8 hr at room temperature. The resulting solution was filtered and allowed for slow evaporation which gave pale yellow crystals in the form of prisms. Yield 80%. m. pt. 148°C.

^{1}H-NMR (400 MHz, d_6-DMSO + $CDCl_3$, ppm): 2.45(s br, 6H, H^a); 2.7(s br, 6H, H^b); 3.1(s br, 6H, H^e); 3.95(s, 6H, H^c); 4.25(t, 6H, H^d); 7.01(t, f & g); 7.25(d, 3H, h) and 7.45(t, 3H, i). The spectrum is shown in Fig. 5.32.

^{13}C-NMR (100 MHz, d_6-DMSO + $CDCl_3$, ppm): 44.5, 46.4, 51.3, 55.4 and 64.8 (alphatic carbons); 110.8, 120, 130.2, 130.9, 132 and 156 (aromatic carbons). The spectrum is shown in Fig. 5.33.

FAB-mass showed three peaks at m/z 598, 582 and 560. The spectrum is shown in Fig. 5.34.

When the ligand was dissolved in acetone and allowed to crystallize in air, a pale yellow crystalline solid was obtained in 65% yield. 80 MHz ^{1}H-NMR spectrum of 2 was found not to be different from the free ligand at 298 K. However, the FAB-mass spectrum (Fig. 5.35) showed two prominent peaks at m/z 582 and 560. It did not show the m/z 598 peak as in the case of 1 above.

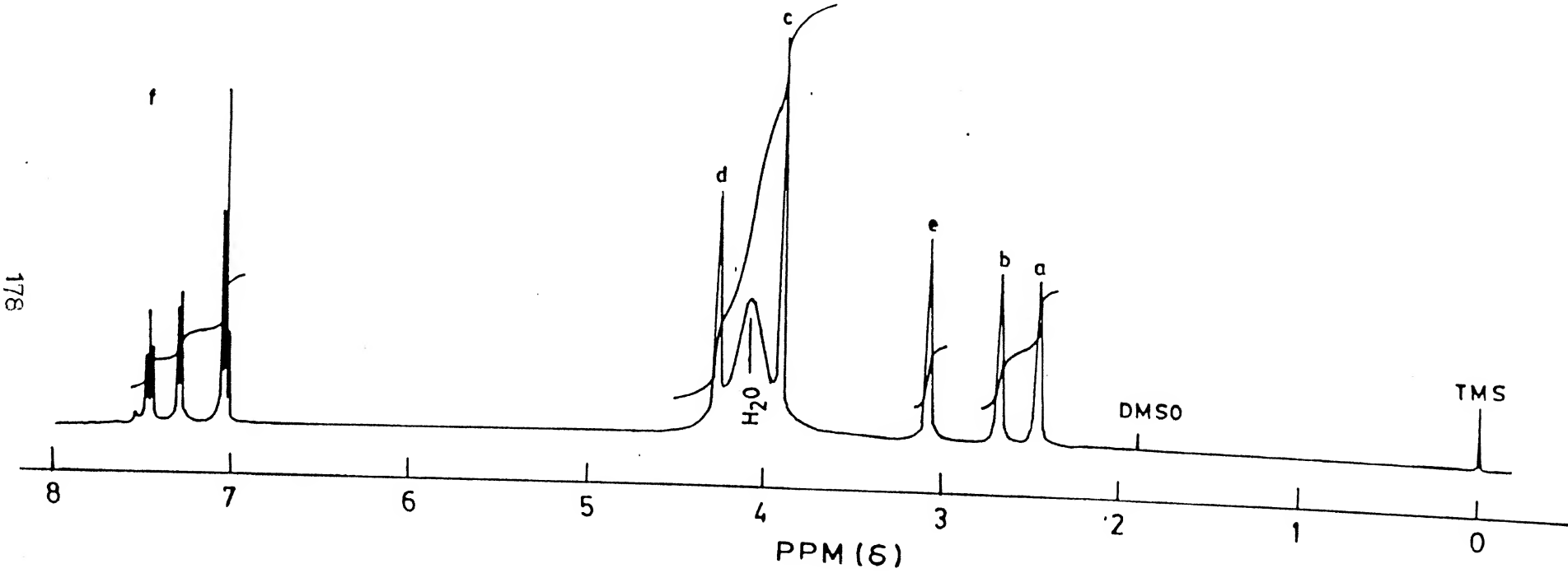

Fig. 5.32 400 MHz ^{1}H-NMR spectrum of 1

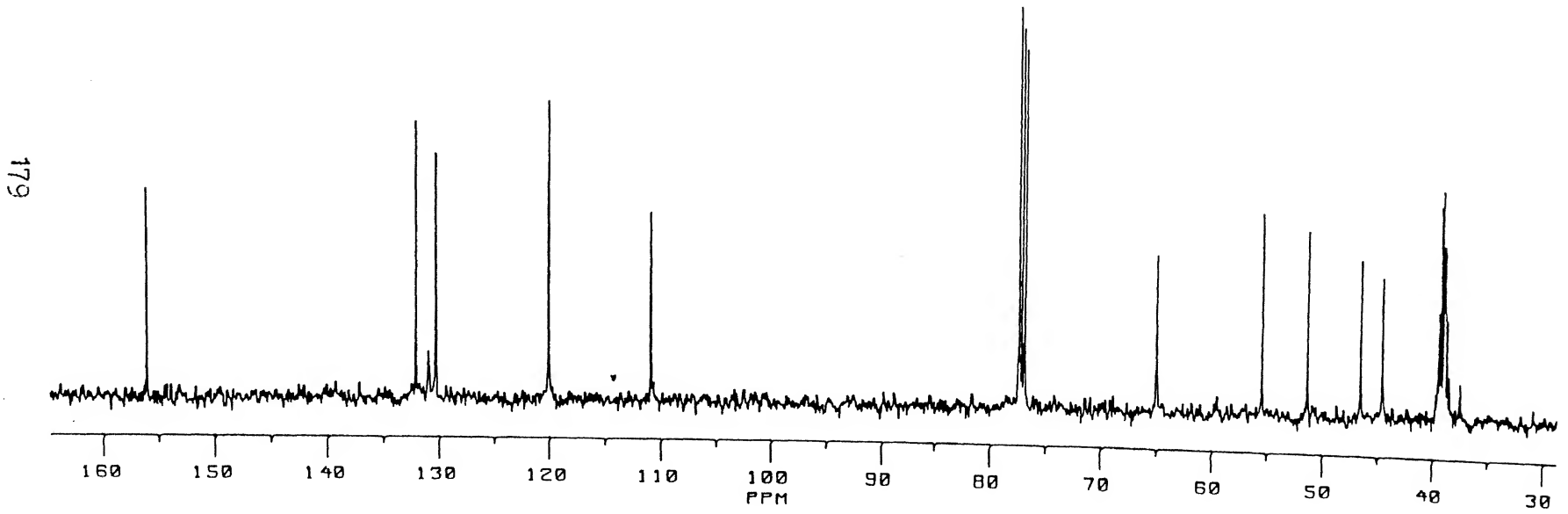

Fig. 5.33 100 MHz ^{13}C-NMR spectrum of 1

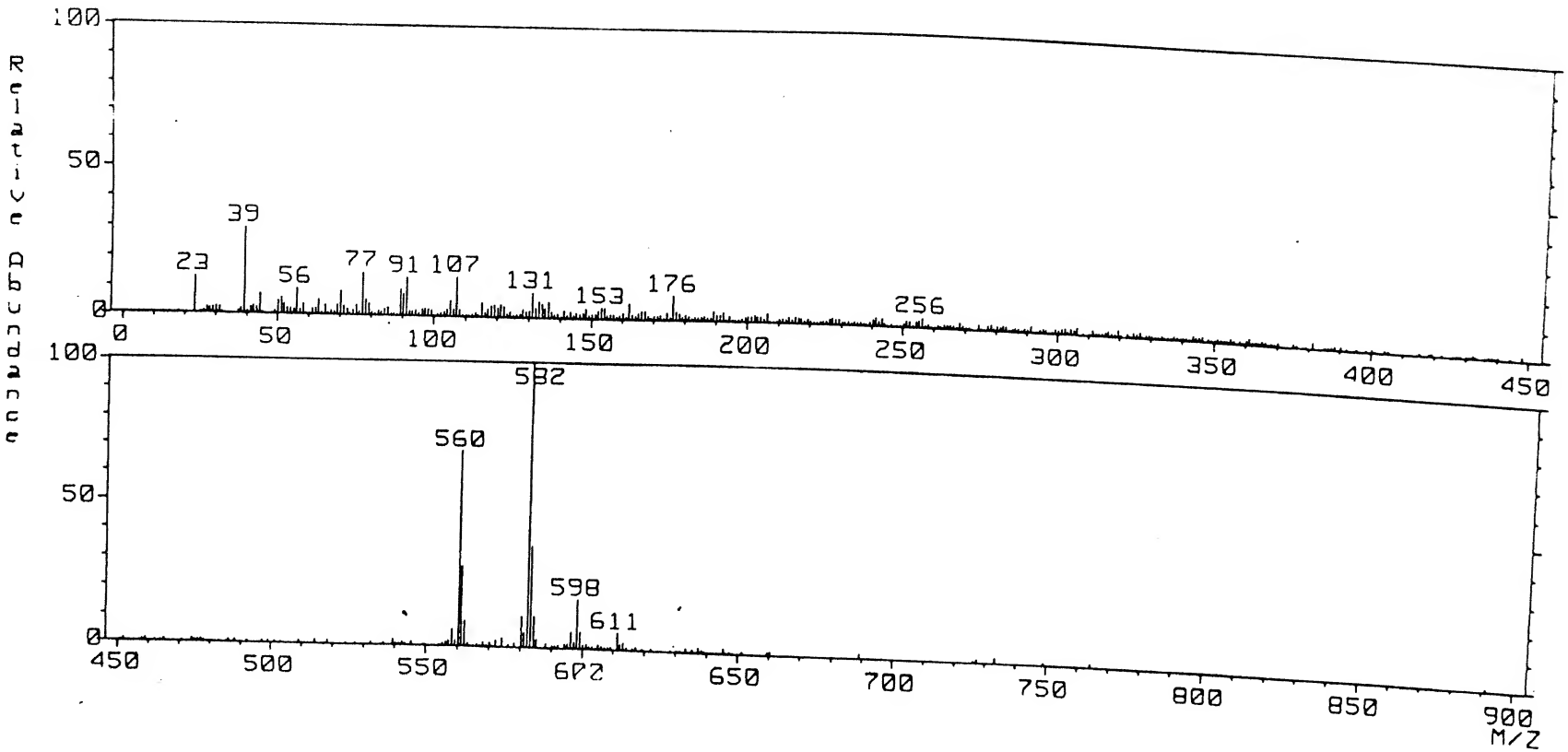

Fig. 5.34 FAB-mass spectrum of 1

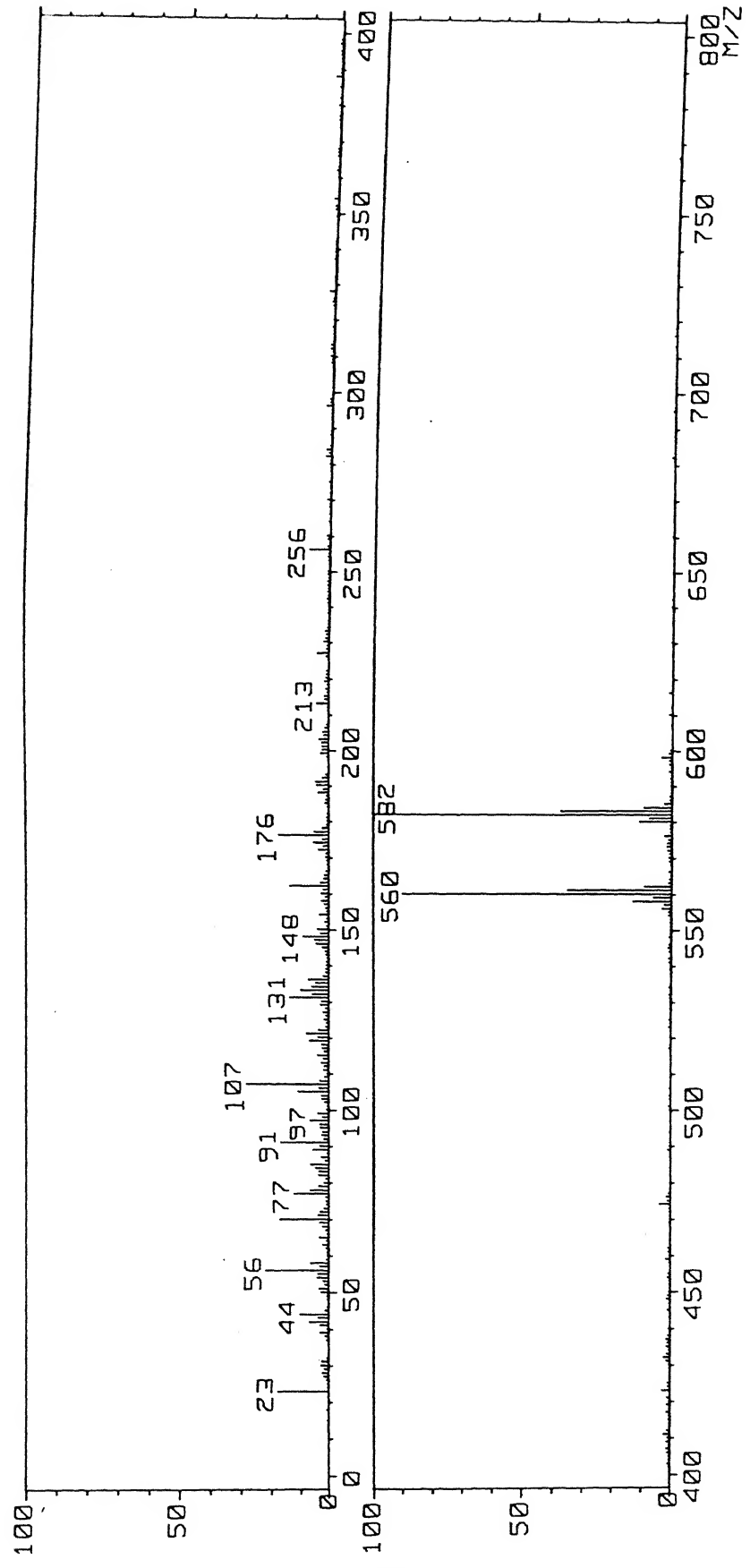

Fig. 5.35 FAB-mass spectrum of 2

$4H^+]$.

In a similar manner, when the ligand L^4 was dissolved in acetone and allowed to crystallize in air, again a pale yellow crystalline solid was obtained in about 56% yield. The FAB-mass spectrum (Fig. 5.36) showed three peaks at m/z 748, 732 and 710. Comparing the FAB-mass results with the two compounds above, it may be concluded that at least one water molecule is trapped inside the cavity of the cryptand, L^4. It is relevant to point out here that during purification of the cryptand, L^4, one water molecule gets trapped inside the cavity as the FAB-mass data indicate (vide supra).

5.9 X-ray Crystallography on 1

Colorless crystals suitable for X-ray diffraction studies were obtained from a chloroform solution on slow evaporation at room temperature. Crystal data, data collection, structure solution and refinement details are given in Table 5.7. All diffraction measurements were made at RT (21°C) with a Nicolet R2m/V diffractometer system using graphite monochromated MoK radiation. Intensity data were corrected for decay, L_p and absorption effects. The structure was solved by direct method [154] and refined on F by full-matrix least squares techniques

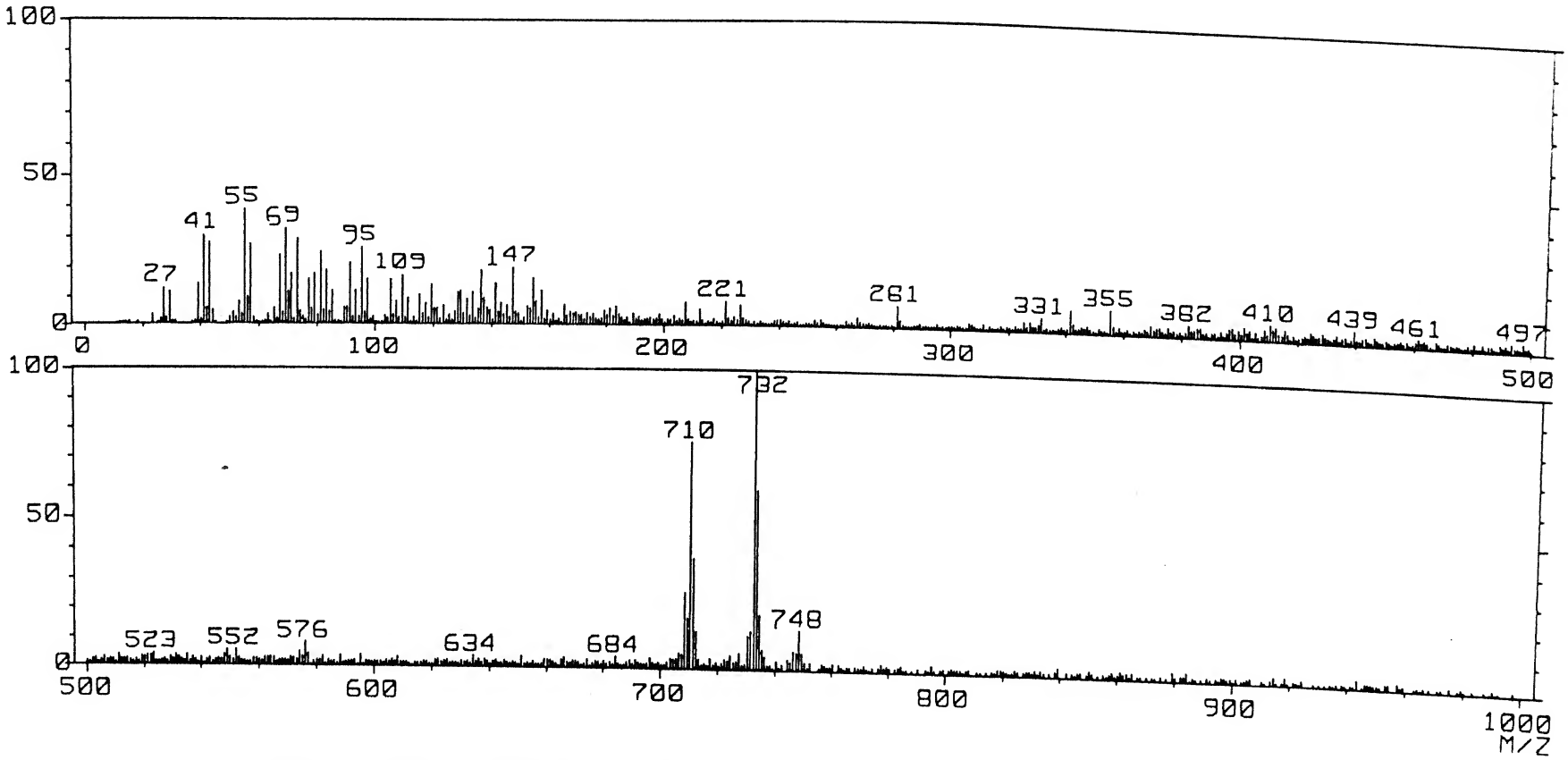

Fig. 5.36 FAB-mass spectrum of the water inclusion cryptate of L^4

using the SHELXTL-PLUS program package [155] on a DEC microvax-II computer. Most of the hydrogen atoms were located in successive difference fourier maps and the rest were generated geometrically (C-H 0.9 A; N-H 0.87 A). All the non-hydrogen atoms were refined anisotropically. The H-atoms were refined isotropically with the thermal factors of the mother atoms and included in the structure-factor calculations. Analytic expressions of neutral-atom scattering factors were employed and anomalous dispersion corrections [156] were incorporated. Fractional coordinates for all the atoms, bond lengths and bond angles and anisotropic thermal parameters are listed separately.

5.10 Results and Discussion

A perspective view of the complex cation is shown in Fig. 5.37 while the packing of the molecule in the crystal lattice is illustrated in Fig. 5.38. The molecule consists of the cation $[H_2L^3]^{2+}$ and two thiocyanate anions. Thus, when ethylenediammonium thiocyanate is treated with the cryptand L^3 transfer of two protons from the ethylenediammonium moiety to the secondary amino nitrogens takes place. One water molecule present in the solvent enters the cavity and forms the inclusion complex. The water molecule is held inside the cavity through H-

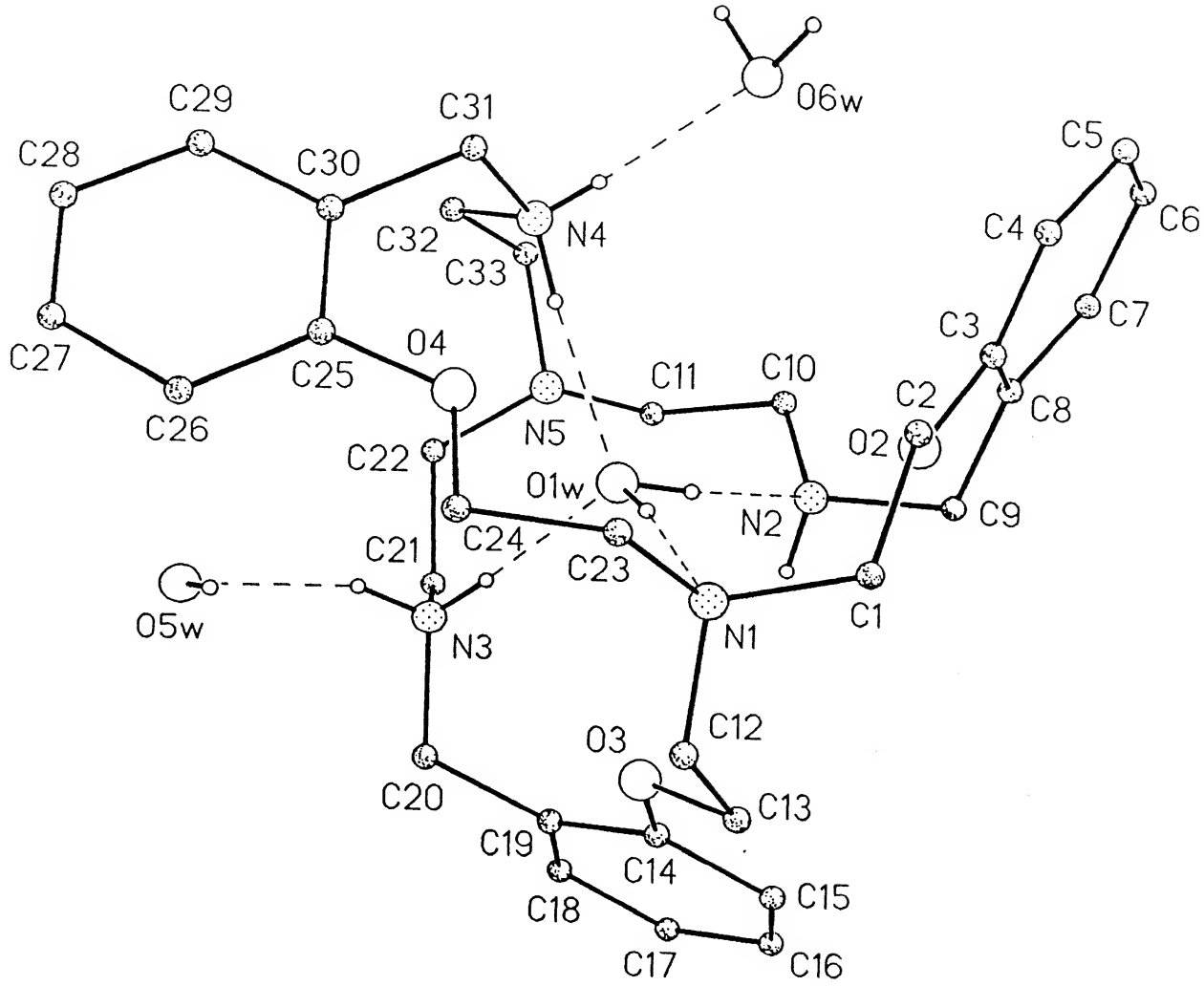

Fig. 5.37 A perspective view of 1 showing the atom numbering scheme; H atoms bonded to carbons are omitted for clarity

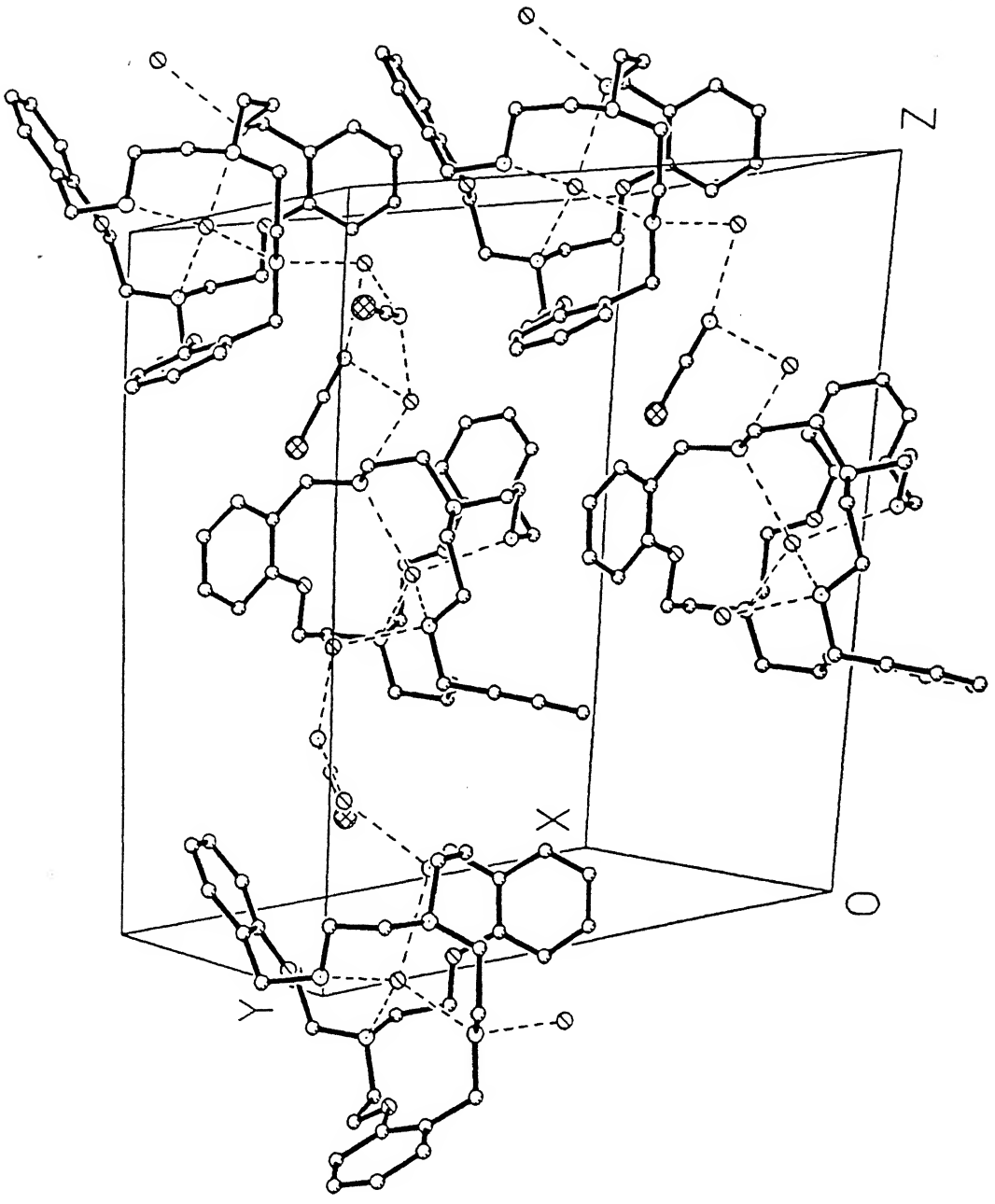

Fig. 5.38 An illustration of the packing diagram of **1**

Molecular formula	$[C_{33}H_{47}N_5O_3.H_2O](SCN)_2.2H_2O$
Molecular weight	731.0
Color and habit	light yellow prism plate
Crystal size	0.50 x 0.50 x 0.60 mm^3
Crystal system	monoclinic
Space group	Cc (No. 9)
Unit cell parameters	a = 13.701(2)Å β = 107.61(3)°
	b = 15.284(2) V = 1087.4(8)Å^3
	c = 19.685(3) Z = 4 $F(000)$ = 1564
Density (calcd)	1.236 g cm^{-3}
Radiation	graphite-monochromatized Mo$K\alpha$, λ = 0.71073 Å
Standard reflections	(1,1,-9); (4,4,-6)
Intensity variation	±0.9%
Absorption coefficient	1.86 cm^{-1}
Mean μr	0.04
Transmission factors	0.908 to 0.915
Scan type and rate	ω-scan; 1.01-14.65 deg min^{-1}
Scan range	0.85° below $K\alpha_1$ to 0.85° above $K\alpha_2$
Background counting	stationary counts for one-fifth of scan time at each end of scan range
Collection range	$0 \le h \le 16$, $0 \le k \le 18$, $-23 \le \ell \le 22$; $2\theta_{max}$ = 50°
Unique data measured	3608
Obs. data with $\|F_o\| \ge 3\sigma(\|F_o\|)$, n	3098
No. of variables, p	449
Weighting scheme	$w = [\sigma^2\|F_o\| + 0.002\|F_o\|^2]^{-1}$
$R_F = \sum\|\|F_o\| - \|F_c\|\| / \sum\|F_o\|$	0.033
$wR = [\sum w^2(\|F_o\| - \|F_c\|)^2 / \sum w^2\|F_o\|^2]^{1/2}$	0.046
$S = [\sum w(\|F_o\| - \|F_c\|)^2/(n-p)]^{1/2}$	0.84
Residual extrema in final difference map	+0.18 to -0.15 eÅ^{-3}

Atom	x	y	z	U_{eq}
O(1W)	0	-1399(1)	0	484(3)
N(1)	1364(2)	-1425(2)	-918(1)	530(3)
C(1)	2104(2)	-699(2)	-742(2)	592(3)
C(2)	2471(2)	-478(2)	35(2)	594(3)
O(2)	1658(2)	-31(1)	195(1)	638(3)
C(3)	1892(2)	451(2)	809(2)	558(3)
C(4)	2839(2)	393(2)	1341(2)	685(3)
C(5)	3029(3)	926(2)	1937(2)	776(3)
C(6)	2305(3)	1493(2)	2002(2)	798(3)
C(7)	1363(3)	1541(2)	1491(2)	720(3)
C(8)	1124(2)	1006(2)	875(2)	583(3)
C(9)	109(2)	1050(2)	323(2)	677(3)
N(2)	-560(2)	285(2)	347(1)	560(3)
C(10)	-836(2)	265(2)	1011(2)	563(3)
C(11)	-1709(2)	-368(2)	971(2)	528(3)
C(12)	749(2)	-1357(2)	-1673(2)	653(3)
C(13)	-43(2)	-656(2)	-1821(2)	676(3)
O(3)	-860(2)	-947(1)	-1568(1)	638(3)
C(14)	-1732(2)	-459(2)	-1716(1)	535(3)
C(15)	-1817(3)	406(2)	-1945(2)	664(3)
C(16)	-2744(3)	821(2)	-2089(2)	765(3)
C(17)	-3584(3)	408(2)	-1999(2)	749(3)
C(18)	-3500(2)	-450(2)	-1764(2)	623(3)
C(19)	-2577(2)	-892(2)	-1623(1)	493(3)
C(20)	-2469(2)	-1840(2)	-1399(1)	512(3)
N(3)	-2057(2)	-1961(2)	-610(1)	493(3)
C(21)	-2783(2)	-1661(2)	-227(1)	584(3)
C(22)	-2369(2)	-1811(2)	565(1)	534(3)
C(23)	1956(2)	-2255(2)	-788(2)	713(3)
C(24)	1365(3)	-3033(2)	-702(2)	709(3)
O(4)	1240(2)	-3000(1)	-11(1)	716(3)
C(25)	926(2)	-3736(2)	242(2)	560(3)
C(26)	557(2)	-4486(2)	-166(2)	667(3)
C(27)	285(2)	-5204(2)	161(2)	749(3)
C(28)	369(3)	-5198(2)	862(2)	804(3)
C(29)	715(2)	-4462(2)	1258(2)	717(3)
C(30)	1002(2)	-3716(2)	962(2)	567(3)
C(31)	1417(2)	-2923(2)	1406(1)	590(3)
N(4)	648(2)	-2203(2)	1325(1)	493(3)
C(32)	-251(2)	-2442(2)	1561(1)	534(3)
C(33)	-899(2)	-1654(2)	1600(1)	492(3)
N(5)	-1450(2)	-1290(1)	904(1)	437(3)
O(5W)	-1929(2)	-3725(2)	-717(2)	1019(3)
O(6W)	1484(2)	-889(2)	2335(1)	861(3)
S(1)	4439(1)	2230(1)	3636(1)	922(2)
C(34)	5218(2)	2986(2)	3552(2)	616(3)
N(6)	5803(2)	3505(2)	3497(2)	878(3)
S(2)	9135(1)	2967(1)	1830(1)	1109(3)
C(35)	8912(2)	3381(3)	2512(2)	874(3)
N(7)	8750(3)	3703(3)	3018(2)	1164(3)

*U_{eq} defined as one third of the trace of the orthogonalized U tensor.

N(1)-C(1)	1.471	(4)	N(1)-C(12)	1.474	(3)
N(1)-C(23)	1.486	(4)	C(1)-C(2)	1.497	(4)
C(2)-O(2)	1.422	(4)	O(2)-C(3)	1.368	(4)
C(3)-C(4)	1.403	(4)	C(3)-C(8)	1.388	(4)
C(4)-C(5)	1.385	(5)	C(5)-C(6)	1.353	(5)
C(6)-C(7)	1.378	(4)	C(7)-C(8)	1.415	(4)
C(8)-C(9)	1.485	(4)	C(9)-N(2)	1.495	(4)
N(2)-C(10)	1.467	(4)	C(10)-C(11)	1.522	(4)
C(11)-N(5)	1.468	(3)	C(12)-C(13)	1.489	(4)
C(13)-O(3)	1.426	(4)	O(3)-C(14)	1.364	(3)
C(14)-C(15)	1.391	(4)	C(14)-C(19)	1.392	(4)
C(15)-C(16)	1.370	(5)	C(16)-C(17)	1.370	(5)
C(17)-C(18)	1.383	(4)	C(18)-C(19)	1.386	(4)
C(19)-C(20)	1.509	(4)	C(20)-N(3)	1.495	(3)
N(3)-C(21)	1.490	(4)	C(21)-C(22)	1.506	(4)
C(22)-N(5)	1.468	(3)	C(23)-C(24)	1.477	(5)
C(24)-O(4)	1.422	(4)	O(4)-C(25)	1.354	(4)
C(25)-C(26)	1.403	(4)	C(25)-C(30)	1.388	(4)
C(26)-C(27)	1.380	(5)	C(27)-C(28)	1.351	(6)
C(28)-C(29)	1.369	(5)	C(29)-C(30)	1.389	(5)
C(30)-C(31)	1.503	(4)	C(31)-N(4)	1.498	(4)
N(4)-C(32)	1.488	(4)	C(32)-C(33)	1.512	(4)
C(33)-N(5)	1.461	(3)	S(1)-C(34)	1.615	(3)
C(34)-N(6)	1.157	(5)	S(2)-C(35)	1.596	(5)
C(35)-N(7)	1.189	(7)			

C(1)-N(1)-C(12)	109.1(2)	C(1)-N(1)-C(23)	107.6(2)
C(12)-N(1)-C(23)	110.5(2)	N(1)-C(1)-C(2)	113.9(3)
C(1)-C(2)-O(2)	107.0(2)	C(2)-O(2)-C(3)	117.7(2)
O(2)-C(3)-C(4)	122.9(3)	O(2)-C(3)-C(8)	115.5(2)
C(4)-C(3)-C(8)	121.6(3)	C(3)-C(4)-C(5)	119.3(3)
C(4)-C(5)-C(6)	120.1(3)	C(5)-C(6)-C(7)	121.1(3)
C(6)-C(7)-C(8)	121.1(3)	C(3)-C(8)-C(7)	116.6(2)
C(3)-C(8)-C(9)	121.8(3)	C(7)-C(8)-C(9)	121.5(3)
C(8)-C(9)-N(2)	112.9(2)	C(9)-N(2)-C(10)	111.7(2)
N(2)-C(10)-C(11)	112.2(2)	C(10)-C(11)-N(5)	114.0(2)
N(1)-C(12)-C(13)	114.1(3)	C(12)-C(13)-O(3)	108.1(3)
C(13)-O(3)-C(14)	119.0(2)	O(3)-C(14)-C(15)	124.8(3)
O(3)-C(14)-C(19)	114.9(2)	C(15)-C(14)-C(19)	120.2(3)
C(14)-C(15)-C(16)	119.2(3)	C(15)-C(16)-C(17)	121.5(3)
C(16)-C(17)-C(18)	119.5(3)	C(17)-C(18)-C(19)	120.5(3)
C(14)-C(19)-C(18)	119.1(3)	C(14)-C(19)-C(20)	118.9(2)
C(18)-C(19)-C(20)	122.0(3)	C(19)-C(20)-N(3)	113.2(2)
C(20)-N(3)-C(21)	112.8(2)	N(3)-C(21)-C(22)	112.2(2)
C(21)-C(22)-N(5)	113.0(2)	N(1)-C(23)-C(24)	114.7(3)
C(23)-C(24)-O(4)	108.0(3)	C(24)-O(4)-C(25)	117.8(2)
O(4)-C(25)-C(26)	124.6(3)	O(4)-C(25)-C(30)	115.1(2)
C(26)-C(25)-C(30)	120.4(3)	C(25)-C(26)-C(27)	118.9(3)
C(26)-C(27)-C(28)	121.4(3)	C(27)-C(28)-C(29)	119.6(3)
C(28)-C(29)-C(30)	121.9(3)	C(25)-C(30)-C(29)	117.8(3)
C(25)-C(30)-C(31)	120.6(3)	C(29)-C(30)-C(31)	121.5(3)
C(30)-C(31)-N(4)	113.6(2)	C(31)-N(4)-C(32)	114.2(2)
N(4)-C(32)-C(33)	112.0(2)	C(32)-C(33)-N(5)	113.6(2)

C(11)-N(5)-C(22)	111.3(2)	C(11)-N(5)-C(33)	110.5(2)
C(22)-N(5)-C(33)	110.4(2)	S(1)-C(34)-N(6)	177.6(3)
S(2)-C(35)-N(7)	179.0(4)		

Hydrogen bonding scheme (donor atom precedes acceptor atom in each bond)

O(1W)...N(1)	2.968	O(1W)...N(2)	2.828
N(3)...O(1W)	2.841	N(3)...O(5W)	2.714
N(4)...O(1W)	2.776	N(4)...O(6W)	2.813
O(5W)...N(6a)	3.041	O(5W)...N(7a)	2.910
O(6W)...N(6b)	2.873	O(6W)...N(7b)	3.051

N(1)...O(1W)...N(2)	115.2	N(1)...O(1W)...N(3)	117.7
N(1)...O(1W)...N(4)	119.0	N(2)...O(1W)...N(3)	94.0
N(2)...O(1W)...N(4)	102.1	N(3)...O(1W)...N(4)	104.9
N(3)...O(5W)...N(6a)	81.4	N(3)...O(5W)...N(7a)	95.7
N(6a)...O(5W)...N(7a)	96.1	N(4)...O(6W)...N(6b)	99.9
N(4)...O(6W)...N(7b)	107.9	N(6b)...O(6W)...N(7b)	96.6
O(1W)...N(3)...O(5W)	104.7	O(1W)...N(4)...O(6W)	107.1

Symmetry transformations: a *(-1 + x, -y, -1/2 + z)*;
b *(-1/2 + x, -1/2 + y, z)*

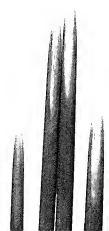

Table 5.10 Anisotropic thermal parameters* ($Å^2 \times 10^4$).

Atom	U_{11}	U_{22}	U_{33}	U_{12}	U_{13}	U_{23}
O(1W)	472(4)	596(4)	442(4)	-71(4)	228(4)	-30(4)
N(1)	564(4)	581(4)	534(4)	-65(4)	299(4)	-67(4)
C(1)	528(4)	697(5)	629(4)	-130(4)	291(4)	-37(4)
C(2)	468(4)	701(5)	634(4)	-37(4)	199(4)	-68(4)
O(2)	483(4)	773(4)	643(4)	-59(4)	149(4)	-204(4)
C(3)	588(4)	560(4)	571(4)	-165(4)	242(4)	-80(4)
C(4)	573(4)	833(5)	646(5)	-187(4)	181(4)	-79(4)
C(5)	694(5)	991(5)	634(5)	-297(5)	188(4)	-96(5)
C(6)	892(5)	887(5)	704(5)	-416(5)	377(4)	-250(4)
C(7)	914(5)	584(5)	861(5)	-158(4)	569(4)	-86(4)
C(8)	666(4)	501(4)	686(4)	-135(4)	358(4)	-2(4)
C(9)	758(5)	551(4)	844(5)	67(4)	427(4)	193(4)
N(2)	529(4)	620(4)	560(4)	22(4)	212(4)	78(4)
C(10)	601(4)	553(4)	605(4)	9(4)	286(4)	-25(4)
C(11)	443(4)	637(4)	548(4)	75(4)	214(4)	10(4)
C(12)	709(4)	856(5)	486(4)	-177(4)	318(4)	-126(4)
C(13)	685(4)	878(5)	496(4)	-200(5)	226(4)	107(4)
O(3)	548(4)	754(4)	648(4)	-91(4)	235(4)	187(4)
C(14)	610(4)	592(5)	382(4)	-112(4)	118(4)	4(4)
C(15)	865(5)	566(5)	524(4)	-136(4)	156(4)	42(4)
C(16)	1125(5)	544(5)	600(5)	37(5)	224(5)	12(4)
C(17)	859(5)	770(5)	558(4)	246(5)	126(4)	-67(4)
C(18)	625(4)	766(5)	463(4)	3(4)	142(4)	-83(4)
C(19)	551(4)	551(4)	351(4)	-85(4)	101(4)	-54(4)
C(20)	547(4)	586(4)	407(4)	-141(4)	151(4)	-59(4)
N(3)	416(4)	608(4)	428(4)	-111(4)	88(4)	-15(4)
C(21)	400(4)	885(5)	447(4)	-44(4)	96(4)	-61(4)
C(22)	419(4)	745(5)	456(4)	-122(4)	158(4)	-7(4)
C(23)	772(4)	714(5)	810(5)	23(4)	474(4)	-65(4)
C(24)	924(5)	652(5)	665(4)	-24(5)	411(4)	-116(4)
O(4)	1095(4)	574(4)	608(4)	-29(4)	452(4)	-93(4)
C(25)	578(4)	537(4)	588(4)	89(4)	209(4)	-4(4)
C(26)	635(5)	669(5)	676(5)	78(4)	170(4)	-89(4)
C(27)	577(5)	568(5)	1080(5)	32(4)	217(4)	-67(5)
C(28)	701(5)	669(5)	1126(5)	81(5)	402(4)	123(5)
C(29)	682(5)	745(5)	770(5)	174(4)	287(4)	178(4)
C(30)	482(4)	667(5)	529(4)	175(4)	120(4)	29(4)
C(31)	488(4)	833(5)	419(4)	128(4)	89(4)	10(4)
N(4)	441(4)	640(4)	384(4)	6(4)	102(4)	-6(4)
C(32)	503(4)	680(5)	441(4)	45(4)	174(4)	63(4)
C(33)	470(4)	644(4)	382(4)	46(4)	156(4)	-10(4)
N(5)	382(4)	550(4)	392(4)	-23(4)	134(4)	1(4)
O(5W)	1098(5)	623(4)	1244(5)	-72(4)	214(5)	160(4)
O(6W)	631(4)	1114(5)	778(4)	-182(4)	124(4)	-189(4)
S(1)	585(3)	974(4)	1090(4)	-24(3)	78(3)	-41(4)
C(34)	528(4)	710(5)	552(4)	244(4)	78(4)	-46(4)
N(6)	812(4)	788(5)	1150(5)	185(4)	472(4)	83(5)
S(2)	833(4)	1018(4)	1449(4)	64(4)	303(4)	219(4)
C(35)	487(4)	884(5)	1192(5)	-10(5)	166(5)	332(5)
N(7)	830(5)	1393(5)	1229(5)	-27(5)	251(5)	212(5)

Table 5.11 Hydrogen atom coordinates (x 10^4) and assigned isotropic temperature factors* (Å^2 x 10^3).

Atom	*x*	*y*	*z*	*U*
H(1WA)	421	-1387	-240	70
H(1WB)	-41	-855	62	70
H(1A)	2686	-853	-893	80
H(1B)	1779	-190	-998	80
H(2A)	3066	-110	135	80
H(2B)	2638	-1005	312	80
H(4)	3352	-10	1293	100
H(5)	3675	892	2303	100
H(6)	2448	1865	2414	100
H(7)	861	1947	1553	100
H(9A)	-231	1574	397	80
H(9B)	212	1070	-138	80
H(2N)	-1161	356	-19	80
H(10A)	-248	85	1391	80
H(10B)	-1038	842	1107	80
H(11A)	-2274	-215	564	80
H(11B)	-1908	-306	1396	80
H(12A)	1204	-1239	-1949	80
H(12B)	411	-1907	-1818	80
H(13A)	-295	-549	-2325	80
H(13B)	246	-128	-1579	80
H(15)	-1232	710	-2000	100
H(16)	-2807	1413	-2258	100
H(17)	-4224	713	-2096	100
H(18)	-4087	-741	-1700	100
H(20A)	-3133	-2109	-1563	80
H(20B)	-2016	-2121	-1620	80
H(3NA)	-1494	-1752	-421	80
H(3NB)	-1928	-2513	-524	80
H(21A)	-2906	-1047	-314	80
H(21B)	-3415	-1976	-409	80
H(22A)	-2200	-2419	647	80
H(22B)	-2889	-1658	779	80
H(23A)	2221	-2356	-1180	80
H(23B)	2514	-2187	-358	80
H(24A)	1722	-3558	-752	80
H(24B)	706	-3024	-1058	80
H(26)	500	-4498	-664	100
H(27)	32	-5719	-116	100
H(28)	182	-5707	1081	100
H(29)	764	-4463	1755	100
H(31A)	1984	-2703	1265	80
H(31B)	1652	-3095	1898	80
H(4NA)	447	-1992	892	80
H(4NB)	959	-1869	1553	80
H(32A)	-664	-2852	1227	80
H(32B)	-13	-2709	2024	80
H(33A)	-460	-1208	1876	80
H(33B)	-1391	-1825	1834	80
H(5WA)	-1350	-3698	-830	150
H(6WA)	1406	-1120	2714	150
H(6WB)	2125	-807	2510	150

bonding as shown in Fig. 5.37. The oxygen atom is hydrogen bonded to two hydrogen atoms from the two protonated nitrogens. The two hydrogens of the water molecule are in turn, hydrogen bonded to one bridgehead nitrogen and the secondary nitrogen atom of the chain which is not protonated. Therefore, the oxygen atom is tetrahedrally coordinated. The H-O-H bond angles are slightly distorted from the ideal tetrahedral value as the bond angle data suggest. Similar structures have been proposed by Lehn and coworkers [13]. There are two more lattice water molecules which are outside the cavity and are H-bonded to the two protonated amino nitrogens. The two thiocyanate anions are H-bonded to these lattice water molecules forming a chain-like structure. The bond distances and angles in the ligand are within the normal values. Also, the overall ellipsoidal topology of the cavity is observed upon complexation with the water molecule.

The 400 MHz ^{1}H-NMR shows that the water molecul is fast exchanging with the medium since the bonded water molecule does not show up in the spectrum. The ^{13}C-NMR spectrum shows five types of aliphatic carbons and six types of aromatic carbons.

5.11 Conclusion

The facile synthesis of the two cryptands with hetero-

ditopic receptor sites in presence of Cs(I)/Rb(I) ion, proves the effectiveness of these alkali metal ions as templates in the synthesis of cryptands. The ethereal oxygens, being poor donors for transition metal ions, only mononuclear cryptates are formed so that a part of the cavity remains vacant. This type of cryptands, therefore, affords to study cavitand chemistry. The two H_2S complexes with the Cu(II)-cryptates are air-stable. Thus, the cryptand affords to study transition metal-H_2S bonding (in this case Cu(II)-H_2S). This is due to the fact that the cryptands are able to provide an effective protective environment against decomposition of such species. The nitrogens present in the ring can be protonated easily to trap uncharged planar molecules like H_2O.

Table 5.1 Molar Conductances, Magnetic Moments(301K) and Elemental Analyses of the Cryptates

Cryptate	λ_M / ohm^{-1}cm^{2}mol^{-1}	μ_{eff}/μ_B	% Analysis							
			Found				Calcd			
			C	H	N	S	C	H	N	S
1	243		48.18	5.32	8.23		48.10	5.50	8.50	
2	239	1.97	48.17	5.47	8.60		48.21	5.52	8.52	
3	223	2.89	48.63	5.50	8.39		48.50	5.55	8.57	
4	152	1.93	50.97	5.72	14.44		51.83	5.93	14.65	
5	140	2.91	52.31	5.77	14.39		52.16	5.97	14.75	
6	139	2.04	56.10	6.16	21.72		56.04	6.41	21.78	
7	147	2.97	56.23	6.31	21.77		56.42	6.46	21.93	
8	227	1.9	46.37	5.37	8.16	3.78	46.27	5.30	8.18	3.74

Table 5.2 Electronic Absorption Spectral Data of the cryptates

Cryptate	λ_{max}/nm	ϵ_{max}/ $dm^3 mol^{-1} cm^{-1}$	Assignment
2	810	230	d-d band
	680	225	d-d band
	275	7120	σ(N)-->Cu(II) LMCT + intra-ligand transitions
3	940	18	d-d band
	565	15	d-d band
	360	45	d-d band
	270	4520	σ(N)-->Ni(II) LMCT + intra-ligand transitions
4	805	220	d-d band
	670	250	d-d band
	390	1370	(N_3)-->Cu(II) LMCT
	275	7900	σ(N)-->Cu(II) LMCT + intra-ligand transitions
5	950	15	d-d band
	570	15	d-d band
	380	80	d-d band + (N_3)-->Ni(II) LMCT
	270	4720	σ(N)-->Ni(II) LMCT + intraligand transitions

...co

Table 5.2 contd.

8	865	155	d-d band
	460	135	(H_2S)-->Cu(II) LMCT
	275	5280	σ(N)-->Cu(II) LMCT

4 and **6** have indistinguishable electronic spectral properties. So is the case between **5** and **7**.

Table 5.3 EPR spectral data of the cryptates

Cryptate	g_{av}	g_1	g_2	g_3	$A_{\|\|}^{Cu}$	
2	2.07					(298 K solid sample)
	2.06					(77 K solid sample)
		2.12($g_{\|\|}$)	2.07($g_{\perp}$)		61	(298 K in MeCN)
		2.18($g_{\|\|}$)	2.06($g_{\perp}$)		93	(77 K in MeCN)
4	2.09					(298 K solid sample)
	2.09					(77 K solid sample)
		2.14	2.07	2.03	65	(298 K in MeCN)
		2.21	2.07	2.02	97	(77 K in MeCN)
8	2.06					(298 K solid sample)
	2.07					(77 K solid sample)
		2.13	2.07	2.03	60	(298 K in MeCN)
		2.17	2.07	2.02	103	(77 K in MeCN)

The EPR spectral properties of **4** and **6** have no noticeable differences. So, the data for only **4** is presented.

Unit for hyperfine couplings is $cm^{-1} \times 10^{-4}$

Table 5.4 Molar Conductance, Magnetic Moment (301 K) and Elemental Analysis of the cryptates

Cryptate	λ_m/ohm^{-1}cm^{2}mol^{-1}	μ_{eff}/μ_B	Analysis (%)							
			Found				Calculated			
			C	H	N	S	C	H	N	S
9	227	-	55.49	5.12	7.01		55.48	5.28	7.2	
10	232	2.02	55.31	5.42	7.31		55.59	5.29	7.2	
11	176*	3.07	55.91	5.42	7.39		55.86	5.30	7.24	
12	215	2.09	53.60	5.21	7.21	3.27	53.70	5.31	7.00	3.

*Solvent in this case was DMF. In all other cases the solvent was acetonitrile

Table 5.5 Electronic Spectral Data of the Cryptates

Cryptate	λ_{max}/nm	ϵ_{max} ($dm^3\ mol^{-1}\ cm^{-1}$)	Assignment
9	330	6500	ligand absorptio
	320	6250	"
	301	10500	"
	280	10900	"
10	800	225	d-d band
	690	195	d-d band
	332	7550	Ligand absorptio
	301	11700	Ligand absorptio
	282	12530	σ(N)--->Cu(II)LM
			ligand absorptic
11	960	27	d-d band
	575	31	d-d band
	375	93	d-d band
	333	7090	Ligand absorpti
	301	10500	Ligand absorpti
	288	12300	σ(N)--->Ni(II)
			ligand absorpti
12	890	120	d-d band
	717	95	d-d band
	450	450	(S)--->Cu(II)LM
	333	7419	Ligand absorpti
	320	7274	Ligand absorpti
	301	15966	Ligand absorpti
	281	15654	σ(N)--->Cu(II)
			ligand absorpti

Table 5.6 EPR Spectral Data of the Cu(II) cryptates

Cryptate	g_{av}	$g_{\parallel}$	$g_{\perp}$	$A_{\parallel}^{Cu}$	
10	2.08	-	-	-	(298K solid sample)
	2.07	-	-	-	(77K solid sample)
	-	2.13	2.07	60	(298K CH_3CN solution)
	-	2.19	2.07	94	(77K CH_3CN glass solution)
12	2.07	-	-	-	(298K solid sample)
	-	2.17	2.01	-	(77K solid sample)
	2.07	-	-	65(av)	(298K CH_3CN solution)
$g_1 = 2.17$, $g_2 = 2.07$, $g_3 = 2.03$				103	(77K CH_3CN glass)

The unit for hyperfine couplings is $cm^{-1} \times 10^{-4}$

SCOPE OF THE FUTURE WORK

The research presented in this thesis indicate that alkali metal ions can be used as templates for the synthesis of macrobicyclic cryptands. In most cases, the template ion is not present inside the cavity. However, in case it is trapped inside, it can be easily replaced by transition metal ions of interest. Synthesis of four macrobicyclic cryptands are described here. Each of them form transition metal cryptates showing interesting electronic structure and bonding properties. However, the complexation studies with other transition as well as non-transition metal ions should be carried out in order to probe the effectiveness of these cryptands as ligands.

The stability constant measurements of various metal cryptates should provide valuable data regarding stability and selectivity of different metal ions towards these cryptands.

The X-ray structures of the metal cryptates should be determined whenever suitable single crystals are available. In the present thesis, only one X-ray structure has been given as other complexes have not been obtained in single crystal forms. Once X-ray structures are available, the electronic structure and bonding studies can be made on a more quantitaive fashion.

The use of alkali metal ions as templates in the synthesis of other types of cryptands should be undertaken.

The above aspects of supramolecular chemistry should provide important results and some of these are already being undertaken in the laboratory by the present investigator as well as other workers.

REFERENCES

1. J.M. Lehn, Struct. Bonding, Berlin, 1973, **16**, 1.

2. E. Weber and F. Vogtle, Top. Curr. Chem., 1981, **98**, 1.

3. J.M. Lehn, Angew. Chem. Int. Ed. Engl., 1988, **27**, 89.

4. D.J. Cram, Angew. Chem. Int. Ed. Engl., 1988, **27**, 1009.

5. I.O. Sutherland, Chem. Soc. Rev., 1985, **15**, 63.

6. J.M. Lehn,Science, 1985, **227**, 849.

7. F. Vogtle, H. Sieger and W.M. Muller, Top. Curr. Chem., 1981, **98**, 107.

8. D.J. Gram, Nature, 1992, **356**, 29.

9. J.M. Lehn, Pure Appl. Chem., 1980, **52**, 2441.

10. G.P. Potvin and J.M. Lehn, in Progress in Macrocyclic Chemistry, Vol. 3, Eds., R.M. Izatt and J.J. Christensen, Wiley, New York, 1987, p. 167.

11. J.M. Lehn, in Perspectives in Coordination Chemistry, Eds. A.F. Wiliams, C. Floriani and A.F. Merbach, V.C.H., New York, 1992, 447.

12. R.D. Hancock and A.E. Martell, Chem. Rev., 1989, **89**, 1875.

13. J.M. Lehn, Acc. Chem. Res., 1978, **11**, 49.

14. (a) J.M. Lehn, Pure Appl. Chem., 1977, **47**, 857.

    (b) E. Kauffmann, J.M. Lehn and J.P. Sauvage, Helv. Chim.

Acta, 1976, **59**, 1099.

15. B. Dietrich, J.M. Lehn, and J.P. Sauvage, Tetrahedron Lett., 1969, 2885 and 2889.

16. J.M. Lehn, Pure Appl. Chem., 1980, **52**, 2303.

17. L. Rossa and F. Vogtle, Top. Curr. Chem., 1983, **113**, 1.

18. (a) G. Illuminati and L. Mandolini, Acc. Chem. Res. 1981, **14**, 95.

(b) M.A. Winnik, Chem. Rev., 1981, **81**, 491.

19. (a) B. Dietrich, J.M. Lehn, J.P. Sauvage and J. Blanzat, Tetrahedron, 1977, **29**, 1629.

(b) H. An, J.S. Bradshaw and R.M. Izatt, Chem. Rev., 1992, **92**, 543 and references therein.

20. D.H. Busch and C. Cairns in progress in Macrocyclic Chemistry, Vol. 3, Eds., R. M. Izatt and J.J. Christensen, Wiley, New York, 1987, p. 1.

21. M.D.S. Healy and A.J. Rest, Adv. Inorg. Chem. Radiochem., 1978, **21**, 1.

22. N.F. Curtis, J. Chem. Soc., 1969, 3, 3.

23. D.A. Laidler, J.F. Stoddart, in "Synthesis of Crown Ethers and Analogues", ed., S. Patai, The Chemistry of Functional Groups, supp. E., Part 1, Wiley, New York, 1980, p. 1.

24. W.H. Kruizinga, R.M. Kellog, J. Am. Chem. Soc., 1981, 103, 5183.

25. W. Baker, J.F.W. McOmie, W.D. Ollis, J. Chem. Soc.,1951, 200.

26. C.J. Pederson, J. Am. Chem. Soc., 1967, 89, 2495.

27. C. J. Pederson, J. Am. Chem. Soc., 1967, 89, 7017.

28. (a) C.W. Gokel, S.H. Korzeniwski in "Macrocyclic Polyether Synthesis", Eds. K. Hafner, J.M. Lehn, C.W. Rees, P.V.R. Schleyer, B.M. Trest and R. Zahnradnik, Springer, New York, 1982.

(b) A.V. Bajaj, N.S. Poonia, Coord. Chem. Rev., 1988, 87, 55.

(c) C.J. Pedersen, Angew. Chem., Int. Ed. Engl., 1988, 27, 1053.

29. H.E. Simmons and C.H. Park, J. Am. Chem. Soc., 1968, 90, 2428.

30. F. Arnand-Neu, B. Spiess and M.J. Schwing-weill, J. Am. Chem. Soc., 1982, **104**, 5641.

31. R.M. Izatt, K. Pawlak, J.S. Bradshaw and R.L. Bruening, Chem. Rev.,1991, **91**, 1721 and references therein.

32. A.M. Sargeson, Pure Appl. Chem., 1984, **56**, 1603.

33. L.F. Lindoy in The Chemistry of Macrocyclic Ligand

Complexes, Cambridge University Press, Cambridge 1989.

34. J.M. Lehn, Angew. Chem. Int. Ed. Engl., 1990, 29, 1304.

35. Perspectives in Coordination Chemistry, Eds. A..F. Williams, C. Floriani and A.E. Merbach, V.C.H., New York, 1992, p. 31, 109, 153.

36. B.L. Vallee and R.J.P. Williams, Proc. Natl. Acad. Sci., (USA), 1968, **59**, 398.

37. E.I. Solomon, M.J. Baldwin and M.D. Lowery, Chem. Rev., 1992, **92**, 521.

38. P.K. Bharadwaj, J. Sci. Ind. Res., India, (in press).

39. M.P. Ngwenya, A.E. Martell and J. Reibenspies, J. Chem. Soc., Chem. Commun., 1990, 1207.

40. R. Louis, Y. Agnus and R. Weiss, J. Am. Chem. Soc., 1978, **100**, 3604 and references therein.

41. P. Chauduri, M. Winter, P. Fleischhauer, W. Hanse, U. Florke and H. J. Haupt, J. Chem. Soc. Chem. Commun., 1990, 1728.'

42. Biological and Inorganic Copper Chemistry, Eds. K.D. Karlin and J. Zubieta, Adenine Press, Guilderland, New York, 1983 and 1986.

43. S.J. Lippard, Angew. Chem. Int. Ed. Engl., 1988, **27**, 344.

44. Metal Clusters in Proteins, Eds., L. Que. Jr., ACS Symposium Series 372, American Chemical Society, Washington D.C. 1988.

45. J.B. Vincent and G. Christou, Adv. Inorg. Chem. 1989, 33, 197.

46. (a) I.I. Creaser, R.J. Geve, J.M. Harrowfied, A.J. Herlt, A.M. Sargeson, M.R. Snow and J. Springborg, J. Am. Chem. Soc., 1982, **104**, 6016.

(b) R.J. Geue, T.W. Hambley, T.M. Harrowfield, A.M. Sargeson and M.R. Snow, J. Am. Chem. Soc., 1984, **100**, 5478.

(c) H.A. Boucher, G.A. Lawrence, P.A. Lay, A.M. Sargeson, A.M. Bond, D.F. Sangster and J.C. Sullivan, J. Am. Chem. Soc., 1983, **105**, 4652.

(d) J. Harrowfield, B. Mac, A.J. Herlt, P.A. Lay, A.M. Sargeson, A.M. Bond, W.A. Mulac and J.C. Sullivan, J. Am. Chem. Soc., 1983, **105**, 5503.

(e) P. Osvath, A.M. Sargeson, B.W. Skelton and A.H. White, J. Chem. Soc., Chem. Commun., 1991, 1036.

(f) M.T. Donlevy, R.L. Gahan, W.T. Hambley and R. Stranger, Inorg. Chem. 1992, **31**, 4376.

47. A. Bencini, A. Bianchi, A. Borselli, S. Chimichi, M. Ciampolin, P. Dappaorto, M. Micheloni, N. Nardi, P. Paoli, B. Valtancoli, Inorg. Chem., 1990, **29**, 3282.

48. J.M. Lehn, S.H. Pine, E. Watanabe and A.K. Willard, J. Am. Chem. Soc., 1977, **99**, 6766.

49. Y. Agnus, R. Louis and R. Weiss, J. Am. Chem. Soc., 1979, **101**, 3381.

50. P. Chaudhuri, M. Winter, F. BIrkelbach, P. Fleischhauer, W. Haese, U. Florke and H.J. Haupt, Inorg. Chem., 1991, **30**, 4291.

51. J. Mendoza, E. Mesa, J. Redriquez-U bis, P. Vazquez, F. Vogtle, P. Winsdscheif, K. Rissanen, J.M. Lehn, D. Lilienbaum and R. Ziessel, Angew. Chem. Int. Ed., Engl., 1991, **30**, 1331.

52. P.D. Beer, O. Kocian, R.J. Mortimer and P. Spencer, J. Chem. Soc., Chem. Commun., 1992, 602.

53. (a) R.J. Motekaitis, A.E. Martell, J.M. Lehn and E.I. Watanabe, Inorg. Chem., 1982, **21**, 4253.

(b) R.J. Motekaitis, P.R. Rudolf, A.E. Martell and A. Clearfield, Inorg. Chem., 1989, **28**, 112.

54. A.E. Martin and J.E. Bulkowski, J. Am. Chem. Soc., 1982, **104**, 1434.

55. M.G.B. Drew, J. Hunter, D. Marrs, J. Nelson and C. Harding, J. Chem. Soc. Dalton Trans., 1992, 3435.

56. R. Menif, J. Reibenspies and A.E. Martell, Inorg. Chem.

1991, **30**, 3446.

57. R.J. Motekaitis, A.E. Martell, B. Dietrich and J.M. Lehn, Inorg. Chem., 1984, **23**, 1588.

58. R.J. Motekaitis, A.E. Martell, I. Murass, J.M. Lehn and M.W. Hosseini, Inorg. Chem., 1988, **27**, 3630.

59. J. Franke and F. Vogtle, Top. Curr. Chem., 1986, **132**, 135.

60. M.C. Etter, Acc. Chem. Res., 1990, **23**, 120.

61. R. Foster, Molecular Association, Academic Press, London, Vol. 1, 1975; Vol. 2, 1979.

62. (a) F. Diedrich, in "Cyclophanes", Royal Soc. Chem., Cambridge, 1991.

(b) W. Saenger, in Inclusion Compounds, Eds. J.L. Atwood, J.E.D. Davies, D.D. MacNicol, Vol.2, Ch.8 and R.J. Bergeron, ibid, Vol.3, Ch.12.

63. F. Vogtle and W. M. Muller, Top. Curr. Chem., 1984, **125**,131.

64. S. Kulstad and L.A. Malmsten, Tetrahedron Lett., 1980, **21**, 643.

65. F. Mathien and R. Weiss, J. Chem. Soc. Chem. Commun., 1973, 816.

66. S.B. Larson, J.N. Ramsden, S.H. Simonsen and J.J. Lagowski, Acta Cryst., 1983, **C39**, 1646.

67. J.M. Lehn and F. Montovan, Helv. Chim. Acta, 1978, **61**, 67.

68. Y. Sun and A.E. Martell, J. Am. Chem. Soc., 1989, **111**, 8023.

69. M.T. Garrett, J.T. Mc Murry, W.M. Hosseini, E.Z. Reyes, E.F. Hahn and K.N. Raymond, J. Am. Chem. Soc., 1991, **113**, 2965.

70. J. Hunter, J. Nelson, C. Harding, M. McCann and V. McKee, J. Chem. Soc. Chem. Commun., 1990, 1148.

71. B. Dietrich, M.W. Hosseini, J.M. Lehn, and R.B. Sessions, Helv. Chim. Acta, 1985, **68**, 289.

72. C. Harding, V. Mckee and J. Nelson, J. Am. Chem. Soc., 1991, **113**, 9684.

73. M.G.B. Drew, D. Marrs, I. Hunter and J. Nelson, J. Chem. Soc. Dalton Trans., 1992, 11.

74. J. Jazwinski, J.M. Lehn, D. Lilienbaum, R. Ziessel, J. Guilhem and C. Pascard, J. Chem. Soc. Chem. Commun., 1987, 1691.

75. R.J. Motekaitis, A.E. Martell, I. Murase, J.M. Lehn and M.W. Hosseini, Inorg. Chem., 1988, **27**, 3630.

76. C.M. Frey and J. Stuehr, Metal Ions in Biological Systems, Ed. H. Sigel, Marcel Dekkar, N.Y. (1974), Vol. 1, p. 69.

77. E. Deutsh, M.J. Rot and D.L. Nosco, Adv. Inorg. Bioinorg. Mech., 1982, **1**, 269.

78. A. Bencini and D. Gatteschi, Electron Paramagnetic Resonance of

Exchange Coupled Systems, Springer, Berlin, 1990 ,

79. J.A. Fee, Struct. Bonding, Berlin, 1975, **23**, 1.

80. B. Dietrich, J.M. Lehn, J. Guilhem and C. Pascard, Tetrahedron Lett., 1989, **30**, 4125.

81. D.D. Perrin, W.L.F. Armargo and D.R. Perrin, Purification of Laboratory Chemicals, Pergamon Press, New York, 1st edn., 1966.

82. M. Ray, S. Mukherjee and R.N. Mukherjee, J. Chem. Soc. Dalton Trans. 1990, 3635.

83. R.M. Silverstein, C.C. Bassler and T.C. Morrill, Spectrometric Identification of Organic Compounds, 3rd edn., Wiley, New York, 1991, p. 126.

84. A.M. Heyns, Spectrochim. Acta, Part A, 1977, **33**, 315.

85. D. Moras, B. Metz and R. Weiss, Acta Cryst., 1973, **B29**, 388.

86. W.J. Grey, Coord. Chem. Rev., 1971 **7**, 81.

87. Q. Lu, Q.H. Luo, A.B. Dai, Z.Y. Zhou and G.Z. Hu, J. Chem. Soc. Chem. Commun., 1990, 1429.

88. D.L. Rabenstein and G. Blakney, Inorg. Chem., 1973, **12**, 128.

89. (a) B.J. Hathaway and A.E. Underhill, J. Chem. Soc. (A), 1961, 3091.

(b) A.E. Wickenden and R.A. Krause, Inorg. Chem., 1965, **4**,

404.

(c) S.F. Pavkovic and D.W. Meek, Inorg. Chem., 1965, 4, 1091.

90. D.L. Lewis, W.E. Hatfield and D. J. Hodgson, Inorg. Chem., 1974, 13, 147.

91. V.M. Miskowski, J.A. Thich, R. Solomon and H.J. Schugar, J. Am. Chem. Soc., 1976, 98, 8344.

92. (a) B.J. Hathaway and D.E. Billing, Coord. Chem. Rev. 1970, 5, 143

(b) R.J. Dudley, B.J. Hathaway, P.G. Hodgson, P.C. Power and D.J. Loose, J. Chem. Soc. Dalton Trans., 1974, 1005.

93. A.W. Addison, H.M.J. Hendricks, J. Reedijk and L.K. Thompson, Inorg. Chem., 1981, 20, 103 and refs. cited therein.

94. (a) M. Duggan, N. Ray, B.J. Hathaway, A.A.G. Tomlinson, P. Brint and K. Pelin, J. Chem. Soc. Dalton Trans., 1980, 1342

(b) R. Kuroda, S.F. Mason, T. Prosperi, S. Savage and G.E. Tranter, J. Chem. Soc. Dalton Trans., 1981, 2565.

95. A.B.P. Lever, Inorganic Electronic Spectroscopy, Elsevier, Amsterdam, 2nd ed., 1984, p. 175.

96. (a) R.C. Slade, A.A.G. Tomlinson, B.J. Hathaway and D.E.

Billing, J. Chem. Soc. A, 1968, 61.

(b) D.M. Duggan and D.N. Hendrickson, Inorg. Chem., 1973, **12**, 2422; 1974, **13**, 1911.

(c) E.J. Laskowski, D.M. Duggan and D.N. Hendrickson, Inorg. Chem., 1975, **14**, 2429.

97. (a) T.D. Smith and J.R. Pilbrow, Coord. Chem. Rev., 1974, **13**, 173.

(b) E.I. Solomon, A.A. Gewirth and T.D. Westmoreland, in Advanced EPR-Applications in Biology and Biochemistry, ed., A.J. Hoff, Elsevier, Amsterdam, 1989, p. 865.

98. (a) R. Burbucci and M.J.M. Campbell, Inorg. Chim. Acta, 1975, **L15**, 15.

(b) R. Burbucci, A. Bencini and D. Gatteschi, Inorg. Chem., 1977, **16**, 2117.

99. M.I. Pilo, G. Manca, M.A. Zoroddu and R. Seeber, Inorg. Chim. Acta., 1991, **180**, 225.

100. N. Nakamoto, Infrared and Raman Spectra of Inorganic and Coordination Compounds, 4th ed., John Wiley, New York, 1987, p.251.

101. H. Elliot and B.J. Hathaway,Inorg. Chem., 1966, **4**, 885.

102. H.J. Prochaska, W.F. Schwindinger, M. Schwartz, M.J. Burk, E. Bernarducci, R.A. Lalancette, J.A. Potenza and H.J. Schugar,

J.Am.Chem.Soc., 1981, **103**, 3446.

103. W.E. Blumberg and J. Peisach, Arch. Biochem. Biophys., 1974, **165**, 691.

104. B.N. Figgis and J. Lewis, Prog. Inorg. Chem., 1964, **6**, 37.

105. R. C. Rosenberg, C.A. Root, P.K. Bernstein and H.B. Gray, J.Am.Chem.Soc., 1975, **99**, 21.

106. A.B.P. Lever, "Inorganic Electronic Spectroscopy", Elsevier, New York, 1984, p. 448.

107. J.E. Wertz and J.R. Bolton, Electron Spin Resonance - Elementary Theory and Practical Applications, Mcgraw Hill, N.Y. (1972), p. 224; A. Abragam and B. Bleany, Electron Paramagnetic Resonance of Transition Ions, Clarendon Press, Oxford (1970), p. 436.

108. C. Branden, Acta Chem. Scand., 1967, **21**, 1000.

109. J.A. Thich, D. Mastropaolo, J. Potenza and H.J. Schugar, J. Am. Chem. Soc., 1974, **96**, 726.

110. (a) M.M. Kadooka, L.G. Warner and K. Seff, J. Am. Chem. Soc., 1976, **98**, 7569.

(b) M.M. Kadooka, L.G. Warner and K. Seff, J.Chem.Soc.Chem. Commun., 1975, 990.

(c) L.G. Warner, T. Ottersen and K. Seff, Inorg. Chem.,

1974, 13, 2819.

111. J.M. Downes, J. Whelan and B. Bosnich, Inorg. Chem., 1981, 20, 1081.

112. P.E. Riley and K. Seff, Inorg. Chem., 1972, 11, 2993.

113. L.G. Warner, T. Ottersen and K. Seff, Inorg. Chem., 1974, 13, 2529.

114. L.G. Warner, M.M. Kadooka and K. Seff, Inorg. Chem., 1975, 14, 1773.

115. J.A. Bertrand and J.L. Breece, Inorg. Chim. Acta, 1974, 8, 267.

116. L.D. Nosco, R.C. Elder and E. Deutsch, Inorg. Chem., 1980, 19, 2545.

117. M.M. Kadooka, L.G. Warner and K. Seff, Inorg. Chem., 1976, 15, 812.

118. S.E. Livingstone and J.D. Nolan, Aus. J. Chem., 1973, 26, 961.

119. J.L. Corbin and D.E. Work, J. Org. Chem., 1976, 487.

120. N. Bodor, E. Koltai and L. Prokai, Tetrahedron, 1992, 48, 4767.

121. A.V. Joshuo, J.R. Scott, S.M. Sondhi, R.G. Ball and W.J. Lown, J. Org. Chem., 1987, 52, 2447.

122. R.J. Motekaitis, A.E. Martell, I. Murase, J.M. Lehn and M.W.

Hosseini, Inorg. Chem., 1988, 27, 3630.

123. R. Steudel, Angew. Chem. Int. Ed. Engl., 1975, 655.

124. R. Kuroda, S.F. Mason, T. Prosperi, S. Savage and G.E. Tranter, J.Chem.Soc.Dalton Trans., 1981, 2565.

125. E. John, P.K. Bharadwaj, K. Krogh-Jesperson, J.A. Potenza and H.J. Schugar, J. Am. Chem. Soc. 1986, 108, 5016.

126. A. Bencini and D. Gatteschi, Electron Paramagnetic Resonance of Exchange Coupled Systems, Springer, Berlin (1990), p.2.

127. B.J. Hathaway, M. Duggan, A. Murphy, J. Mullane, C. Power, A. Walsh and B. Walsh, Coord. Chem. Rev., 1981, 36, 267.

128. E.I. Solomon, K.W. Penfield and D.E. Wilcox, Top Curr. Chem., 1983, 53, 1.

129. L.F. Lindoy, "The Chemistry of Macrocyclic Ligand Complexes" 1989, Cambridge University Press, Chp. 8, p. 216.

130. Perspectives in Coordination Chemistry, Eds. A..F. Williams, C. Floriani and A.E. Merbach, V.C.H., New York, 1992,

131. M.M. Bernardo, M.J. Heeg, R.R. Schroeder, L.A. Ochrymowycz and D.B. Rorabacher, Inorg. Chem. 1992, 31, 191.

132. K. Ragunathan and P.K. Bharadwaj, J. Chem. Soc. Dalton Trans., 1992, 2417

133. D. L. Tennet and D. R. McMillin, J.Am.Chem.Soc., 1979, **101**, 2307.

134. K. Ward, Jr., J. Am. Chem. Soc., 1935, **57**, 914.

135. S. Liu, L. Gelmini, S.J. Rettig, R.C. Thompson and C. Orvig, J. Am. Chem. Soc., 1992, **114**, 6081.

136. H.I. Schlesinger, H.C. Brown, H.R. Hockstra and L.R. Rapp, J. Am. Chem. Soc., 1953, **75**, 199.

137. (a) R.D. Willet, J.A. Haugen, J. Lebsack and J. Morrey, Inorg. Chem., 1974, **13**, 2510.

(b) R.L. Harlow, W.J. Wells III, G.W. Watt and S.H. Simonsen, Inorg. Chem., 1975, **14**, 1768.

(c) H. Yokoi and A.W. Addison, Inorg. Chem., 1977, **16**, 1341.

138. A.B.P. Lever, Inorganic Electronic Spectroscopy, 2nd ed., Elsevier, New York, 1984, p. 555.

139. (a) H. Yokoi and T. Isobe, Bull. Chem. Soc. Jpn., 1969, **42**, 2187.

(b) B.P. Kennedy and A.B.P. Lever, J. Am. Chem. Soc., 1973, **95**, 6907.

140. S. Knapp, T.P. Keenan, X. Zhang, R. Fikar, J.A. Potenza and H.J. Schugar, J. Am. Chem. Soc., 1990, **112**, 3452.

141. E.I. Solomon, J.W. Hare, D.M. Dooley, J.H. dawson, P.J.

Stephens and H.B. Gray, J.Am.Chem.Soc., 1980, **102**, 174.

142. F.A. Cotton and G. Wilkinson, Advanced Inorganic Chemistry, 5th ed., John Wiley, New York, 1988, p. 747.

143. (a) W.E. Hill, J.G. Taylor, C.A. McAuliffe, K.W. Muir and L. Manojlovic-Muir, J. Chem. Soc. Dalton Trans., 1982, 833.

(b) W.E. Hill, J.G. Taylor, C.A. McAuliffe and M. Levason, J. Chem. Soc. Dalton Trans., 1982, 841.

144. C.J. Ballhausen, Introduction to Ligand Field Theory, McGraw Hill, New York (1962).

145. K. Nakamoto, Infrared and Raman Spectra of Inorganic and Coordination Compounds, 4th ed., John Wiley, New York, 1987, p. 290.

146. R. Cortes, J.I.R. de Larramendi, L. Lezama, T. Rojo, K. Urtiaga and M.I. Arriorlua, J.Chem.Soc.Dalton Trans., 1992, 2723.

147. M.I. Arriorlua, R. Cortes, L. Lezama, T. Rojo, X. Solens and M. Font-Bardia, Inorg. Chim. Acta, 1990, **174**, 263.

148. H.J. Schugar in Copper Coordination Chemistry: Biochemical and Inorganic Perspectives, eds. K.D. Karlin and J. Zubieta, Adenine Press, New York, 1983, p. 43.

149. H. M. Herberhold and G. Suss, Angew. Chem., Int. Ed. Engl.,

1976, **15**, 366.

150. C.G. Kuehn and H. Taube, J. Am. Chem. Soc., 1976, **92**, 1089.

151. (a) J.J. Christensen, D.J. Eatough, R.M. Izatt, Chem. Rev., 1974, **74**, 351.

(b) F. de Jong, D.N. Reinhoudt and C.J. Smit, Tetrahedron Lett., 1976, 1371.

152. P. Labbe, R. Le Goallery, H. Handel, G. Pierre and J.L. Pierre, Electrochim. Acta, 1982, **27**, 257.

153. M.R. Johnson, I.O. Sutherland and R.F. Newton, J. Chem. Soc., Perkin Trans., 1, 1979, 357.

154. P. Main, S. Fiske, S.E. Hull, L. Lessinger, G. Germain, J.P. Declercq and M.M. Woolfson, MULTAN 82, A system of Computer Programs for the Automatic Solution of Crystal Structures from X-ray Diffraction Data, Univs. of York, England and Louvin, Belgium, 1982.

155. G.M. Sheldrick, SHELXTL-PLUS 88, Structure Determination Software Programs, Nicolet Instrument Corp., Madison, WI. 1988.

156. International Tables for X-ray Crystallography, Kynoch Press, Birmingham, 1974, Vol. 1 (present distributors, Kluer Academic Publishers, Dordrect).

LIST OF PUBLICATIONS

1. Synthesis and Characterisation of an Octaazamacrobicyclic Ligand Using Alkali Metal Ions as Templates;Characterisation of a Dicopper Complex as the Perchlorate Salt, K. Ragunathan and P.K. Bharadwaj, J.Chem.Soc.Dalton Trans., 1653 (1992).

2. Nickel(II) Complexes with Tripodal Ligands: Synthesis, X-ray Structural and Spectroscopic Studies, K. Ragunathan and P. K. Bharadwaj, J. Chem. Soc. Dalton Trans. 1992, 2417.

3. Template Synthesis of a Cryptand Having Hetero-Ditopic Receptor Sites, K. Ragunathan and P.K. Bharadwaj, Tetrahedron Lett., 7581 (1992).

4. Synthesis of a Macrobicyclic Cryptand Having Mixed Donors by [2+3] Schiff Base Condensation, K. Ragunathan and P.K. Bharadwaj, Proc. Ind. Acad. Sci. (submitted).

5 Imposition of Pseudotetrahedral Geometry by a Cryptand with Hetero-Ditopic Receptor Sites: Synthesis and Characterisation of Cu(II) and Ni(II) Cryptates with the Chromophore MN_4 and Their Interactions with the Azide Ion, K. Ragunathan and P. K. Bharadwaj, J.Chem.Soc.Dalton Trans., (submitted).

6. Dinuclear Hexadentate Cu(II) and Ni(II) Cryptate Complexes: Synthesis, Spectroscopic and Electrochemical Characterisation of the Perchlorate Salts, K. Ragunathan and P. K. Bharadwaj, J.Chem.Soc. Dalton Trans., (submitted).

7. Template Synthesis of a Hetero-Ditopic Cryptand with Three Naphthyl Side-Groups: Effects of Donor Atoms' Topology on the Electronic Structures of Cu(II) and Ni(II) Cryptates, K. Ragunathan and P. K. Bharadwaj, J.Chem.Soc.Chem.Commun. (submitted).

8. Facile Synthesis of Cryptands Using Alkali Metal Ions as Templates and Their Ligating Behaviour Towards Transition Metal Ions, K. Ragunathan and P.K. Bharadwaj, 29th.Int.Conf. Coord.Chem., Lausanne, Switzerland, July 19-24, 1992.